NTNU

Norwegian University of
Science and Technology

Study of frequency dependent loss in magnetic steel by the Jiles-Atherton method

Magnus Erlend Tangen

Master of Science in Electric Power Engineering
Submission date: June 2018
Supervisor: Arne Nysveen, IEL
Co-supervisor: Anyuan Chen, IEL

Norwegian University of Science and Technology
Department of Electric Power Engineering

NORGES TEKNISK-NATURVITENSKAPELIGE UNIVERSITET

NTNU

M A S T E R O P P G A V E

Kandidatens navn : Magnus Erlend Tangen

Fag : **ELKRAFTTEKNIKK**

Oppgavens tittel (norsk) : *En studie av frekvensavhengige tap i magnetisk stål med bruk av Jiles-Atherton metoden*

Oppgavens tittel (engelsk) : *Study of frequency dependent loss in magnetic steel by the Jiles-Atherton method*

Oppgavens tekst:
Direct electrical heating system (DEHs) are used for safeguarding the well-stream through pipelines for processing topside or shore. The heating source is conductive and hysteresis power losses in the pipeline due to electric current injected into pipeline. For DEHs design, it is critical to predict the heating power as function of input current and frequency so that proper frequency and current can be selected correspondingly. This master thesis concerns using Jiles-Atherton modelling to simulate the induced loss in magnetic steel materials and verification with sample tests:

The project study will include:

- Improving MATLAB script to be suitable for generic measured B-H Curves, creating five required parameters by Jiles-Atherton in Comsol.
- FEM simulation to calculate the frequency dependent loss in a rod sample conducting AC currents
- Measuring AC loss of a rod samples with different frequencies and currents in Lab

Further details to be clarified with the supervisors.

Oppgaven gitt	: 15. januar 2018
Oppgaven revidert:	: 4. juni 2018
Besvarelsen leveres innen	: 11. juni 2018
Besvarelsen levert	:
Utført ved (institusjon, bedrift)	: Institutt for elkraftteknikk/NTNU
Kandidatens veileder	: Anyuan Chen/NTNU
Faglærer	: Professor Arne Nysveen

Trondheim, 4. juni 2018

Arne Nysveen
faglærer

Preface

This project is performed during the fall of the 4th semester in a two-year master program as a master thesis project. The thesis is a continuation of the specialization project presented in [1]. The author, Magnus E. Tangen, is a trained electrician and has a bachelor's degree from the University College of Southeast Norway. This thesis is his final work in the master's program Electric Power Engineering at the Norwegian University of Science and Technology.

Readers with a basic understanding of electromagnetic theory and terms related to finite element methods (FEM) will have the highest benefit of reading this report.

I would especially like to thank Marte, Jenny and the rest of my family for the unconditional support throughout my period as a student. I would also like to thank my supervisor Arne Nysveen and co-supervisor Anyuan Chen for their help and guidance during the project period. An additional thanks to my grandfather Harald O. Danielsen for introducing me to the concept of electromagnetism and my fellow student Lars Erik Pettersen for insightful discussions and feedback.

Sammendrag

Denne avhandlingen er en videreføring av spesialiseringsprosjektet som undersøkte muligheten for å simulere hysterese- og virvelstrømstap i karbonstål [1]. Arbeidet i denne avhandlingen omfatter en undersøkelse av hvordan man effektivt definerer Jiles-Atherton (J-A) parameterverdier for magnetiske materialer. Dette forenkler tapssimuleringer gjennom effektiv J-A-implementering av materialer i finite element method (FEM)-programvare. J-A-metoden implementeres i en FEM-modell og verifiseres av simulerte og målte tap i to forskjellige ferromagnetiske materialer.

Den generiske programvaren JAMPS (Jiles-Atherton Parameter Search) ble utviklet som en del av arbeidet og brukt som verktøy for å bestemme parameterverdiene til J-A metoden. JAMPS er utviklet med et grafisk brukergrensesnitt for å øke brukervennligheten til programvaren.

Verifikasjonen av J-A parameterne ble utført i FEM-programvaren Comsol Multiphysics hvor en modell ble utviklet for å simulere måleutstyret som ble brukt til å måle tapet i materialprøver. Måleinstrumentet blir undersøkt og forklart for å oppnå en sammenlignbar tapssimulering i FEM-modellen. Den utviklede FEM-modellen er relativt effektiv når det gjelder beregningstid og resultatoppløsning.

Simuleringene og målingene ble utført med flukstetthetene 100, 200, 300 og 400mT ved frekvensene 50, 100, 150 og 200Hz. De målte AC-tapene ble brukt som referanser og sammenlignet med de simulerte tapene fra FEM-modellen. Generelt ble simuleringen av de totale tapene utført med tilstrekkelig nøyaktighet, og implementeringen av Jiles-Atherton-metoden betraktes som en suksess. Forskjellen mellom simulerte de og målte totale tap i materiale 1 ligger i området -15% til 5%. Forskjellen mellom de simulerte og målte totale tap i materiale 2 ligger i området 0% til 37%

Sammenligningen av målt og simulert virvelstrøm og hysteresetap viste en signifikant forskjell mellom de målte og simulerte tap i begge materialer. De separerte tapene kunne ikke uttrykkes analytisk med tilfredsstillende nøyaktighet. Dette indikerer at forskjellen mellom målt og simulert virvelstrøm- og hysteresetap kan skyldes andre grunner enn unøyaktige materialbeskrivelser i FEM-modellen.

Abstract

This thesis is a continuation of the specialization project presented in [1] which investigated the possibility of simulating the hysteresis and eddy current losses in carbon steel. The work comprises an investigation of how to efficiently obtain Jiles-Atherton (J-A) parameter values for magnetic materials and thus ease the J-A implementation of new materials in a finite element method (FEM) software for loss simulations. The J-A method is implemented in a FEM model and verified by simulated and measured AC losses. Two different ferromagnetic materials are investigated.

The generic software 'JAMPS' (Jiles-Atherton Parameter Search) was developed and used as the tool for obtaining the J-A parameter values. JAMPS was developed with a graphical user interface (GUI) to increase the usability of the software.

The verification of the J-A parameters was performed in the FEM software Comsol Multiphysics where a model was developed to simulate the measurement equipment used to measure the loss in the material samples. The operation principle of the measuring instrument is investigated and explained to obtain a comparable loss simulation in Comsol. The resulting FEM model is relatively efficient in terms of computation time and result resolution.

The simulations and measurements were performed with the target flux densities 100, 200, 300 and 400mT at the frequencies 50, 100, 150 and 200Hz. The measured AC losses were used as references and compared with the simulated losses from the FEM model. In general, the simulation of the total losses was performed with a low error and the implementation of the J-A method is regarded as a success. The difference between the simulated and measured total losses in material 1 is in the range of -15% to 5%. The difference between the simulated and measured total losses in material 2 is in the range of 0% to 37%,

The comparison of the measured and simulated eddy current and hysteresis loss showed a significant difference between the measured and simulated losses in both materials. The separated losses could not be expressed analytically with a satisfactory low error. This indicates that the difference between the measured and simulated eddy current and hysteresis losses may be due to other reasons than inaccurate material descriptions in the FEM model.

Table of content

List of figures

List of tables

Abbreviations

DEH	Direct Electrical Heating
EMF	Electromotive force
FEM	Finite element method
GUI	Graphical user-interface
J-A	Jiles-Atherton
JAMPS	Jiles-Atherton method parameter search
MMF	Magnetomotive force

1 Introduction

The background for this master thesis originates from a specialization project [1] which was written in the fall of 2017 at NTNU by Magnus E. Tangen. The specialization project investigated the possibility of simulating the hysteresis and eddy current losses in carbon steel.

There are many advantages and applications of such loss calculations, but the main application investigated in the specialization project was related to safeguarding well streams through pipelines used in oil production. This application is known as Direct Electrical Heating (DEH) and the main objective was to study how the power (or energy) changed with the AC frequency. The heating source is power loss due to the injected AC current in the pipeline. With alternating flux in a ferromagnetic material, it is difficult to calculate the loss in the time domain with a satisfactory low error.

The specialization project [1] and the wide range of applications are the most important motivations for this thesis. The work carried out in the specialization project lay the groundwork for further development and testing of the Jiles-Atherton implementation in a finite element method (FEM) analysis for studies in the time domain. This thesis will investigate how to efficiently obtain Jiles-Atherton parameter values for new materials and thus ease the Jiles-Atherton implementation of new materials in FEM software. This should be accomplished by developing a software that does not require programming skills. The manual tasks, such as preparing input values, should be automated as much as possible. The script developed in the specialization project [1] should be used as the basis for the software development. Further, the required material characteristics of the material samples should be determined carefully in order to obtain a satisfactory method implementation.

Measured losses are compared to the simulated losses to determine if the Jiles-Atherton method is suitable for loss simulation. In this case, the losses in isotropic bulk steel material samples are investigated. An efficient Comsol model is developed in terms of computation time and result resolution. The operation principles of the measuring instrument used to measure losses in the material samples should be investigated to understand how to obtain a comparable loss simulation in Comsol.

The previous work carried out in the specialization project was merely an investigation to check the possibility of calculating the Jiles-Atherton parameter values, based on measured B- and H-field values in carbon steel. The study resulted in a Matlab script that enabled calculation of the Jiles-Atherton parameters for a given set of measurements. The script developed in [1] is

comprehensive and not user-friendly. Hence, one of the main motivators for this thesis is to make the script more generic and user-friendly. By developing a graphical user interface (GUI), the script is possible to deploy as a standalone Windows program (.exe file), which enables a wider range of potential users.

2 Theoretical background

The theory presented in this chapter is used throughout the thesis and lays the foundation of the presented work. Basic electromagnetic theory will be covered in combination with ferromagnetic material properties. The separated losses are presented in terms of eddy current, hysteresis and anomalous loss. Lastly, the Jiles-Atherton method and its parameter values are presented.

2.1 Electromagnetic fields in ferromagnetic materials

The basic theory describing the magnetic field in this chapter is based on [2]. The magnetic field from a current flowing in a wire can be found by applying amperes law in equation (2.1).

$$\oint_C \mathbf{H}\, d\boldsymbol{l} = \begin{cases} \boldsymbol{I}, if\ C\ encloses\ I \\ 0, otherwise \end{cases} \tag{2.1}$$

H is the magnetic field strength vector, d**l** is the differential vector from any closed path C. The current enclosed by the path is denoted **I**. If a coil of wire has N turns equation (2.2) can be derived from equation (2.1).

$$H * l = I * N \tag{2.2}$$

H is the electromagnetic field strength [A/m], l the magnetic length of the solenoid (coil), I the injected current and N the number of turns in the coil. Equation (2.2) is often used to describe the magnetomotive force (MMF) related to coils.

The magnetic domains in materials has to be understood in order to predict how a material reacts to an externally applied magnetic field. All materials consist of small domains with a small magnetization. For unmagnetized materials, the magnetic orientation is random in each domain, as can be seen in Figure 2.1. The small domains are represented by arrows and can be regarded as small permanent magnets. The interpretation of the magnetic domain in a material is based on [3].

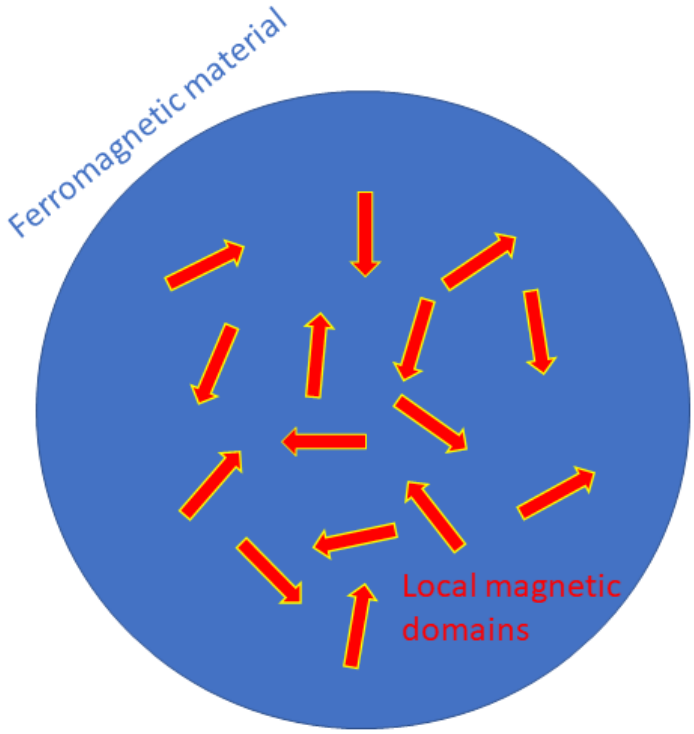

Figure 2.1: Illustration of random magnetization in a ferromagnetic material

If the domains are subjected to a magnetic field, the influence of the magnetic orientation depends on the magnetic property of the material. There are five main categories of magnetic materials: Ferro-, Para-, Dia-, Ferri and Antiferromagnetism. The descriptions of the magnetic material categories are based on [4].

The magnetic domain orientation aligns with the externally applied field for para- and ferromagnetic materials. The small permanent magnets in diamagnetic materials aligns in the opposite direction of the external field. In each case, the new orientation causes a new global magnetization of the material depending on the type of material and the magnetic field strength. The global magnetization will either reduce or strengthen the total magnetic field in the material. This effect is described further in [3] and illustrated for a ferromagnetic material in Figure 2.2. Figure 2.2 illustrates that the orientation of the magnetic domains changes when the material is exposed to a magnetic field. The field strength variation is of importance when ferromagnetic materials are considered, which is covered later in this chapter.

In antiferromagnetic materials there is no net spontaneous magnetization, thus the orientation of the magnetic domains is not changed when the material is exposed to a magnetic field.

Ferrimagnetic materials have material properties similar to both anti- and ferromagnetic materials. The ferrimagnetic material properties will not be described further as it is beyond the scope of this thesis.

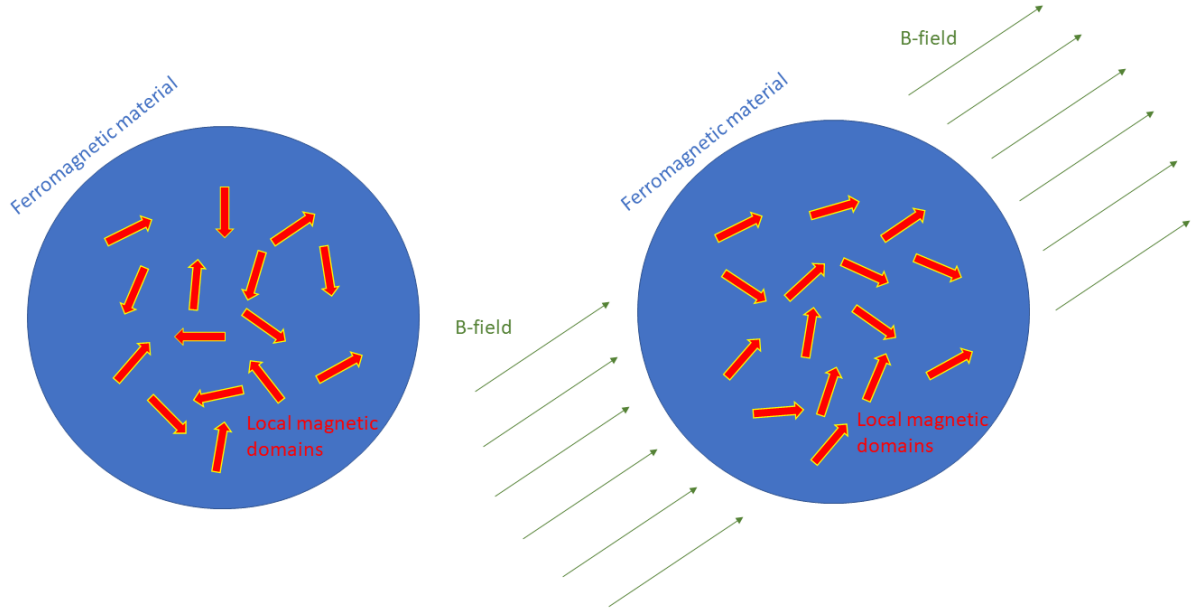

Figure 2.2: Illustration of magnetization of a ferromagnetic material due to an external magnetic field

In Figure 2.2 it can be observed that the orientations of the magnetic domains are changed from the left to the right figure illustration. The direction of the global magnetization in Figure 2.2 due to the externally applied field (figure to the right) is illustrated in Figure 2.3.

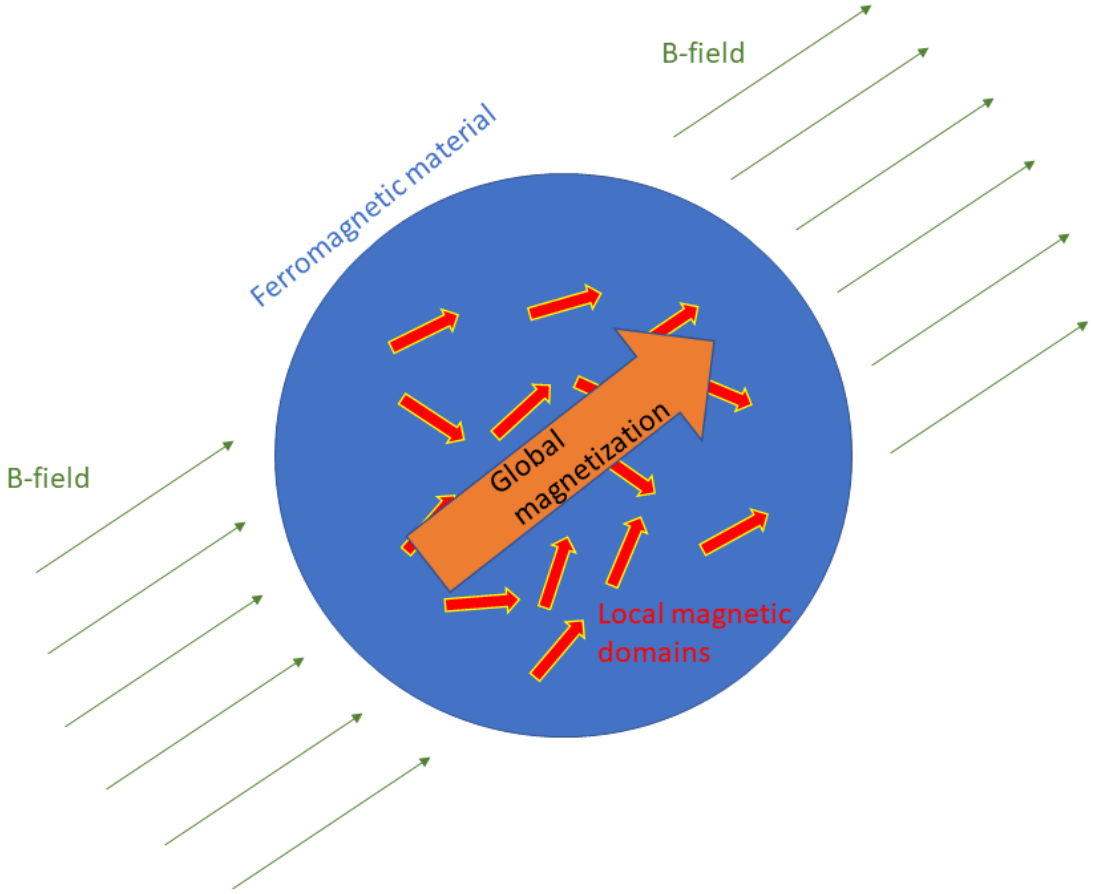

Figure 2.3: Illustration of the global magnetization in a ferromagnetic material due to an external magnetic field

Another way of interpreting this phenomenon is the expansion of the domain walls in the small domains with the same magnetic orientation as the externally applied magnetic field. This domain wall model is discussed in [5].

The antiferromagnetic materials have a zero net magnetic moment. In diamagnetic materials, the internally induced electromagnetic field has a direction opposite to the externally applied field. The internal field is weak and reduces the net field in the material. The paramagnetic materials have an induced electromagnetic field in the same direction as the applied field and thus acts as a field enhancer. The internally induced fields are weak in both para- and diamagnetic materials. Most materials are either para- or diamagnetic and the relationship between the H- and B-field can be described as approximately linear in both cases. The following theory is based on [2] and the relationship is described in equation (2.3).

$$B = \mu H \tag{2.3}$$

B is the electromagnetic field density, H is the electromagnetic field strength and μ is the permeability of the material. The permeability of 'free space' is $4\pi * 10^{-7}$H/m and is represented by the symbol μ_0. The relative permeability of a material, μ_r, is introduced in equation (2.4) and the usage of the relative permeability is described in equation (2.5).

$$\mu = \mu_0 \mu_r \tag{2.4}$$

$$B = \mu_0 \mu_r H \tag{2.5}$$

Para- and diamagnetic materials have a low relative permeability (close to one). Paramagnetic materials have a relative permeability slightly higher than one and are attracted to the magnetic field. The diamagnetic materials have a relative permeability slightly lower than one and are repelled by magnetic fields. As mentioned, the para- and diamagnetic materials can be regarded as linear materials. In addition, the equations are only valid if the materials are homogenous and isotropic. Isotropic materials have the same material properties in all directions. In this case, it means that a magnetic field can be applied from any direction and the material response would be the same if the geometrical aspect is ignored. In this thesis, materials with $\mu_r \approx 1$ are regarded as non-magnetic.

In ferromagnetic materials, the induced field is stronger and has an influence on the net field in the material. If an initial unmagnetized state is considered, this implies that the small domains will need some time to align with the applied magnetic field. If the applied field is sinusoidal, the local induced field is delayed due to the movement. The effect is also present when the polarization changes. This phenomenon causes the total field to become non-linear and dependent on the applied field. Another important phenomenon is that there is a limit to how much the local field can increase the total field. The magnetic field strength of the externally applied magnetic field determines how many and to which degree the small magnetic domains are affected. The material becomes saturated when the magnetic domains are aligned with the external field. An increase in the magnetic field will not be enhanced by the material, meaning

that the behavior of the material is changed. A further increase of the H-field will only change the B-field as it would in ‘free air’. This characteristic behavior results in the hysteresis loop, shown in Figure 2.4.

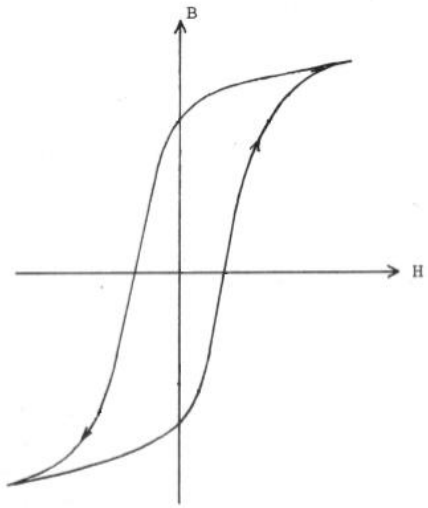

Figure 2.4: Illustration of the characteristic hysteresis loop

2.2 Losses in a ferromagnetic material

The characteristic hysteresis loop is a property in ferromagnetic materials. There is a loss in the material when an externally applied field is subjected to the ferromagnetic material. According to [6] it is commonly accepted to separate the total loss into hysteresis loss, eddy current loss and often anomalous loss (also known as excess loss). These losses are described in the following chapters.

2.2.1 Hysteresis loss

As described in chapter 2.1, the magnetic orientation of the domains in the ferromagnetic material changes. This change requires electromagnetic energy which dissipates in the material as heat. The hysteresis loss originates from the change in domain wall motion [2]. Ferromagnetic materials are divided into hard magnetic and soft magnetic materials. Hard magnetic materials require a lot of electromagnetic energy to move the magnetic domains. This causes a larger delay between the change in the externally applied field and the change in the locally induced field. This causes the hysteresis effect. The magnetic domains in soft magnetic materials move faster, thus the magnetic energy needed is significantly less than in hard magnetic materials.

The magnetizing process is described in Figure 2.5. It can be seen that the area confined by the hysteresis loop illustrates the energy that dissipates as heat in the material. The area confined by the hysteresis loop is the difference between the supplied energy to the material and the energy delivered back to the source. The supplied electromagnetic energy during magnetization of the material is illustrated by the area a-b-0-d-a. The electromagnetic energy transferred back to the source during demagnetization is illustrated by the area a-b-c-a.

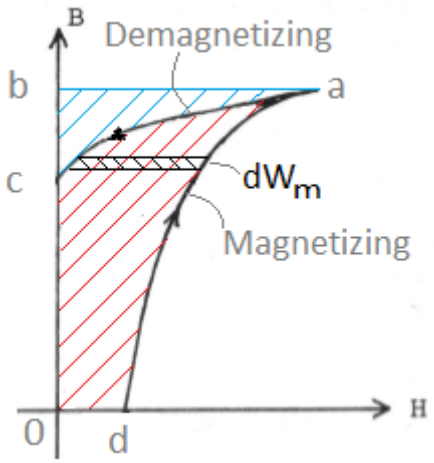

Figure 2.5: Energy dissipation due to the hysteresis effect.
The figure is found in [1] on page 11 and is used with permission in this thesis.

Equation (2.6) describes how energy loss, W_e, due to hysteresis is calculated.

$$W_e = \int H \, dB \tag{2.6}$$

When investigating Figure 2.5, it can be understood that during the magnetization of the ferromagnetic material, the material 'consumes' electromagnetic energy and during demagnetization the material delivers electromagnetic energy back to the source. The difference between these quantities is the dissipated energy in the material. This also implies that dB is sensitive to a negative or positive rate of change. Based on the conclusion in [1], equation (2.7) is used to calculate the volumetric hysteresis loss in this thesis.

$$P_h = k_h f B_{max}^n \quad (2.7)$$

The qualitative hysteresis loss described in equation (2.7) is based on the original work of Steinmetz [7]. The parameter description and recommendations are found in [2].

P_h is the volumetric loss in Watt, k_h is the loss constant, f is the frequency, B_{max} the peak magnetic flux density and n is the exponent in the range of 1.5 to 2.5 based on the material type.

2.2.2 Eddy current loss

The classical losses consist of the ohmic losses (in a current carrying conductor) and the eddy current losses. The conductive ohmic losses will not be treated further in this thesis. The eddy current is a consequence of the materials reluctance to magnetize. When the conductive material is exposed to an alternating electromagnetic field the material will act against the external field by generating a local counter field. This effect is illustrated in Figure 2.6.

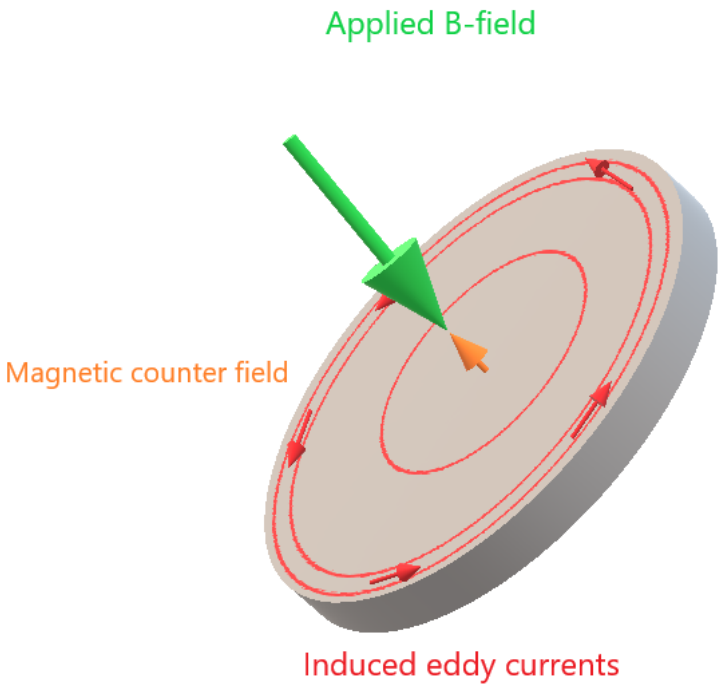

Figure 2.6: Illustration of induced eddy currents and magnetic counter field

This phenomenon can be explained by Lenz law. Lenz law can be illustrated with the negative sign in the law of induction by Faraday in equation (2.8) found in [8].

$$e_{ind} = -\frac{\partial \phi}{\partial t} \tag{2.8}$$

Where e_{ind} is the induced voltage and $\frac{\partial \phi}{\partial t}$ is the time derivative of the flux in the test object. This equation is often easy to understand when relating to coils. The induced voltage in the coil is determined based on the change in the flux passing through it.

Lenz law states that if there is a magnetic flux in a material, an induced electromotive force (EMF) will initiate a current with a magnetic field in the opposite direction of the original field. If the direction of the magnetic field is known, the direction of the induced current is also known (right hand rule).

Figure 2.6 illustrated the induced currents due to the eddy current effect. The induced current distribution and density is strongly related to the flux path in the material. The induced eddy currents are also dependent on the material geometry, which in this case is a cylindric rod. The magnetic field will be directed through the longitudinal axis of the rod. This implies an induced current with a magnetic orientation that acts against the external field. Thus, the current has to circulate around the surface of the cylindric rod. This phenomenon is similar to the well-known skin effect that appears in current carrying conductors.

The eddy current losses can be regarded as regular ohmic losses due to induced currents in the material. In [1], several approaches for calculating the volumetric eddy current losses compared with simulated losses are presented. Based on the conclusions in [1], this thesis use equation (2.9) to calculate the analytical eddy current loss in magnetic steel. The parameter descriptions related to equation (2.9) are based on the explanations in [2].

$$P_e = k_e f^2 B_{max}^2 \tag{2.9}$$

In equation (2.9), P_e is the volumetric eddy current loss in Watt, k_e the loss constant, f the applied excitation frequency and B_{max} the maximum magnetic flux density.

2.2.3 Anomalous losses

The classical method is described in [9] and it is assumed that losses can be divided into hysteresis loss, eddy current loss and anomalous loss. Further, it is described that the anomalous loss often is assumed to be an excess eddy current loss related to microscopic effects in the material. The Pry-Bean model described in [10] tries to account for the magnetic domain wall movement and introduces the anomalous loss in the loss calculation. The domain walls are assumed to have an equal wall velocity in the material. The model is mainly used to describe loss in magnetic sheet materials and is simplified to describe the loss in large domains as shown in equation (2.10).

$$P_{Pry-Bean} = 1.628 * \left(\frac{2L}{d}\right) * P_{class} \tag{2.10}$$

The sheet depth (into the plane) is assumed to be infinite, L is the sheet width and d is the thickness.

Non-oriented electrical steel sheets with identical textures was investigated in [11] and the findings indicate that the grain size in a material influences the total loss but not necessarily the magnetic flux density. The crystallographic texture and grain size in the material samples investigated in this thesis is unknown to the author. Thus, the contribution of the anomalous loss is uncertain in the materials investigated in the thesis.

The measured losses, found by use of the measuring equipment described in chapter 3.3, are used as references throughout the thesis. The manufacturer of the measuring instrument does not separate the anomalous loss from the total loss. Thus, the total loss is assumed to be without anomalous loss in the simulations. This thesis will focus on the hysteresis loss and the eddy current loss.

The modified conductivity in an iron-loss model, described in [12], is utilized in a simplified numeric model to include the excess eddy current loss. This modelling will not be described further in this thesis, but is of interest for potential future work where materials with anomalous loss are to be investigated.

2.3 The Jiles-Atherton method

The Jiles-Atherton method is one of the most used methods when modelling fields in isotropic bulk materials, as discussed in [1]. Vector hysteresis modelling is necessary when modelling electromagnetic field relations in isotropic bulk materials.

The method comparison listed in [13] and briefly discussed in [1] show that there exist several methods that describes the relation between electromagnetic fields, such as Jiles-Atherton, Preisach, Globus modified and Stoner-Wolhfarth extended. The methods have different advantages in terms of computation time, number of parameters, appropriate material properties and ease of implementation. The comparison in [13], show that the Jiles-Atherton method has several desirable properties when simulating electromagnetic fields. The relatively sparse usage of hardware resources regarding computation time in combination with relatively few parameters are good attributes when solving these kinds of problems.

This thesis is a continuation of the work carried out in [1], thus it is already established that the Jiles-Atherton method is the preferred method for describing electromagnetic fields in bulk isotropic materials. The Jiles-Atherton method is the only method that is covered in this thesis.

The simulation software used in this thesis is the FEM software Comsol Multiphysics[1] which has the Jiles-Atherton method implemented. This reduces the method implementation to determining the required method parameters used to describe a material. The software "Jiles-Atherton Method Parameter Search" (JAMPS), described in chap 4.1, is developed to determine the method parameters based on simple DC hysteresis[2] measurements of a material.

The Jiles-Atherton method is described by five implicit expressions as shown in equation (2.11) to (2.15). The model requires five model parameters that are unique to the specific material and a method description is given in [14]. The model is a simplified Jiles-Atherton model, thus the anisotropy[3], temperature and magneto-elastic effects are not embedded in the method description.

$$H_e = \mathrm{H} + \alpha\mathrm{M} \tag{2.11}$$

[1] Further referred to as Comsol.
[2] The hysteresis curve obtained at a low frequency is referred to as a DC hysteresis curve in the Brockhaus Measstechnik Manual (instrument used for measurements).
[3] Isotropic materials have identical property values in every direction. Anisotropic materials have different material property values depending on the direction in the material.

$$\frac{d\mathrm{M}_{irr}}{dH_e} = \frac{M_{an} - M_{irr}}{k * \delta} \tag{2.12}$$

$$M_{an} = M_s * (coth\frac{H_e}{a} + \frac{a}{H_e}) \tag{2.13}$$

$$\mathrm{M}_{rev} = \mathrm{c} * (M_{an} - M_{irr}) \tag{2.14}$$

$$M = M_{irr} + M_{rev} \tag{2.15}$$

When investigating formula (2.11) to (2.15), the applied field is referred to as H and the effective field is referred to as H_e. M is the total magnetization and consists of the reversible (M_{rev}) and irreversible magnetization (M_{irr}). The relationship between M_{rev} and M_{irr} is described with the anhysteretic magnetization M_{an}. αM is describing the molecular field and δ is the directional factor (± 1) dependent on the change in H (dH).

Table 2.1 provides an overview of the material specific parameters that can be determined with the software JAMPS and simple hysteresis B-H loop measurements at a low frequency.

Table 2.1: Jiles-Atherton parameter names and symbols

Magnetization saturation	**Langevin parameter**	**Pinning factor**	**Domain rotation**	**Local field factor**
M_s	a	k	c	α

The physical interpretation of the model parameters are discussed in [1], [15] and [16]. The pinning factor can be regarded as the most important parameter in field and loss simulations. The domain wall pinning causes the irreversible change in magnetization, this phenomenon is a key factor when simulating losses due to the hysteresis. The Langevin function provides the

saturation magnetization and the Langevin parameter. The reversible magnetization is described by the energy stored in the domain rotation represented by the parameter domain rotation. The magnetic field and adjacent magnetic domains have interactions described by the mean magnetic field parameter known as the local field factor.

3 Preparations to the loss simulation in the ferromagnetic materials

The following chapter describes the assumptions and measurements needed to start the verification process of the Jiles-Atherton method. The motivation and initial description of the planned setup is explained to get a better understanding of the verification process. The ferromagnetic material samples are shaped like cylindric rods and is described further in the following chapters. In order to simulate and verify the losses in the magnetic materials, it is important to get an accurate description of the loss measurements performed with the Brockhaus Messtechnik instrument.

3.1 Overview of the Jiles-Atherton parameter verification process

As mentioned in the introduction, the DEH application is one of the main motivations for examining the possibility of calculating induced loss in ferromagnetic materials based on the Jiles-Atherton description of the material.

The verification process is based on simplified material samples of ferromagnetic material shaped into rods. This is done to isolate the investigated effects as much as possible and thus generalize the application area of the findings in the thesis. The simplification reduces the complexity of the needed simulation model, thus the results become more trustworthy and unambiguous. The losses to be investigated are the frequency dependent losses due to a time variation in the induced flux (AC losses).

Based on the work performed in [17], it is assumed that the magnetic steel will have a flux density up to approximately 500mT at a frequency between 50 and 200Hz in a practical DEH-application. This is the main reason why the investigated flux densities are chosen to be 100, 200, 300 and 400mT at the frequencies 50, 100, 150 and 200Hz.

The loss calculations performed with the Jiles-Atherton method are to be verified by simulating the induced loss and compare the loss with actual measured loss. To achieve this, the work is divided into five parts; measuring DC hysteresis loops in material samples, developing a software to determine Jiles-Atherton parameter values based on DC hysteresis loops, measuring actual AC loss in material samples, implementing the Jiles-Atherton parameters in FEM model and finally comparing the simulated and measured losses. This method can then be used to verify the Jiles-Atherton method implementation used to describe the material. A summary of the process is illustrated in Figure 3.1.

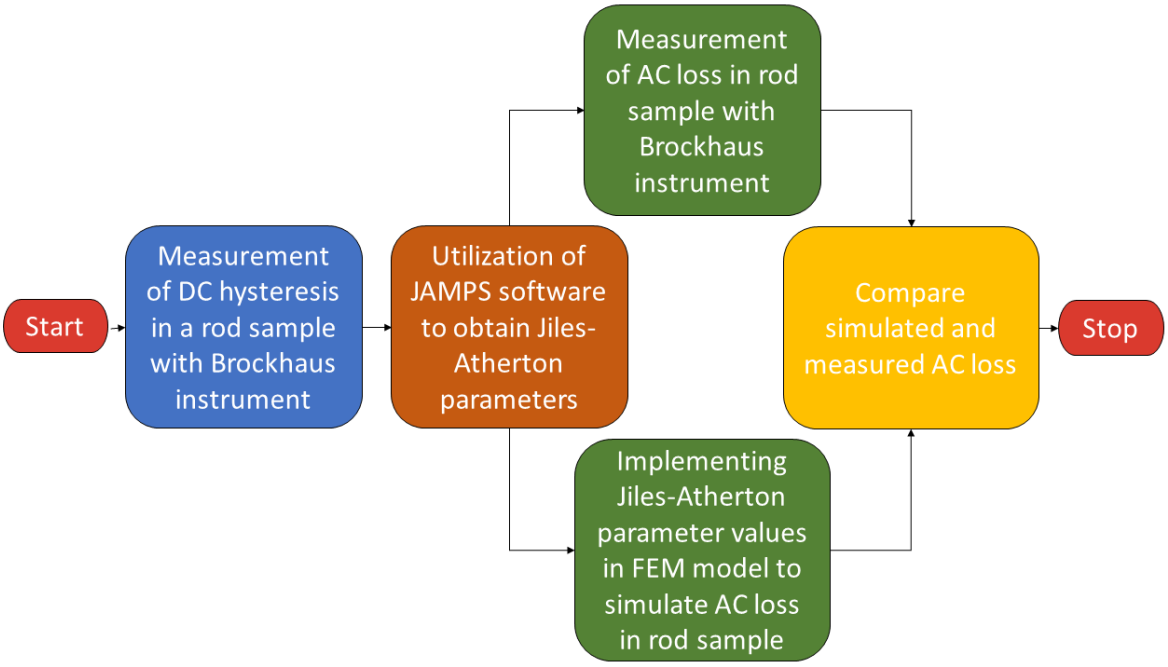

Figure 3.1: Flowchart of work to be presented in the thesis

The development of the FEM model is described with the measured or simulated values needed to advance in the verification process. All needed measurements are described in the following chapters. Relevant operating principles of the measuring equipment is provided to explain choices made during the development of the verification process.

3.2 Properties of the ferromagnetic rods

The rod properties are needed to configurate the measurement setup in the Brockhaus instrument and to develop the material descriptions in a FEM model. The work performed in this thesis will be performed on two different ferromagnetic rod samples, referred to as material 1 and material 2. The exact material composition of the two materials are unknown to the author and confidential. Thus, the provider of the material samples will not be given in the thesis.

3.2.1 Conductivity

The conductivities in the ferromagnetic rods are of importance because they govern the eddy current in the materials. Thus, the error in the loss calculations are increased if the conductivity in each material description is wrong. The conductivity is calculated based on the resistance measurements performed with the digital low resistance ohmmeter ‘Megger DLRO 10X’.

The technique used to obtain the low resistance in the rods is known as the four-point measurement method. This method consists of a voltage and current measurement to determine the low resistivity of the material. The current probes are the outer probes and the voltage probes are the inner probes, as illustrated in Figure 3.2.

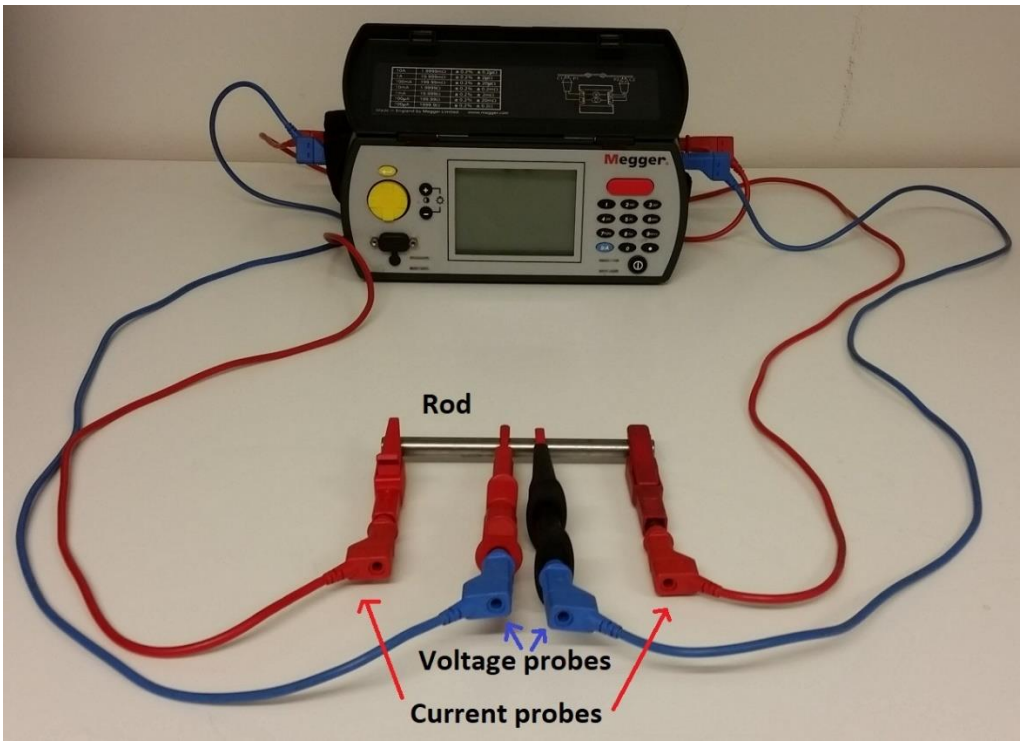

Figure 3.2: Rod conductivity measurement setup

If connected in the opposite order, there would not be any voltage to measure due to the current source in the measuring equipment. The resistance is measured three times in four different positions to get the best representation of the specific resistivity (Ω/m). Table 3.1 and Table 3.2 shows the measured resistances and the calculated conductivity for material 1 and 2 respectively.

Table 3.1: Measured resistance and calculated conductivity for material 1

Space between voltage probes [cm]	**Meas. 1 [μΩ]**	**Meas. 2 [μΩ]**	**Meas. 3 [μΩ]**	**Average resistance [μΩ]**	**Conductivity [S/m]**
2	53.3	55.5	55.7	54.83	$4.6440 * 10^6$
5	138.1	138.5	138.7	138.43	$4.5987 * 10^6$
7	199.9	200.2	200.2	200.10	$4.4541 * 10^6$
10	283.3	283.8	283.8	283.63	$4.4890 * 10^6$
				Average conductivity [S/m]	$4.5465 * 10^6$

Table 3.2: Measured resistance and calculated conductivity for material 2

Space between voltage probes [cm]	**Meas. 1 [μΩ]**	**Meas. 2 [μΩ]**	**Meas. 3 [μΩ]**	**Average resistance [μΩ]**	**Conductivity [S/m]**
2	200.5	201.1	201.7	201.10	$1.2664 * 10^6$
5	499.9	499.9	500.1	499.97	$1.2733 * 10^6$
7	696.3	696	695.9	696.07	$1.2804 * 10^6$
10	984.4	984.3	984.2	984.30	$1.2936 * 10^6$
				Average conductivity [S/m]	$1.2784 * 10^6$

The conductivities implemented in the FEM model is $4.5465 * 10^6$ S/m for material 1 and $1.2784 * 10^6$ S/m for material 2 as shown in Table 3.1 and Table 3.2. The conductivity σ is calculated with formula (3.1).

$$\sigma = \frac{l}{R * A} \tag{3.1}$$

In formula (3.1) l is the length of the measured object, R the resistance and A the cross-section of the measured object.

3.2.2 Mass density and physical dimensions

The measured AC losses, described in chapter 6.1, are given in Watt per kilogram. The weight and volumetric properties are used by the program to calculate the mass density and presents the loss in Watt per kilogram. The development of the FEM model and the comparison of the measured and simulated losses are sensitive to the rod measurements. Thus, the weight and physical dimensions must be measured with care to achieve a satisfactory level of accuracy. The total rod weights are displayed in Table 3.3.

Table 3.3: Total weight of the rod samples

Total weight of rod material 1 [g]	**Total weight of rod material 2 [g]**
82.3	300

The physical dimensions of the ferromagnetic rods are displayed in Table 2.1.

Table 3.4: Dimensions of the rod samples

	Rod material 1	**Rod material 2**
Diameter	10mm	10mm
Length	135mm	501mm

3.3 Important features of the Brockhaus Messteckhnik instrument

The measuring equipment is in general used to determine the magnetic qualities of electric sheets. In this case, a coil measuring system is used to measure the qualities of the material samples shaped like cylindric rods. The descriptions and equations provided in this chapter are collected from the user manual of the measuring instrument Brockhaus Messtechnik MPG 100 D AC/DC, unless explicitly stated otherwise. The user manual was provided by NTNU and is not publicly available.

3.3.1 Dimensions the of Brockhaus Messteckhnik sensor SST 10x100

The Brockhaus instrument is delivered with a software named MPG-Expert. This software organizes the necessary inputs settings needed to define the correct measuring setup. The sensor used in the Brockhaus instrument is named ‘Single-sheet-tester’ (sst 10x150) in the MPG-Expert software. The sensor is illustrated in Figure 3.3 with an inserted rod ready to be measured.

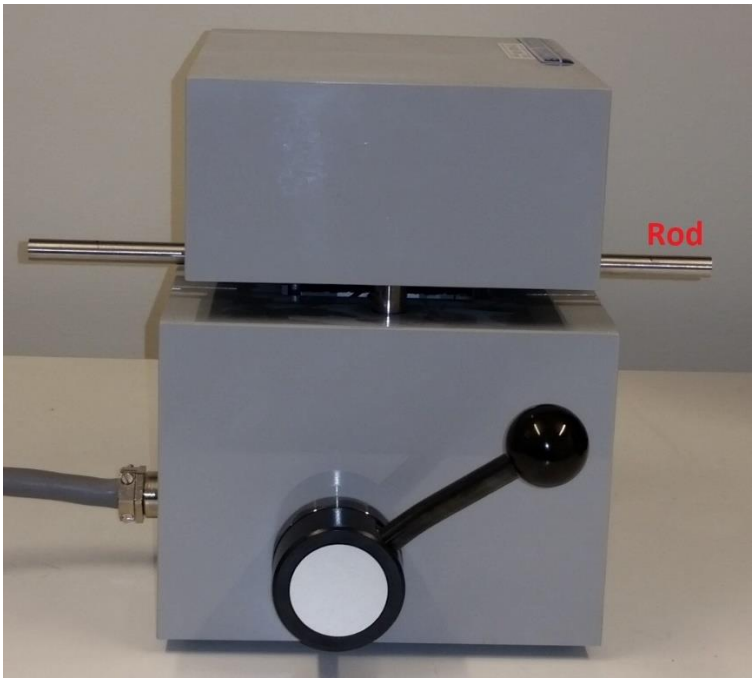

Figure 3.3: Picture of the SST10x150 sensor used to perform DC and AC measurements on the magnetic steel rods

Figure 3.4 is a picture taken from the right side of the sensor in Figure 3.3 to illustrate the physical position of the coil and core, which are the most important parts in the measurement setup.

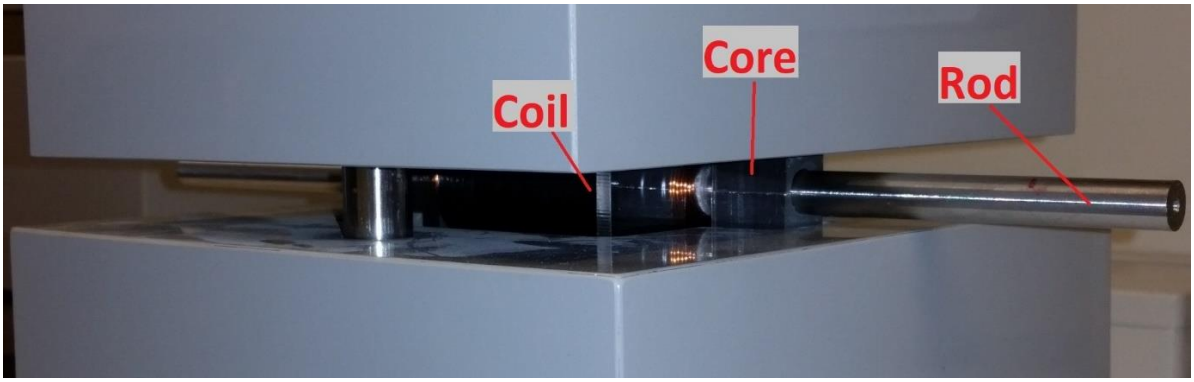

Figure 3.4: Coil, core and rod in the measurement setup of sensor SST 10x150

The main parts of the measuring sensor if the outer casing is removed are illustrated by the means of a 3D model in Figure 3.5. The dimensions presented in the figure will be used later in the thesis to develop a FEM model which replicates the sensor.

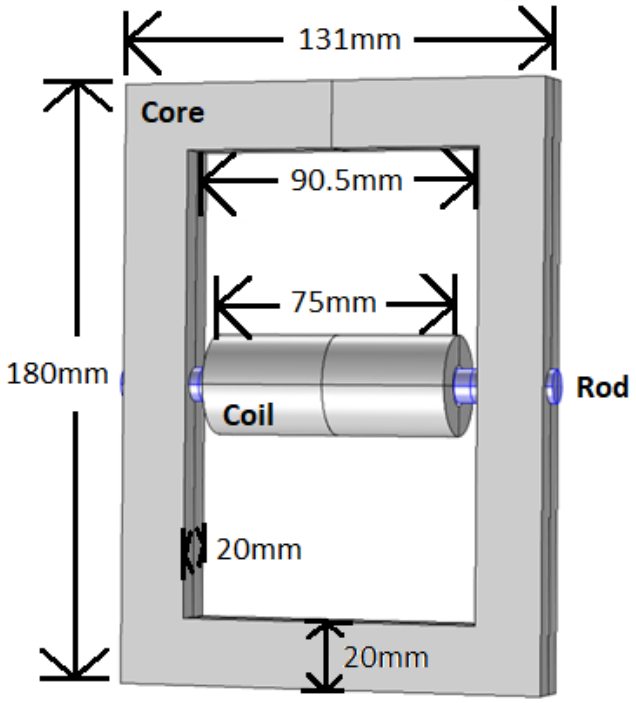

Figure 3.5: Illustration of main parts in the measuring sensor with physical dimensions

3.3.2 General operating principles

The desired quantities to be obtained from the measuring equipment are AC and DC hysteresis curves, field strength [H/m], average maximum field density [T] and specific core losses [W/kg]. The quantities related to the AC measurements are used to simulate the measuring setup in a FEM model and compare the measured specific rod losses with the simulated specific rod losses at different frequencies (50, 100, 150 and 200Hz).

The operating principle of the Brockhaus instrument is to expose the material to a magnetic field with an appropriate coil system. The material sample, in which the magnetic properties are to be measured, must be shaped to fit the sensor. In the measuring equipment there are two windings. The magnetic flux in the steel rod originates from the primary winding which is used to create the magnetic field. The combination of current, number of windings and the magnetic length of the coil determines the magnetic field strength, described by formula (2.2) in chapter 2.1.

The software in the measuring system converts the measured voltage to magnetic field strength, as described in formula (3.2).

$$\mathrm{H(t)} = \frac{N_1}{R_n * l_m} * u_1(t) \tag{3.2}$$

N_1 is the number of turns in the primary winding, l_m the magnetic length and H(t) the magnetic field strength. Formula (3.2) is very similar to formula (2.2) described in chapter 2.1. R_n is the resistance used in combination with the voltage $u_1(t)$ in the primary coil to describe the current from formula (2.2). Formula (3.3) is used to derive formula (3.4). Formula (3.3) and (3.4) shows how the secondary winding in the coil system is used to measure the induced voltage. The induced voltage is used to determine the polarization and/or magnetic flux.

$$\frac{\mathrm{dB}}{\mathrm{dt}} = -\frac{u_2(t)}{N_2 * A_m} \tag{3.3}$$

$$B(t) = -\frac{1}{N_2 * A_m}\int_0^t u_2(t)\,dt \tag{3.4}$$

B is the magnetic flux density, $u_2(t)$ is the voltage in the secondary coil used to measure the induced voltage. N_2 is the number of turns in the secondary coil and A_m is the area of the coil used to calculate the magnetic flux density. The measuring system avoids errors caused by the phase differences by measuring the H and B values in two separate and parallel capture systems. This method ensures simultaneous measurement and high repeatability and stability of the measurements.

3.3.3 DC measurements

The exported excel file of the DC measurements and calculations, referred to as the results in MPG-Expert, are needed as input in the JAMPS-software. The setup file is defined with the H-

field as the target parameter and the B-field is adjusted in steps. The steps are denoted ‘dB’ and are set to 50mT in the setup file.
The DC-setting in the instrument is not translatable to true DC, but AC at a sufficiently low frequency. Sufficiently low frequency in this context is a frequency that reduce the influence of the eddy currents to a negligible level. This ensures that the only measured response in the material is due to the hysteresis effect. The output file contains the measured datasets of H- and B-field values.

The Brockhaus instrument is set in DC mode. The DC hysteresis loops are used to calculate the material parameters for the Jiles-Atherton method with JAMPS. The DC results were exported as excel files for both rods and are presented as plotted DC hysteresis loops in chapter 4.2.

3.3.4 AC measurements

The measuring equipment is sensitive to high currents and the H-field is calculated based on the current with formula (2.2) in chapter 2.1. The length used in the formula is referred to as the magnetic length in the documentation and set to 85mm by the instrument manufacturer.

Either the B-field or the H-field can be used as control parameters in the measurements. The current must be under 2A, which is the limit of the measuring equipment. The maximum H-field in the instrument is approximately 30 000A/m, which is higher than needed in this application. The disadvantage with controlling the H-field (current) is that the equipment software is unable to calculate the eddy current and hysteresis losses. This is solved by controlling the B-field instead of the H-field.

The disadvantage with controlling the B-field is that the coil current needed to achieve the desired B-field is unknown and depends on the material. This introduce a risk of exceeding the 2A limit in the equipment. The risk is avoided by first performing measurements with the H-field as a control parameter. The coil current and corresponding B-field can then be obtained from the result file.

The measurements determined by the H-field as control parameter are defined in a setup file. The relationship between the H-field and B-field is not known. Thus, the setup file must be experimentally obtained based on several measurements to obtain the current at the desired B-field. When the coil current is obtained and under 2A, the AC measurements with the B-field as the control parameter are performed to get the specific and separated losses. The losses are given in Watt per kilogram.

The flux density in this context refers to the volumetric average flux density. This is explained by the fact that the measuring equipment only can derive the flux density based on the induced voltage in the coil due to the flux in the core. Thus, the flux density has to be an average value in the part of the rod which is covered by the coil.

The measuring instrument is equipped with a quartz-controlled digital sine generator that controls the target voltage of the coil. Thus, the flux in the cylindric rod is sinusoidal. This is not the case in the simulations and is discussed in chapter 7.4. The excitation coil and the measuring coil have 900 turns and thus the relation is 1:1 and the induced voltage in the sensor coil can be used directly. This method automatically subtracts the losses in the excitation coil. The instrument manufacturer advertises with no sources of error due to analog multipliers and integrators.

The main measured values are the excitation voltage and current in addition to the induced maximum average flux density. The specific power loss is calculated in the equipment software MPG-Expert, but the calculation is not explained in the user manual. The measuring equipment gives an angle named phi, which suggests that the angle between the voltage and current is given. By trial and error, it was discovered that the magnetic length is used not only to determine the H-field, but in the specific loss calculation as well. There is no further explanation about this provided by the instrument documentation.

Equation (3.5) describes how the specific losses are calculated in the instrument based on the voltage, current and phasor angle.

$$P_{spec.} = \frac{V_{rms-measured} * I_{rms-measured} * \cos(\varphi_{measured})}{m_{rod\ weight} * \frac{l_{mag.\ length}}{l_{rod}}} \tag{3.5}$$

The specific loss in the equation has the notation $P_{spec.}$ [W/kg]. The magnetic length, $l_{mag.\ length}$, is 85mm and regarded as a part of the sensor calibration in order to get the correct measured losses. As mentioned, this length is set by the manufacturer of the measuring equipment. $V_{rms-measured}$ and $I_{rms-measured}$ are the measured rms values of voltage and current in the excitation coil respectively. $\varphi_{measured}$ is the measured phase shift between the voltage and current, l_{rod} is the total length of the rod and $m_{\text{rod weight}}$ is the total rod weight.

Equation (3.5) is not given by the manufacturer but discovered by trial and error. It was essential to know how the specific losses were calculated in order to develop a FEM model and replicate

the losses. The active losses are calculated in the entire rod, based on the supplied current and voltage. It can be deduced that the losses are scaled to fit the weight of a rod with a length equal to 85mm. By investigating the flux path and density in the rod, described in chapter 5.2.2, it is assumed that the magnetic length scales the loss in the rod to an average loss.

The AC results are presented in chapter 6.1 and used as reference values in verification of the loss simulations in following chapters.

4 Obtaining the Jiles-Atherton method parameters

This chapter presents a simplified description of the main functionality in the JAMPS software. The measured DC hysteresis loops will be presented in JAMPS during the investigation of the input curves. Finally, the Jiles-Atherton parameters that will be implemented in the FEM model are presented.

4.1 Operation of the JAMPS software

The computer program Jiles-Atherton Method Parameter Search (JAMPS) is based on the script written in the specialization project by Magnus E. Tangen described in [1]. During the program development, the usability of the program got a higher focus than anticipated. The goal in terms of user-friendliness was that an engineer without programming skills should be able to benefit from the JAMPS software. To broaden the application area the software had to have a lot of adjustments and settings options. The development of a graphical user-interface (GUI) required a lot of work in terms of programming. Further, the software had to be able to manipulate excel-files on a high level. The program became easy to use by removing manual tasks, such as finding the measured values used in the optimization process.

The main objective of the software JAMPS is to obtain Jiles-Atherton parameter values for specific materials based on DC measurements from material samples. The parameters are used in a FEM model with the Jiles-Atherton method implemented. Ideally, this makes it possible to do simulations in the time domain with a satisfactory low error. The required input is exported as an excel-file from the measuring equipment software[4].

The program is based on the Matlab library developed by Magnus E. Tangen in [1] where the Matlab implementation of the Jiles-Atherton method created by R. Szewczyk [18] is utilized. The JAMPS software detects the number of measured loops in the input file and gives the opportunity to reduce the number of measurements and, as a result, the computation time.

The software allows the user to select a maximum of four B-H loops from the input file, from which the optimization is based on. When the loops are separated the software counts the number of measured values in the selected loops and give the user the possibility of reducing the number of measurements. This is beneficial with respect to the computing time in the sense that there are fewer calculations to be carried out.

[4] Brockhaus Messtechnik MPG-Expert software

The Jiles-Atherton method can be regarded as a function that takes a set with H-field values as input and the output is a set of B-field values. The H-field values in the selected loops are sent to the Jiles-Atherton function where the B-field values are calculated. When the values are calculated the difference in measured and calculated B-field values are evaluated with equation (4.1) in the objective function[5]. $B_{Meas.-loop(i)}$ is an array of the measured B-field values in hysteresis loop number i. The corresponding calculated B-field values are stored in the array $B_{Calc.-loop(i)}$. The difference between the array values related to the same H-field value in $B_{Meas.-loop(i)}$ and $B_{Calc.-loop(i)}$ is used in equation (4.1) to calculate $Diff_i$. $Diff_i$ is an accumulated value that depend on the difference between the measured and simulated B-field in a specific hysteresis loop.

$$Diff_i = \sum |B_{Calc.-loop(i)} - B_{Meas.-loop(i)}|^{\sum (B_{Calc.-loop(i)} - B_{Meas.-loop(i)})^2} \tag{4.1}$$

The objective function stores the difference for all values in the hysteresis loop and if there are several selected loops, the software uses the difference in a total difference sum illustrated by the value of $Diff_{tot}$ in equation (4.2).

$$Diff_{tot} = \sum_{i=1}^{n} Diff_i \tag{4.2}$$

i is the number of selected hysteresis loops. This is to get a solution that takes all the selected hysteresis loops into account.

The Jiles-Atherton function needs five parameter values to describe a specific material, in this case isotropic magnetic steel. Five initial parameter values and the H-field values are used to initialize the optimization. The five parameters are the same for all the different loops. The Matlab-function 'fminsearch' is used to change the initial parameter values. It is recommended to keep the parameter value 'c' in the range 0 to 1. The software gives the user the ability to set

[5] The optimizing function is a function in the software code. The objective function calculates the values that are to be optimized by the optimizing function.

a lower boundary for the parameter 'M_S'. The lower boundary value is based on the highest measured B-field in the set of selected hysteresis loops. M_s is calculated in accordance with formula (4.3) where $M_{s\ -\ \text{lower limit}}$ is the constraint added in the script, B_{max} is the highest measured magnetic flux in the selected loops and μ_0 is the relative permeability in vacuum ($4\pi*10^{-7}$ H/m).

$$M_{s-lower\ limit} = \frac{B_{max}}{\mu_0} \tag{4.3}$$

The 'fminsearch' function changes the parameter values in the Jiles-Atherton function in order to minimize the objective function. The objective function is the sum of the differences between measured and calculated B-field values at all the corresponding H-field values.

The software lets the user set a maximum number of iterations. Maximum number of iterations refers to the number of attempts the 'fminsearch' function tries to obtain a solution. The optimization process stops if the convergence criterion is met during the attempts. This is directly translated into how many times the B-fields are calculated in each loop and it is now clear why it is beneficial to reduce the number of measured values prior to the optimizing process.

The convergence criterion is set to 10^{-4} (default) and requires several iterations to be met. In the search for parameter values the software can encounter a local minimum which prevents the convergence criterion to be met. This is why the option 'Improve' was developed into the program. The 'Improve' option rounds up the parameters to the nearest integer. The exceptions are parameters 'c' and 'α', who are rounded up to the five first decimals. This is because the optimizing process uses extreme values in the initial guess and enables the software to skip the local minima.

The software indicates if the parameter search was successful in terms of an error calculation. This error calculation is relative to the area of the measured hysteresis loop. The objective function in the 'fminsearch' function is based on the difference between individual points, but in this project the area of the hysteresis loop is utilized in the power loss calculations. Therefore, the area of the Jiles-Atherton loop calculated in Matlab is compared with the area from the measured hysteresis loop.

The data of one loop must be separated into four to calculate the area confined by the hysteresis loop. The B-field values are evaluated to determine the turning points and zero crossings in the loop. Figure 4.1 displays the calculated areas based on numeric integration with the 'trapz' function in Matlab.

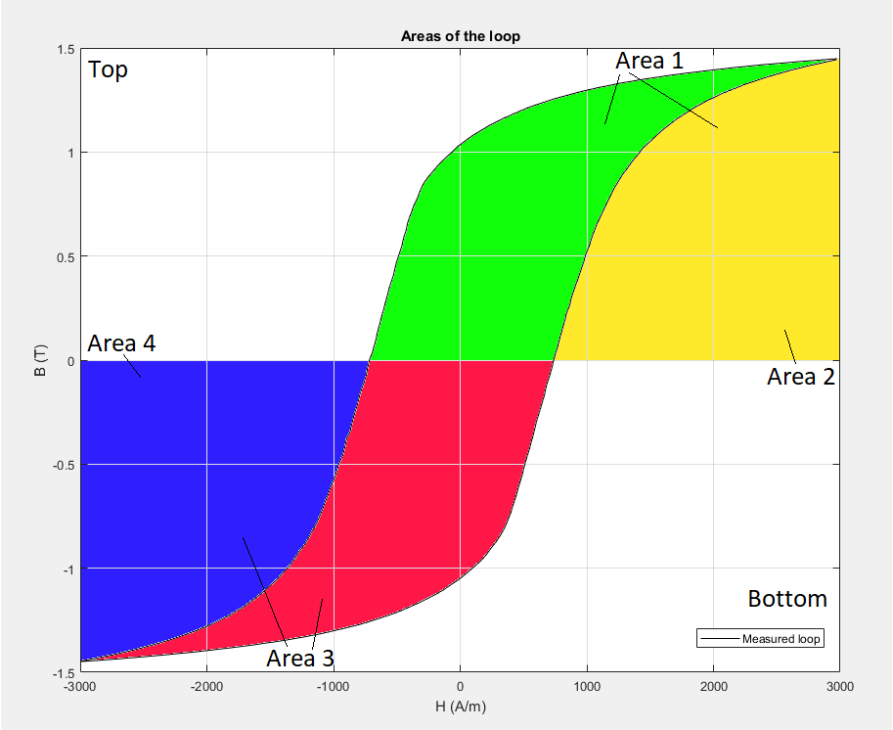

Figure 4.1: Division of curves in hysteresis loop for area calculation

The green area (area 1 – area 2) is defined as the top area and the red area (area 3 – area 4) is defined as the bottom area. The total area of the investigated hysteresis loop is calculated by adding the areas, as shown in expression (4.4) where A is the area.

$$A_{loop} = A_{top} + A_{bottom} \tag{4.4}$$

The calculated and measured loops are compared in JAMPS to determine the error, as shown in equation (4.5).

$$Error = \frac{A_{Matlab\ loop}}{A_{Measured\ loop}} * 100\% - 100\% \quad (4.5)$$

The error is calculated with the measured hysteresis loop as the reference and indicates the accuracy of the Jiles-Atherton parameters. The error indication is displayed in JAMPS after the parameter search is finished.

The developed program (JAMPS) consists of 2799 lines of code. The source code of the program and the compiled Matlab application is made available by the git repository found in [19]. The distribution of the .exe file will be based on email requests[6] to the author due to the file size. Further descriptions of how to obtain the files are given in [19].

4.2 DC measurements and curve selection

There are two material samples to be investigated. The first material is referred to as material 1 and the second material is referred to as material 2. The described measuring equipment is used to obtain the material measurements needed as input in JAMPS. The measured DC hysteresis loops and selected curves in JAMPS are presented in this chapter. The process of obtaining the Jiles-Atherton parameter values in JAMPS is described in the simplified user manual in Appendix A. Figure 4.2 shows four selected curves from the DC measurement file of material 1.

[6] Email: Magnus-tangen@hotmail.com
The thesis will be submitted with the JAMPS software attached as an .exe file

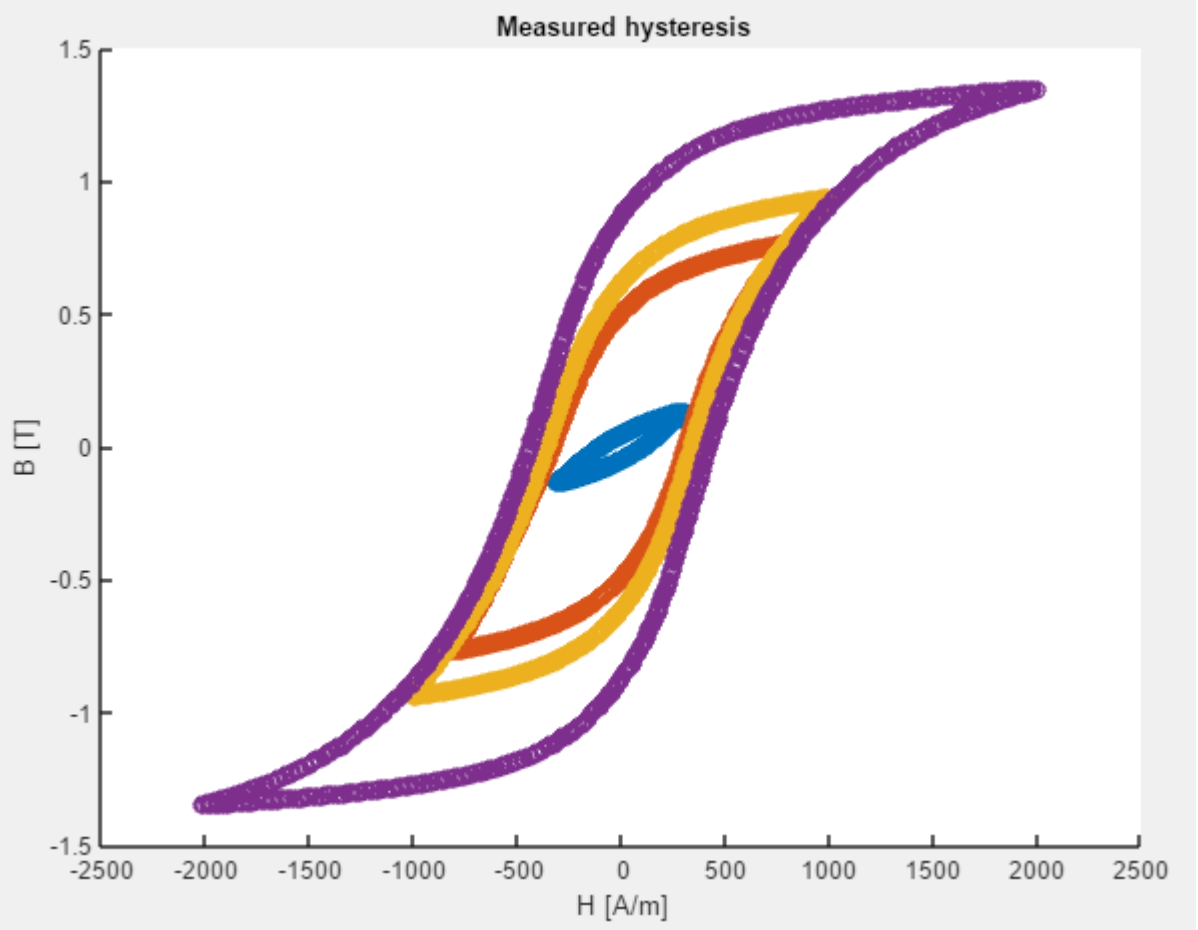

Figure 4.2: Measured hysteresis DC loops in material 1

All the plotted curves in Figure 4.2 was selected as input in the JAMPS software. The argument for selection of the curves are based on the planned maximum flux density in the simulations. The simulations will be performed at 100, 200, 300 and 400mT, as explained in chapter 3.1. Figure 4.3 shows the input curves after a 95% reduction of the dataset in JAMPS.

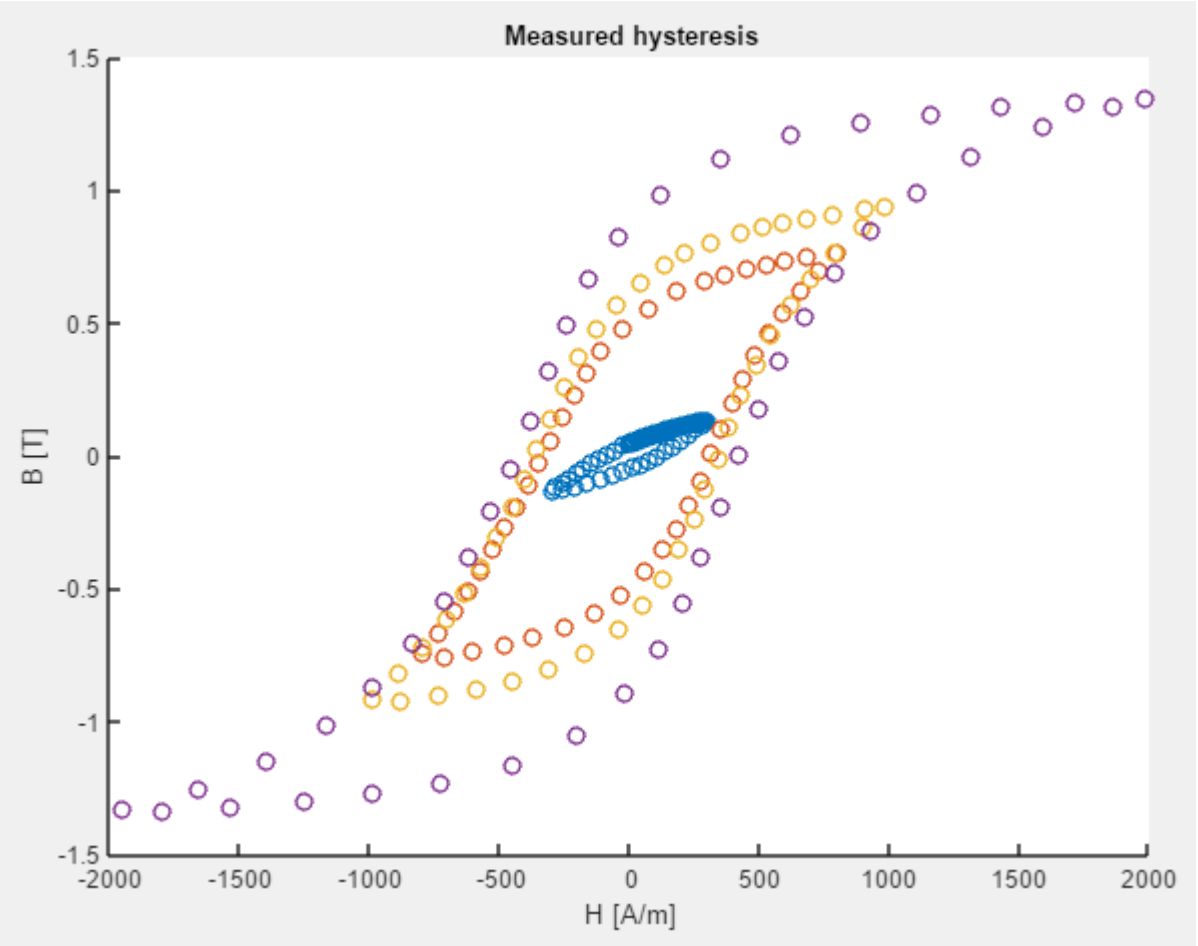

Figure 4.3: Reduced measured hysteresis loops to be utilized in the J-A parameter search for material 1

Figure 4.4 shows four selected curves from the DC measurement file of material 2. It can be observed that the material requires a much higher H-field to operate in a similar B-field range.

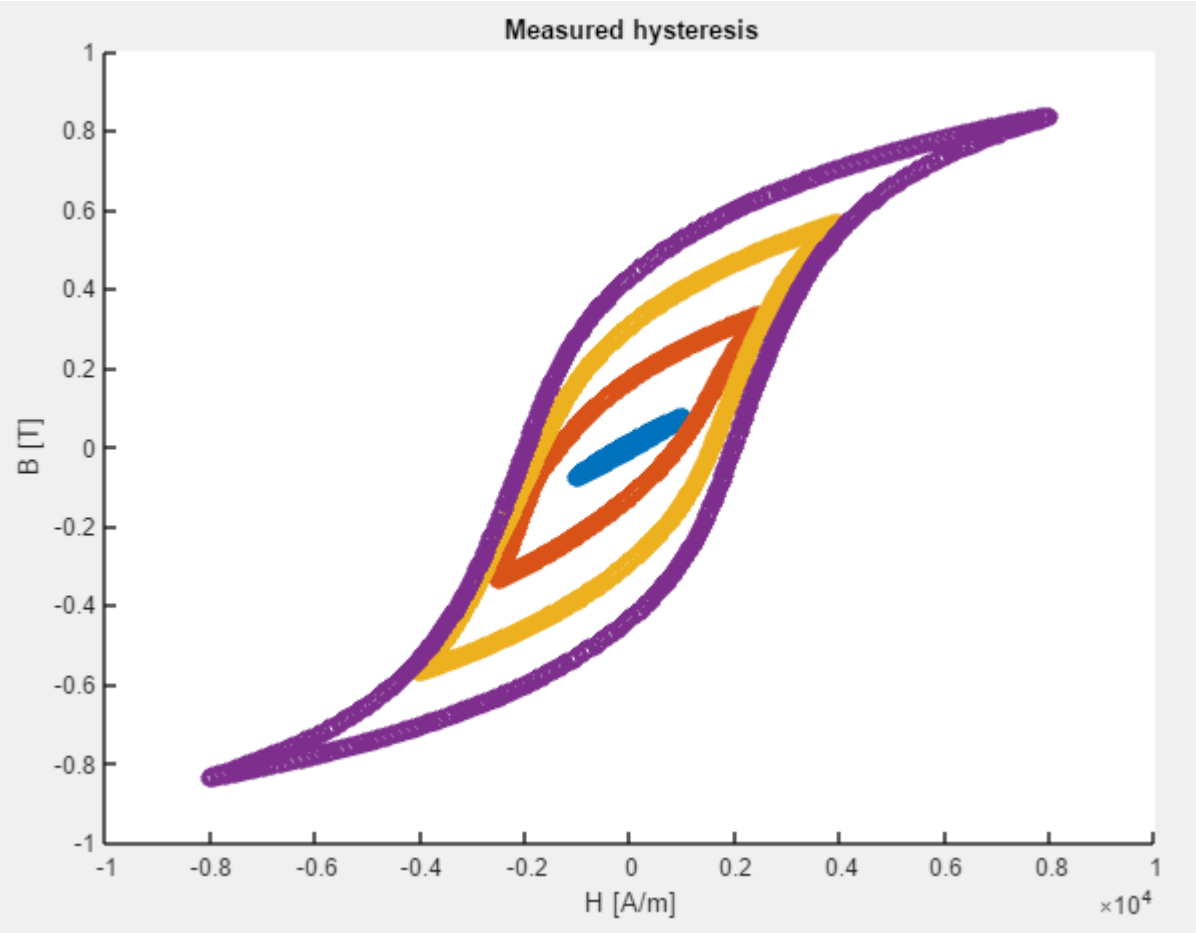

Figure 4.4: Measured hysteresis DC loops in material 2

For several reasons discussed towards the end of this report, the input hysteresis loops are reduced to consist of only two loops. The main argument for selecting two curves is that it was difficult to obtain parameters that described the entire B-field range of the material with a relatively low error. The solution was to select the curves that were closest to the simulation range. Figure 4.5 shows the JAMPS input curves for material 2 with a measurement reduction of 95%.

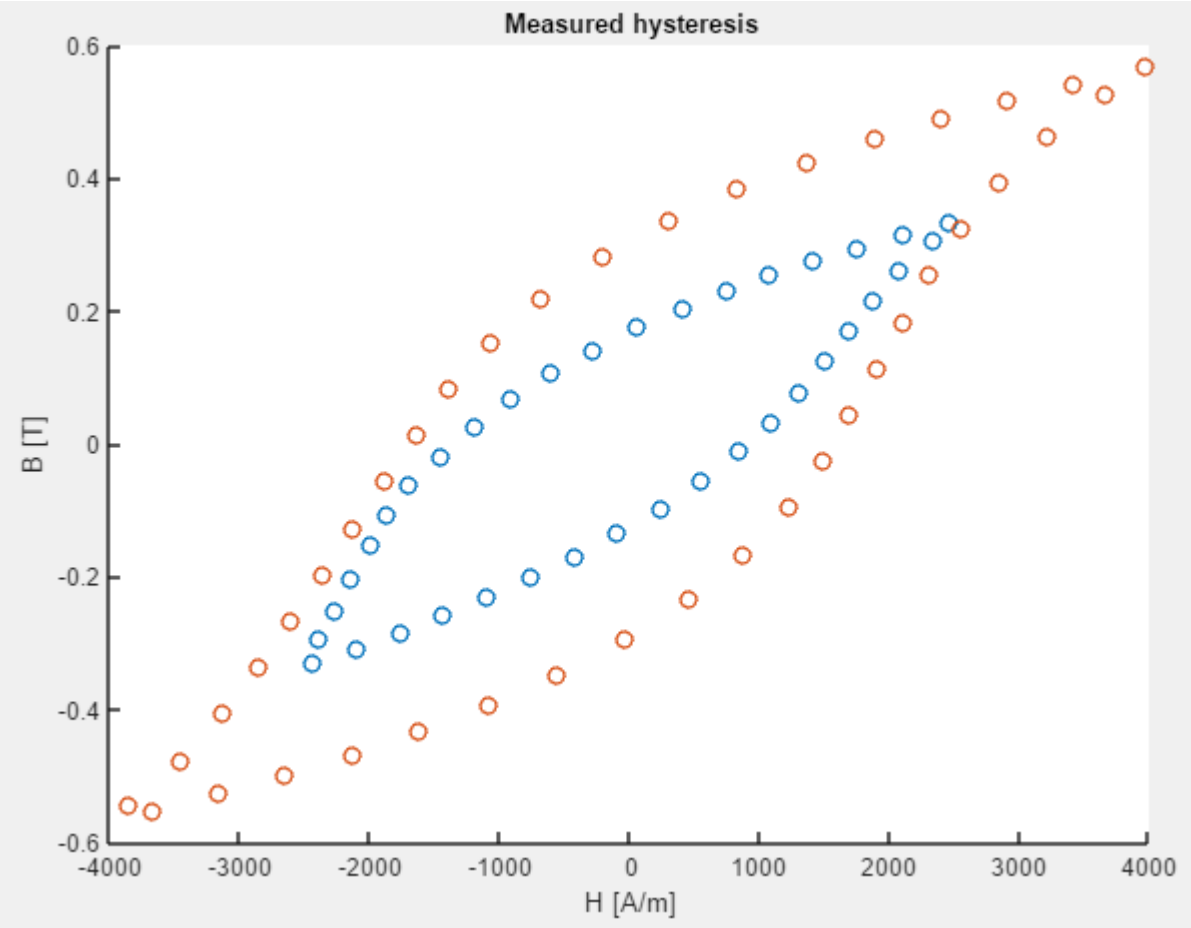

Figure 4.5: Reduced measured hysteresis loops to be utilized in the J-A parameter search for material 2

4.3 Jiles-Atherton parameter values to be used in FEM-simulations

The resulting Jiles-Atherton parameter values (JAMPS result) for material 1 and 2 are based on the specifications in Table 4.1. The listed solvers are selected in JAMPS and represents the numeric solver used in the software. The solvers available in JAMPS are ode23, ode23s, ode45 and rk4. These solvers are described further in the Matlab documentation available in [20].

Table 4.1: Settings in JAMPS used to calculate parameter values for material 1 and 2

Material No.	Number of iterations	Solver	Reduction
1	>400	ODE23	95%
2	>400	RK4	95%

The final Jiles-Atherton parameter values for the investigated materials are shown in Table 4.2. These values are to be implemented and utilized in the FEM simulations. In chapter 6, the AC simulations are compared with AC measurements to verify the validity of the parameter values.

Table 4.2: Calculated Jiles-Atherton parameter values for material 1 and 2

Material No.	M_s	a	k	c	α
1	1427100.592	533.7758585	456.34	0.402872374	0.000782366
2	974672.8	1131.16	2348.45	0.2145793	0.000836528973824

The JAMPS software compares the input curves from the DC measurement file with the hysteresis curves calculated with the Jiles-Atherton method. The Jiles-Atherton method takes the H-field as input and calculates a corresponding B-field. Figure 4.6 is the plot of measured and calculated hysteresis loops in material 1. The total calculated error in material 1 is 4.42% which is assumed to be acceptable for the intended application and verification.

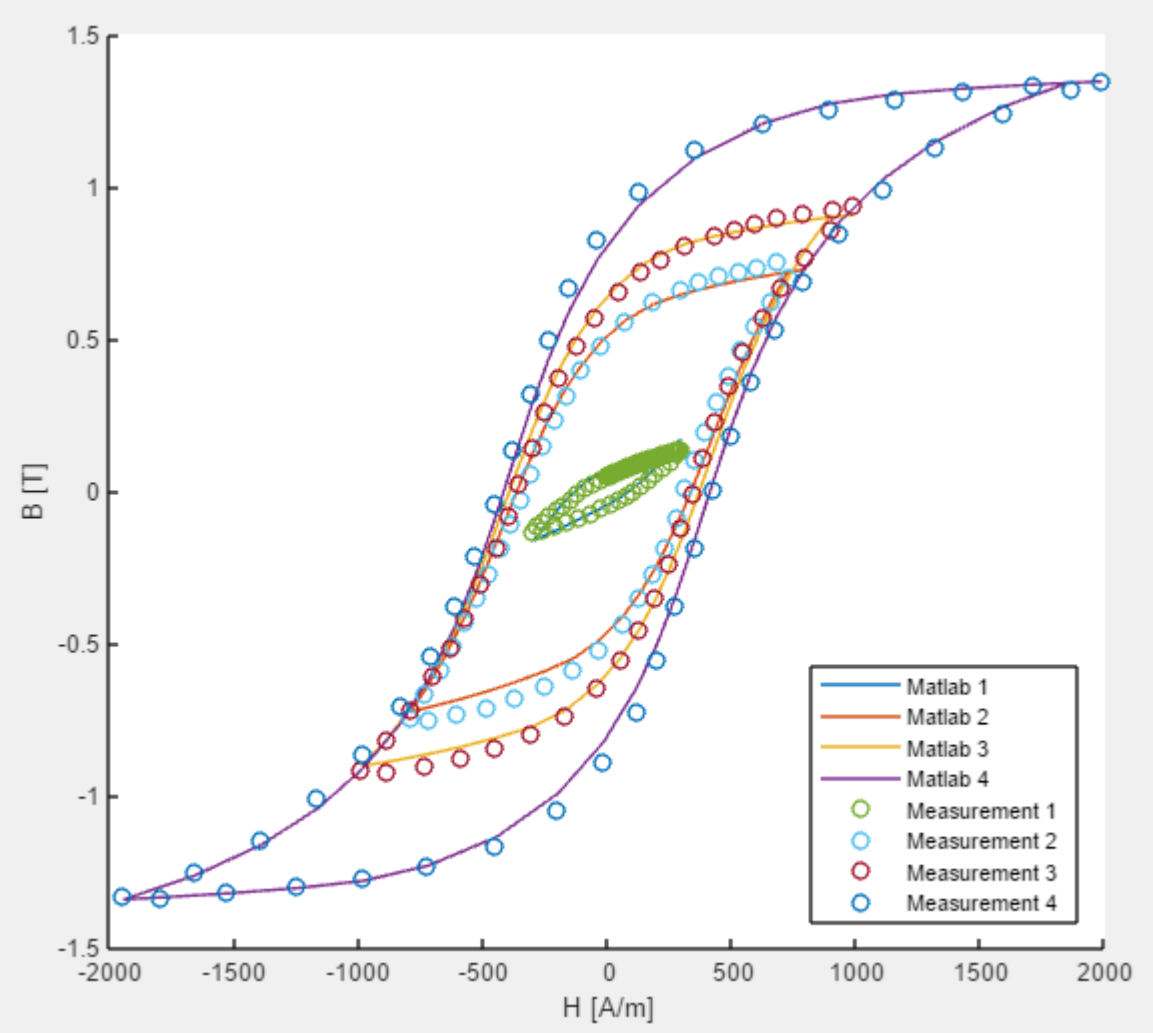

Figure 4.6: Result plot from JAMPS illustrating the simulated and measured hysteresis loops for material 1.

Figure 4.7 is a plot of the calculated and measured hysteresis loops in material 2. The total error of the calculated hysteresis loops of material 2 is 2.60%, which is accepted for further use in the method verification.

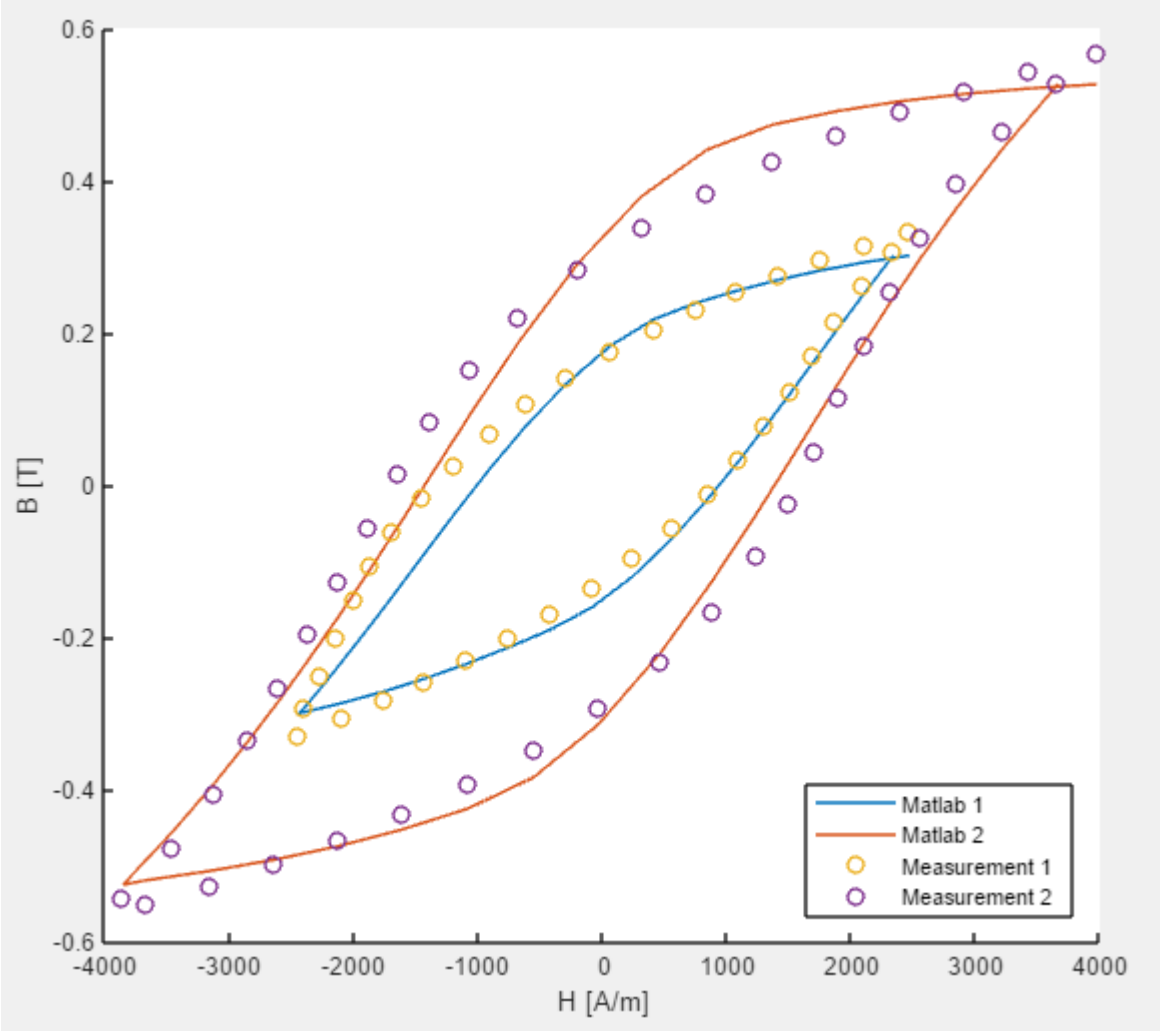

Figure 4.7: Result plot from JAMPS illustrating the simulated and measured hysteresis loops for material 2.

5 Development of FEM model for loss verification

This thesis investigates if the loss in magnetic steel material can be calculated with a FEM model by the implementation of Jiles-Atherton modelling. The modelling is to be verified with sample tests, and in order to achieve this a FEM model was developed. The FEM model is developed in accordance with the actual test setup.

5.1 Simplified geometry and measuring technique

The goal with the model development is to obtain a model where the situation is equal to the actual measuring equipment. This makes the calculated losses from the model comparable with the measured losses. The comparison is used to verify the method of implementing the Jiles-Atherton in the material description.

The main focus in the method development is to replicate the sensor in the measuring equipment with the highest accuracy possible. The model is trustworthy if the assumed difference between the simulated and measured loss is solely caused by the Jiles-Atherton method implementation. This is the main goal of the model development described in the following chapters. The following paragraphs describe the simplifications of the FEM model made in the coil geometry, core geometry and rod geometry.

Rod geometry

The rod is modelled as a perfectly straight cylinder without scratches (smooth surface) and has a constant diameter. This assumption effectively neglects parts of the potential airgaps between the cylindric rod and the core in the measuring sensor. The assumption is that this can be compensated for in terms of the relative permeability of the core.

Coil geometry

The conductor cross section in the modelled coil is based on the recommendation in [21] and assumed to be in accordance with the coil in the measuring sensor. The losses in the coil is assumed to be subtracted from the measured total loss. There is a description of a secondary coil wound on top of the excitation coil in the sensor documentation, which indicates that this assumption is valid.

Core geometry

The core in the FEM model is defined as a solid material with a conductivity set to 1 S/m to simulate the neglectable eddy current loss in the core. The core in the actual sensor consists of laminated sheets which yields low eddy current loss. Physical measurements of the main sensor

parts are performed with the accuracy allowed without dismantling the sensor completely. The metrics are described in Figure 3.5 in chapter 3.3.1 and assumed to be adequate in this application.

The relative permeability is assumed to be constant during one simulation. Thus, the core material is assumed to be linear. The airgaps between the rod and core are included in the relative permeability describing the core in the FEM model. Thus, the relative permeability in the core is assumed to be smaller in the FEM model compared to the actual core value.

5.2 2D-axissymmetric FEM-model

The Comsol model is developed in 2D-axissymmetry to ensure that the computation time is reduced to a minimum compared with traditional 2D- and 3D-models. The final simulations are performed in a 3D model, but first a method will be developed in 2D. This chapter discusses the most important findings during the development of the FEM model.

5.2.1 A brief description of the initial 2D-axisymmetric FEM model

The technical construction of the 2D-axisymmetric model will not be described in detail. This is because the model has endured constant change throughout the model development phase. The objective with the model development phase was to ensure that the simulations were trustworthy and comparable with the losses measured in the laboratory. The important discoveries regarding the model are described and discussed in this chapter.

The model consists of four main elements: air, core, coil and the magnetic steel rod. The Brockhaus instrument is equipped with an SST 10x150 sensor, described in chapter 3.3.1. The sensor and test object must be replicated in the FEM model.

The main function of the model is to simulate one period in steady state at target magnetic flux density. The losses that are calculated in post-processing will later be compared with the measured losses. The most important parts are the flux path, flux density and the externally applied H-field. The closest approximation of the sensor in the 2D-axisymmetric model is illustrated in Figure 5.1. The rod in Figure 5.1 constitutes the test object and is highlighted in blue. The red line is the axis of symmetry in the model.

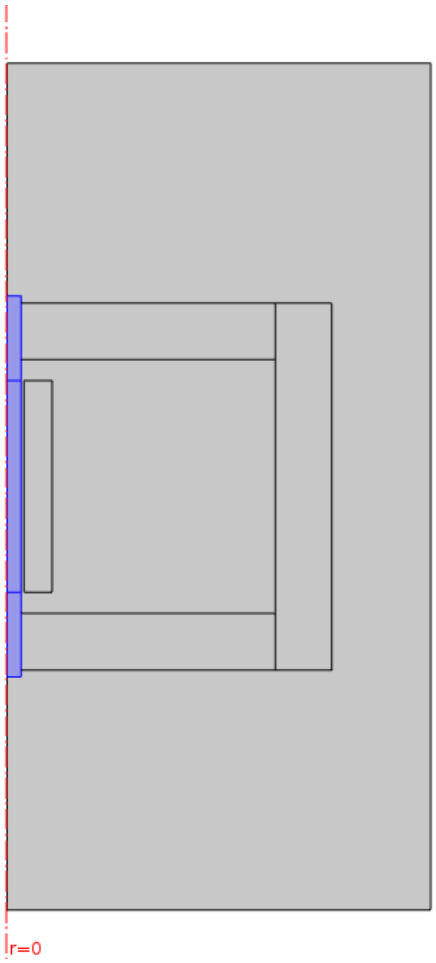

Figure 5.1: 2D-axisymmetric FEM model indicating the red symmetry line

The rod material is described with the help of the Jiles-Atherton method and the parameter values used in the simulations are theoretically valid. It is not possible to confirm the validity of the parameter values until the model is developed further. During the 2D-axisymmetric model development it is assumed that the material description is valid and gives an approximate representation of the material behavior.

The average flux density is the target value, meaning that the simulated peak flux density, $B_{max\text{-}sim}$ has to be equal to the measured peak flux density $B_{max\text{-}meas}$. When the target value is met the losses are to be calculated and compared with the measured losses. During the method development the simulations are performed at the selected frequencies of 50, 100, 150 and 200Hz.

The physics settings in the model are based on the magnetic fields (mf) module. The coil is defined as a homogenized multi-turn coil with a sinusoidal excitation current. Further, the

symmetry arguments are handled by the axial symmetry where the symmetry line is defined. The magnetic insulation is applied to the outer boundaries (except the symmetry line) in the model and Amperes law is utilized in combination with the Jiles-Atherton method to describe the ferromagnetic rod.

The mesh is separated in two different meshes which are adjusted during several simulations. The process of obtaining the mesh is not described in detail, but the highlights are covered in this section. The final mesh size is sufficiently small and prevents potential errors caused by a coarse mesh. The computation time increases with reduced mesh size and the number of nodes increases with a reduction in the mesh size. The flux concentration is assumed to be higher near the surface of the magnetic material samples. Hence, the mesh size should be as small as possible. However, small mesh size implies a long simulation time. A low computation time is a vital constraint on the project because of the high number of simulations needed to develop the FEM model.

In summary, the mesh has to be fine especially in the rod geometry, but not excessively fine in the rest of the model. Hence, the model was divided in two parts. The first mesh is of the type ‘mapped’ with custom maximum mesh size of 0.05cm and covers the carbon steel rod. The second mesh is of the type ‘free triangular’ and covers the remaining geometry, meaning the coil, core and air. The second mesh has a predefined mesh size, extremely fine, with 0.3cm as maximum element size. The solver configuration in the model is set to the direct solver ‘MUMPS’.

5.2.2 Calculating the average magnetic flux density in a volume

The methods for calculating the described loss depends on the model geometry (2D or 3D). This section will describe the principles of the calculation and not the method used in Comsol. The method for calculating the magnetic flux density in Comsol is described in chapter 5.3.7. The calculated magnetic flux density is an important value in the simulation since it is compared with the measured magnetic flux density target. The calculated magnetic flux density indicates if a measurement is successfully simulated. The challenge prior to the simulations is to decide how the magnetic flux density shall be calculated to give the best replication of the measured magnetic density.

The average magnetic flux density was first calculated on a cross-section in the center of the rod. The coil which generates the magnetic field has a leakage field and this leakage indicates that the highest magnetic flux density is in the center of the rod. In the actual measuring sensor,

the secondary coil measures an induced voltage. This means that the magnetic flux density target, found in the measurement results, takes the leakage field into account. The relative permeability of the core material is assumed to be significantly higher than the relative permeability in the test object. This results in a reduced magnetic flux distribution in the center of the rod covered by the core. The Jiles-Atherton implementation in the rod material make the local field response vary in the material. This effect can also be interpreted as a skin effect occurring the rod.

The average flux density calculated in the center of the simulated rod would be higher than the magnetic flux density target from the measurement provided that both scenarios have an equal coil current. Figure 5.2 is a snapshot of the magnetic flux density from a simulation where the flux distribution in the rod is reduced closer to the core interface. Figure 5.2 shows that the magnetic flux density should be calculated as a volume average in the volume covered by the coil.

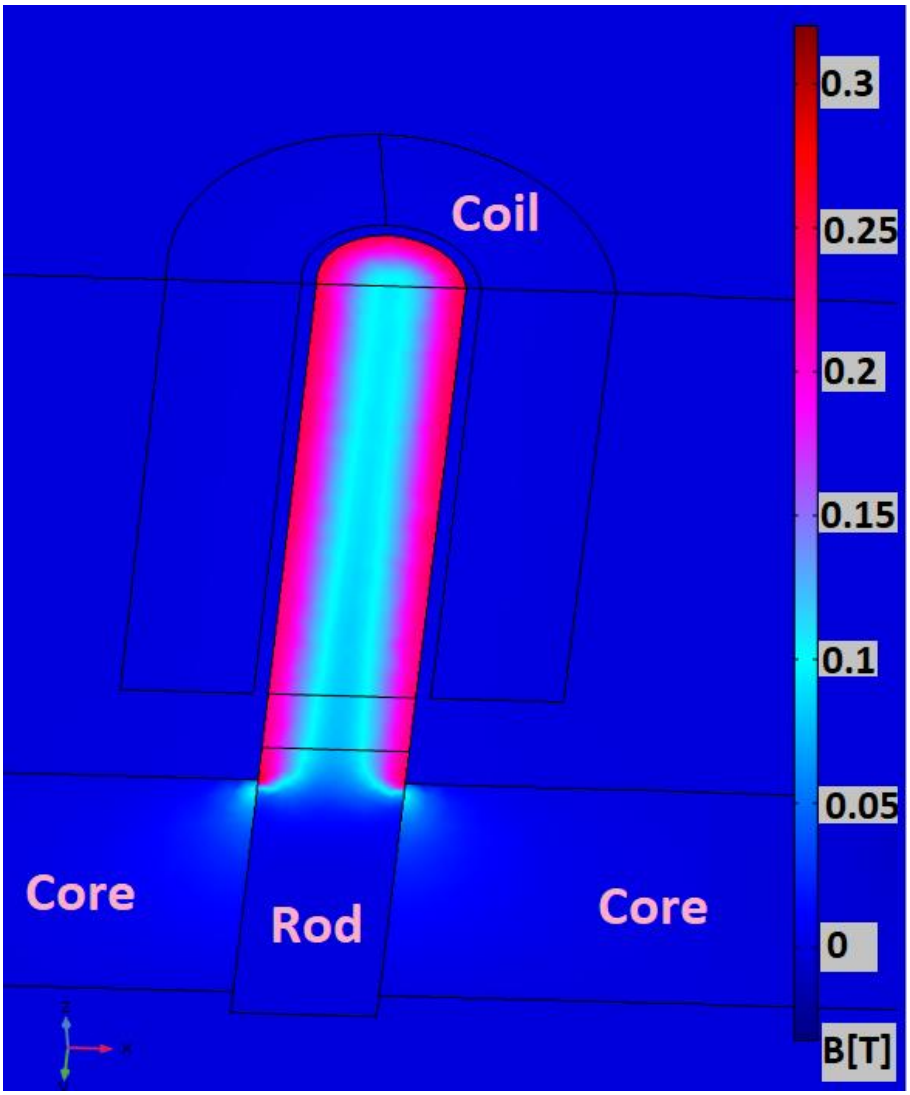

Figure 5.2: Illustration of why the magnetic flux density should be calculated as a volume average

5.2.3 Flux current phase shift

The measuring equipment operates with a voltage source, as described in chapter 3.3.4. The current in the coil must correspond to the measured current in the equipment. The coil current is the parameter that makes the FEM model comparable to the actual measurements. This is because the current dictates the magnetic field strength (H-field), which is the main input in the Jiles-Atherton method that are to be tested. Thus, the coil in the model is defined as a current source. The main challenge with this simplification is the time variation of the flux density which is sinusoidal in the actual measurements due to the voltage source. In the simulated FEM

model, the current source is sinusoidal, and this distorts the ideal sinusoidal time variation of the flux density. It is assumed that this is an acceptable approximation.

It was initially assumed that the flux density in the simulations should be calculated based on the second period of the simulation. That was also the reason why only two periods were simulated initially. The reason for skipping the first period was that the material should magnetize and demagnetize in the first cycle and then be in the regular hysteresis loop. The material is initially unmagnetized, but during the development of the model it was discovered that a significant decaying DC term was added to the flux density in the time domain. The maximum flux density is the target value of the simulation and with the peak caused by the decaying DC term, the needed excitation current in the coil appears to be lower compared to the actual measurements. This is reflected in the calculated power which was low compared to the actual measurement. Figure 5.3 is a plot of the average flux density in the time domain during 5 periods. There is initially an offset due to a decaying DC term in the magnetic flux density.

The purpose of the average magnetic flux density plots in this chapter, is to illustrate the change in the DC term. The value of the magnetic flux density in the plot is not of interest.

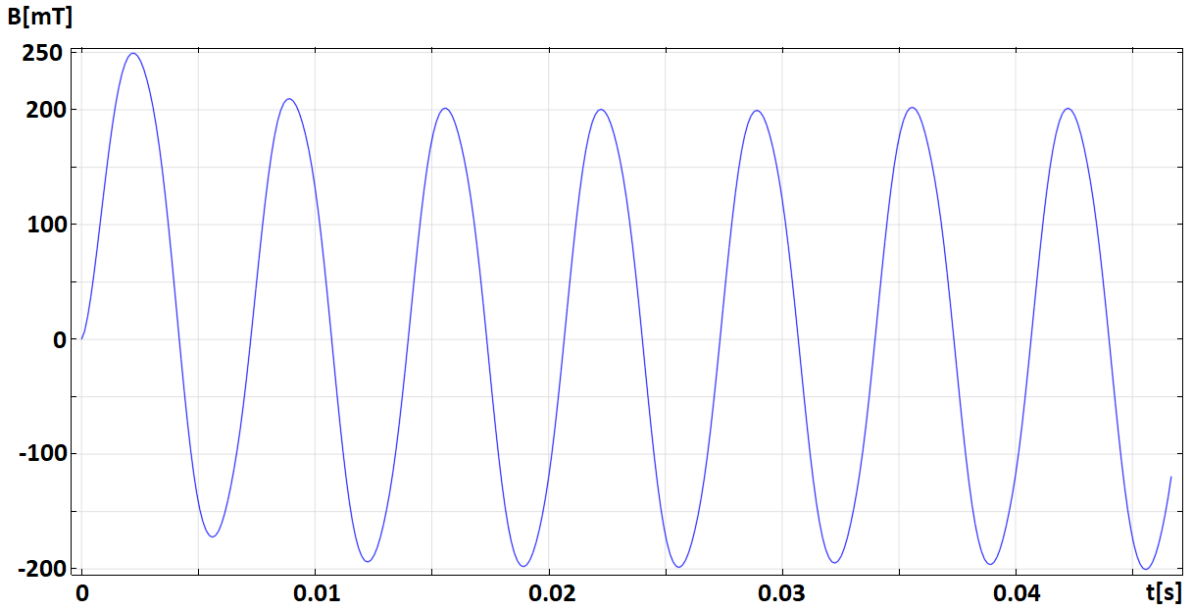

Figure 5.3: Plot of the average magnetic flux density in a rod sample with a decaying DC term

One solution would be to simulate several periods as the measuring instrument does, but that would be very time consuming and reduce the scope of this thesis significantly. Instead, a phase shift could be added in the expression that describes the current in the current source. This phase shift between current and flux density in the rod can be found in two ways. Figure 5.4 displays the hysteresis curve form the DC measurement at 4000 A/m on material 2.

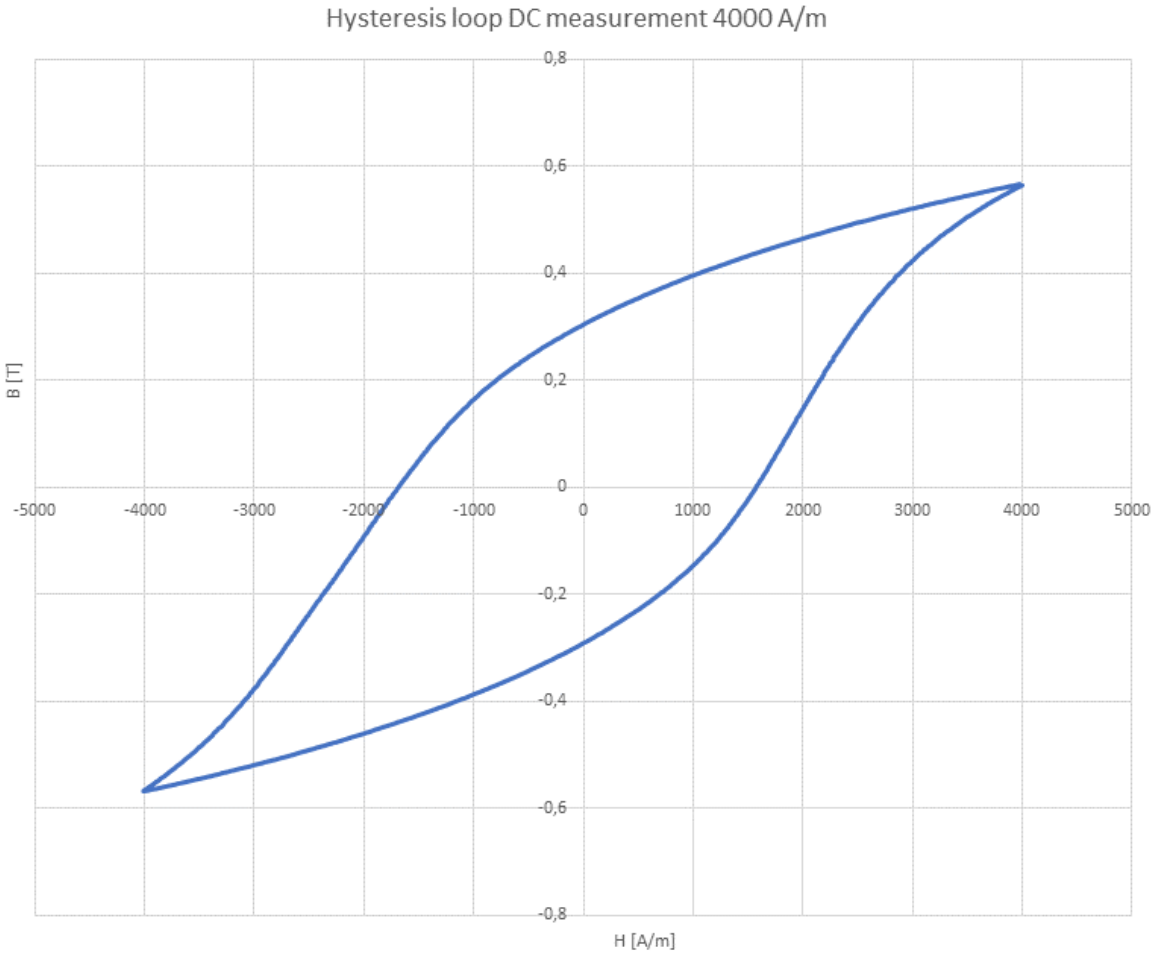

Figure 5.4: Measured DC hysteresis loop in material 2 at 4000 A/m

The magnetic field strength (H-field) is in phase with the current and can be deduced from equation (2.2) in chapter 2.1. This is an important initial condition for further analysis of the phase shift and how to reduce the computation time. The magnetic field strength variation is sinusoidal due to the sinusoidal current. Figure 5.5 illustrates what it would look like if the current was plotted in a hysteresis curve. The amplitude of the current is scaled to fit in the plot, but it is important to imagine how the current traverses back and forth through the plot.

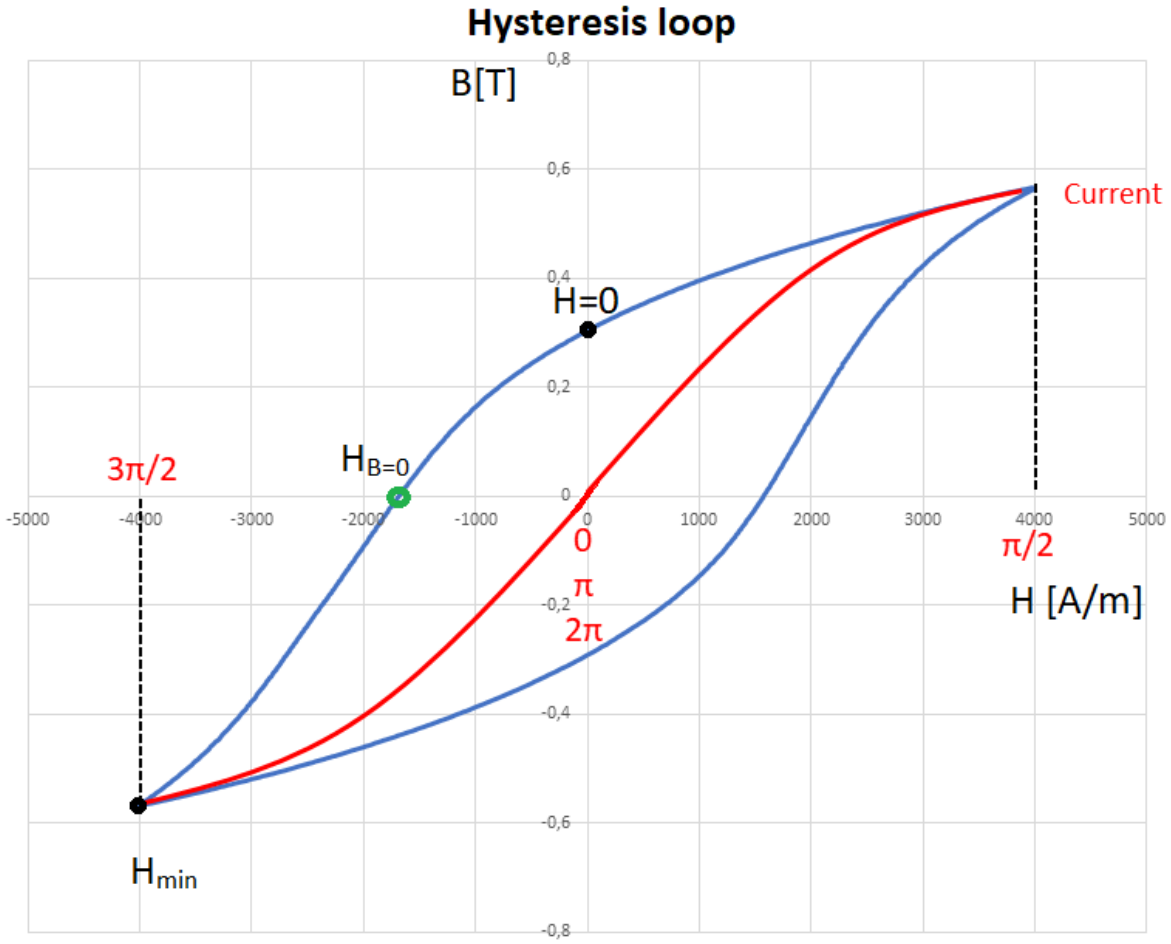

Figure 5.5: Comparison of coil current and hysteresis loop to determine current at the first hysteresis zero-crossing

The green circle in Figure 5.5 is the point where B ≈ 0 and $H_{B=0}$ = -1683.7 A/m. These values are extracted from the measurement file. Figure 5.5 indicates that the phase shift to be determined is between π and $\frac{3\pi}{2}$. Equation (5.1) approximates the phase shift by distributing the $\frac{\pi}{2}$ radians from H=0 to H_{min} and then scale the radians with $H_{B=0}$, in order to get the radians from H=0 to $H_{B=0}$.

$$\varphi = \pi + \frac{H_{B=0} * \frac{\pi}{2}}{H_{min}} = \pi + \frac{-1683.7 * \frac{\pi}{2}}{-4008.4} = 3.801395 \quad (5.1)$$

The phase shift between the current and the flux density is calculated with equation (5.1) and is found to be 3.801395 radians.

The second approach requires a steady state simulation, which is obtained after approximately five periods. When the steady state solution is obtained, the flux density and current are both assumed to be sinusoidal. The time, t_1, found in the first zero-crossing in the flux density steady state is used to obtain the current $i(t_1)$. The initial measured values are described in (5.2) to (5.4).

$$t_1 = 0.01663667312s \tag{5.2}$$

$$B(t_1) = 0T \tag{5.3}$$

$$i(t_1) = 0.1234610299A \tag{5.4}$$

Equation (5.5) to (5.7) describes how the phase shift in the coil current is calculated.

$$B(t) = B_{max} * \sin(2\pi ft) \tag{5.5}$$

$$\text{i(t)} = I_{max} * \sin(2\pi ft + \varphi) \tag{5.6}$$

$$\varphi = 2\pi ft + sin^{-1}\left(\frac{i(t_1)}{I_{max}}\right) \tag{5.7}$$

Table 5.1 describes the parameter values used in the phase shift determination. Equation (5.7) is used to calculate the phase shift, $\varphi = 3.801395$. The scenario used in the phase shift determination is described in Table 5.1. The resulting average magnetic flux density plot is illustrated in Figure 5.6.

Table 5.1: FEM model parameters used in the current phase shift determination

f [Hz]	$\mu_{r\text{-core}}$	I_{max} [A]	$B_{avg\text{-}max\ target}$ [mT]
150	350	0.20912	201.89

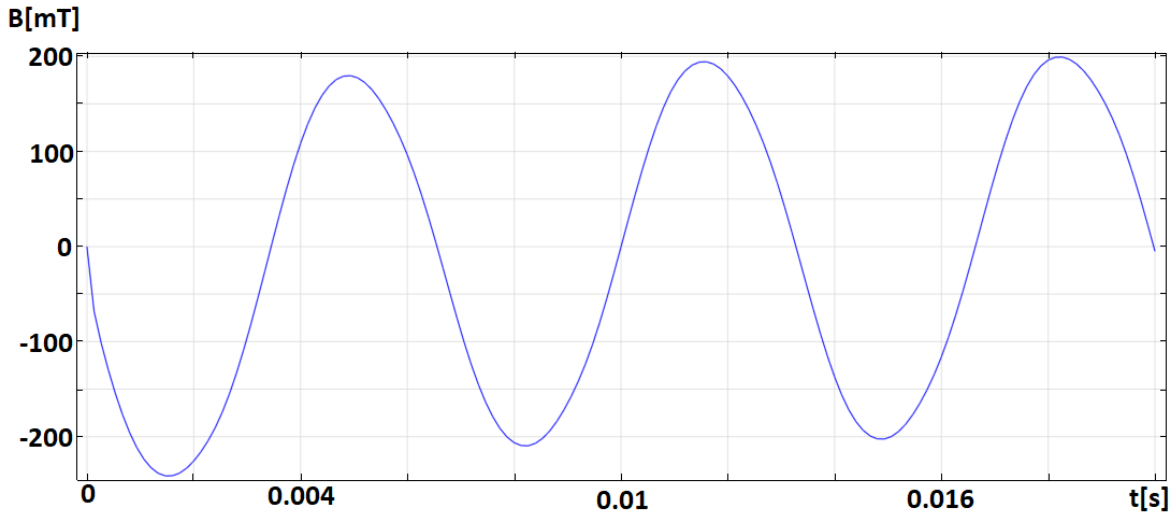

Figure 5.6: Average magnetic flux density in a rod sample with a reduction of the decaying DC term

As can be seen in Figure 5.6, there is still a transient in the solution with the phase shift implemented in the coil current. The steady state is obtained faster, but there are still room for improvements.

There was carried out simulations without conductivity in the material sample, but the simulations yielded the same results. This indicates that the transient originates from the Jiles-Atherton method and the method needs some iterations before the correct values are obtained.

To further reduce the computation time a parametric sweep was initiated. The parametric sweep was performed in several steps. The simulation was performed over two periods with a fixed current amplitude in the current source and a varying phase shift between each sweep. The DC offset is investigated in each loop with equation (5.8).

$$B_{max} - B_{min} = 0 \tag{5.8}$$

When the turning point was discovered and the sum of equation (5.8) starts to increase, a new parameter sweep can be initiated with a new set of parameters. The process of obtaining the final phase shift is described in the illustration found in Appendix B. The process was repeated until a steady state in the magnetic flux density was obtained after one period. Figure 5.7 shows the resulting flux density plot and it is evident that a steady state solution is obtained after approximately 0.01s. This is a significant improvement compared with the 0.02s it took to obtain a steady state solution in Figure 5.6.

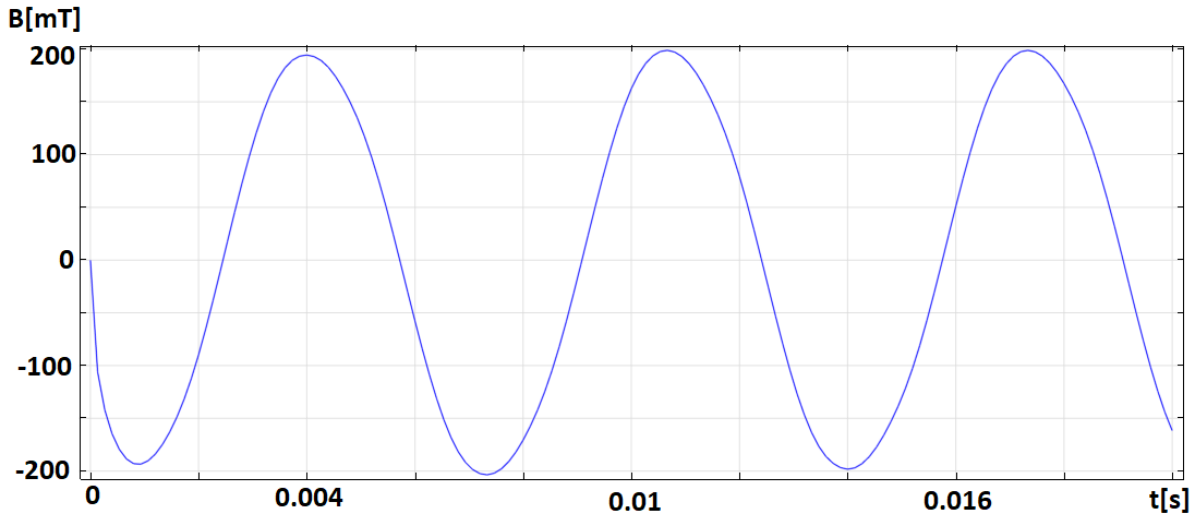

Figure 5.7: Average magnetic flux density in a rod sample in steady state after one simulated period

The steady state must be checked prior to any power calculation, but the phase shift seems to be applicable to different frequencies, coil current amplitudes and types of steel materials.

5.2.4 Obtaining a comparable loss calculation in the FEM model

The measuring equipment is calibrated with a magnetic length equal to 85mm. The calibrating technique is not available, and it is therefore assumed that the calibration accounts for the leakage field in the coil. The calculated losses in the excel file from the measuring equipment are dependent on the magnetic length. The external core in the measuring equipment is assumed to have a high relative permeability compared to the relative permeability in the rod sample.

This indicates that the flux density is higher in the part of the core closest to the core window. To verify the behavior of the flux distribution a displacement test was performed.

The distortion test was created to measure the effect of a smaller contact area between the core material and the test material. This effect will also be important to decide if the specific losses in the FEM model should be calculated in the entire rod geometry. Figure 5.8 describes how the initial position of the measurement setup was configurated.

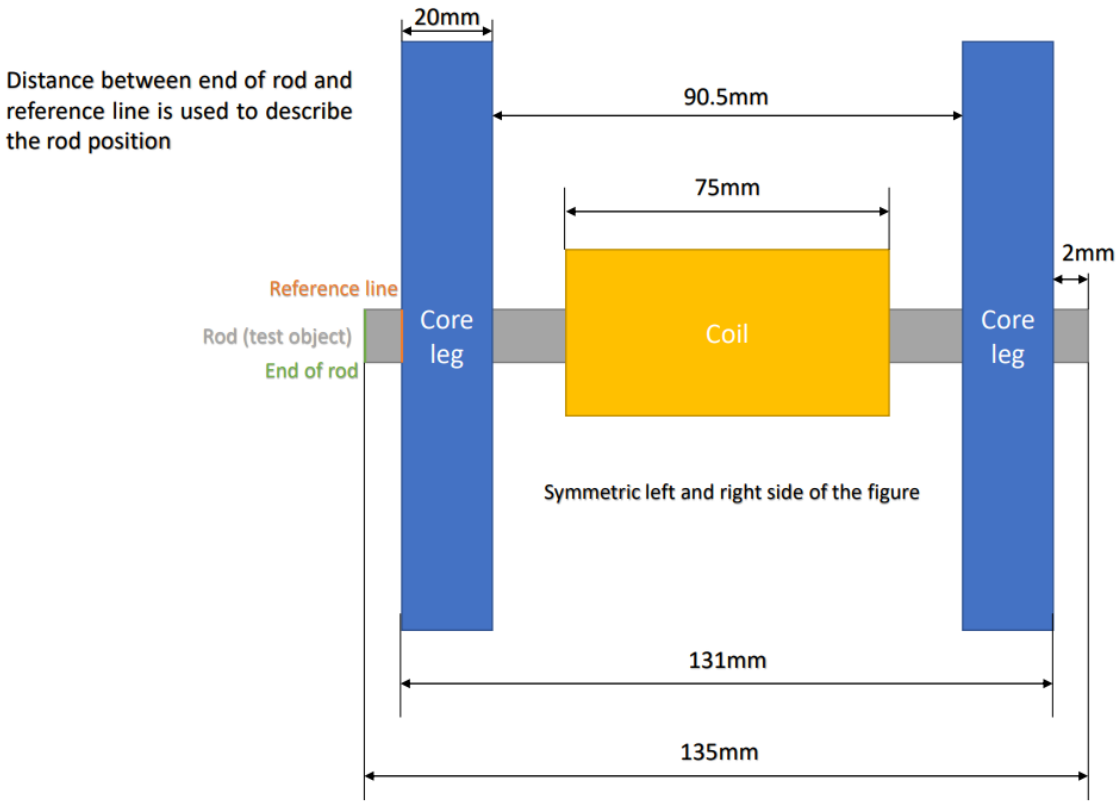

Figure 5.8: Illustration of the measuring setup seen from the side with lengths and reference lines used in the distortion test

The measured values are collected as a function of the rod position. The rod is gradually pulled to the right between each measurement. The measuring equipment has a current limit, and it is expected that the current will increase because the reluctance increases in the reduced contact surface area between the rod and the core. The effect of distorting the position of the test object is difficult to predict. Thus, the measurements have target flux densities at 100mT and 200mT measured at the frequencies 50Hz and 100Hz. The higher frequencies are assumed to have a higher flux density near the inner surface of the core. It is required a higher current to obtain a

certain average flux density in the test object if the frequency increase. The displacement of the test object is likely to cause a current that exceeds the maximum limit of the measuring instrument. Thus, the rod has to be gradually pulled out of the measuring sensor between each measurement.

The distance used as a reference in the displacement results are calculated with equation (5.9). Thus, the initial measurement performed in the setup in Figure 5.8 is at D_{ref} = -2mm.

$$D_{ref} = -2 + D_{displacement} \tag{5.9}$$

$D_{displacement}$ [mm] is the length describing how far the right side of the rod is pulled out of the sensor. D_{ref} is the reference length used in Figure 5.9 and Figure 5.10. The figures illustrate the response in the material in terms of the total specific power in the test object and the H_{max}-value which is linked to the current. Figure 5.9 and Figure 5.10 shows the results from the measurement at 100Hz with 200mT as target flux density. All results are presented as plots in Appendix C.

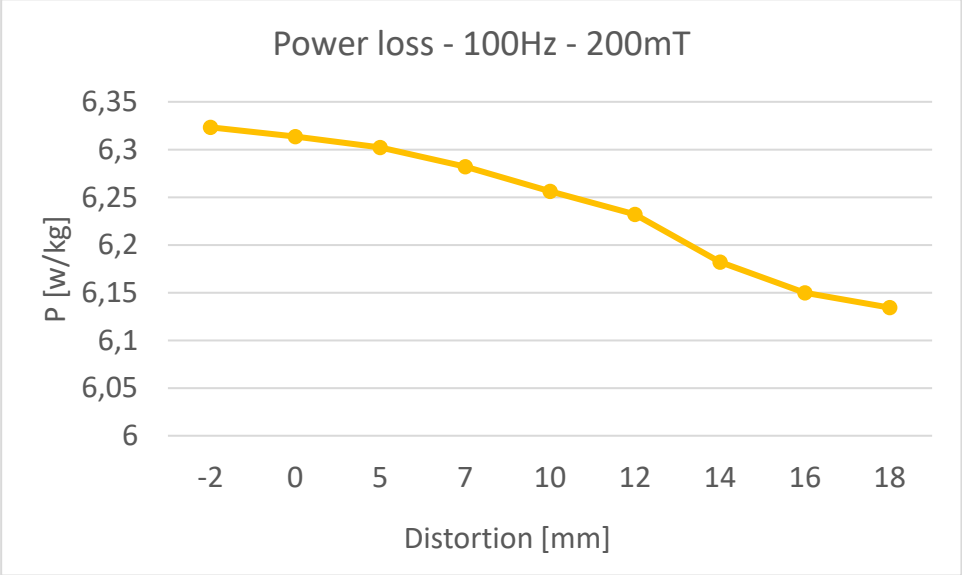

Figure 5.9: Measured total power loss at 100Hz and 200mT target flux density plotted as a function of distortion length

In Figure 5.9 the power loss described as a function of the distortion is decreasing as the rod is pulled out of the core. This indicates that there are losses in the rod volume that are covered by

the core that should be included in the specific loss calculation. Figure 5.10 shows that H_{max} increases when the rod is pulled out of the core. This is as expected, as the reduced contact surface between the rod and the core increases the reluctance in the magnetic circuit. Thus, a higher current is needed to achieve the target flux density.

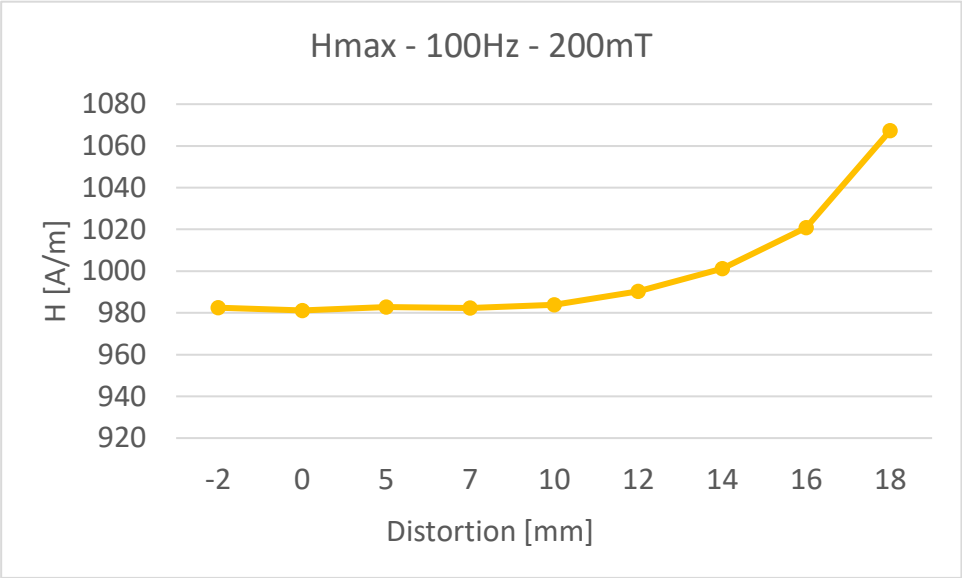

Figure 5.10: Measured H-field at 100Hz and 200mT target flux density plotted as a function of distortion length

The main goal of the distortion test was to measure the effect of a reduced contact surface between the rod and the core. The losses will increase locally due to the enhanced flux density, but it will be a smaller volume in which power can be dissipated. The hypotheses is that a reduced contact surface will influence the losses. A significant loss will be ignored in the FEM model if the loss is in the rod volume covered by the core is neglected. This would not have been the case if the power were to be calculated on 85mm of the rod. The instrument has no way of excluding the dissipated power in the rod volume covered by the core. It should also be mentioned that the effect is only occurring in one side of the rod in the distortion test. The impact of neglecting the dissipated power in the rod volume covered by the core is double of the loss illustrated in Figure 5.9. Further, the findings indicate that the 'pot core' in the axisymmetric 2D model will introduce errors in the loss distribution compared with the actual loss distribution. The loss distribution is different because of the actual core geometry. This will not be investigated further, as the need for a 3D model is presented in the next chapter.

5.2.5 Using the relative permeability as the control parameter

During the method development it was discovered that the excitation current influenced the magnitude of the losses in the model. Initially, it was assumed that the only important parameter was the average flux density and that if the model simulation resulted in a flux density higher than the target value, the current could be used to reduce the flux density in the model.

Tests were performed in terms of a comparison of two simulations. In the first scenario, the current was constant and the relative permeability of the model was adjusted until the simulated flux density was equal to the measured target value. In the second scenario, the relative permeability was constant, and the current amplitude was adjusted to achieve the target flux density in the simulation. When the losses were calculated they turned out to be of different magnitude in the two scenarios. The current should not be a control variable if the magnetic flux density target value is correct and the magnitude of the losses are different when the excitation current is changed.

In further development of the model, the coil current is constant in terms of using the current amplitude from the measurement file corresponding to a specific magnetic flux density. The main argument for choosing the relative permeability as the control parameter is the availability of the current, while the relative permeability in the core is not measured or given in the instrument manual.

When the 2D-axisymmetric model, displayed in Figure 5.1, is revolved the rod and core displayed in Figure 5.11 is similar to the actual sensor and test object. The accurate representation of the rod and the excitation coil is the reason why the 2D-axisymmetric model was chosen in the first place.

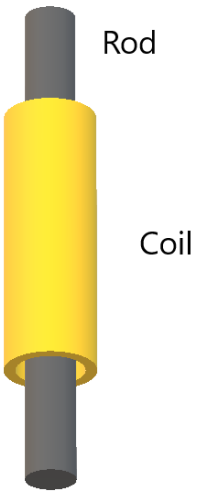

Figure 5.11: Illustration of the revolved rod and coil in the 2D-axisymmetric FEM model

When the sole control parameter of the model is the relative permeability of the core it introduces challenges regarding the usage of the 2D-axisymmetric model. In the FEM model there are no airgaps between the core and the test object and the relative permeability of the core is assumed to be high. In reality it is difficult to predict the relative permeability of the core due to the small airgaps between the test object and the core in the actual measuring setup. The relative permeability of the core has to represent the magnetic circuit consisting of the core and the small airgaps. This will make the total relative permeability significantly lower than assumed. In addition, the airgap influence will vary with the frequency of the excitation current because of the penetration depth of the flux in the core. The main problem with the 2D-axisymmetric model is the core. When the core is revolved around the symmetry axis in the model it becomes a pot core, illustrated in Figure 5.12.

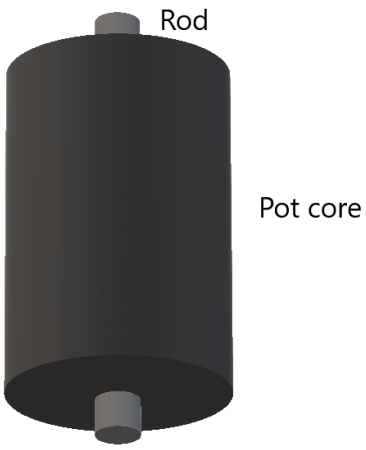

Figure 5.12: Illustration of the revolved 2D-axisymmetric FEM model

The area of the flux path in the pot core is significantly larger than in the sensor core. To obtain the target flux density in the test object, the relative permeability of the core has to be in the range 1 to 2. The low relative permeability of the core distributes the flux over a larger part of the contact surface. As discussed previously, the power dissipated in the rod volume covered by the contact surface between the rod and the core is significant. This implies that the loss calculation will be wrong when the flux distribution is changed due to the low relative permeability. To overcome this issue, different core geometries in the 2D-axisymmetric model were investigated. Adjustment of the core leg thickness, shown in Figure 5.13, and different airgaps, shown in Figure 5.14, were investigated but the flux path was not satisfactory in terms of a realistic distribution.

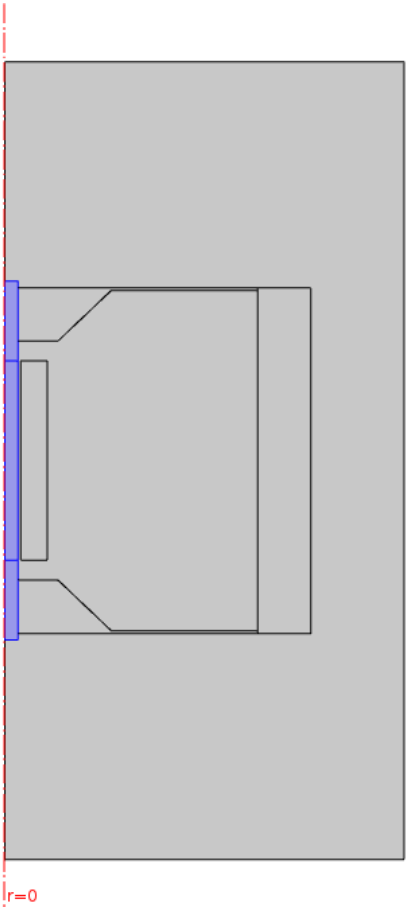

Figure 5.13: Narrow core legs in 2D-axisymmetric FEM model

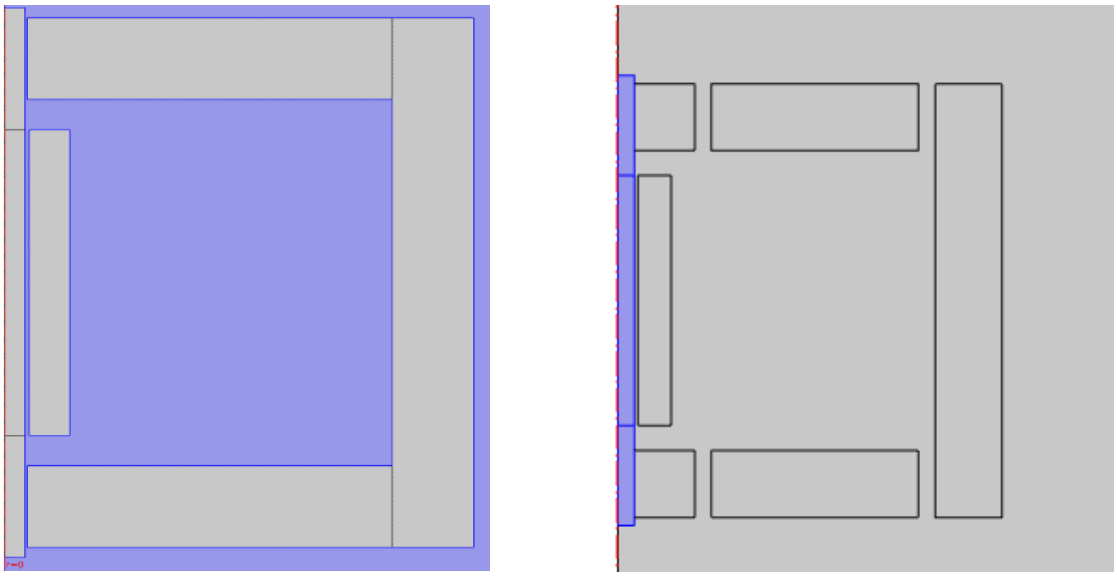

Figure 5.14: Different airgaps tested in 2D-axisymmetric FEM model

Adjusting relative permeability of the core in a 3D model is the only viable option to obtain the target flux density and a reasonable flux path. The 3D model has to have the same physical dimensions as the sensor in the measuring equipment.

5.3 3D FEM model

To obtain a trustworthy simulation in Comsol, a 2D-axisymmetric model was used to develop a model of the measuring equipment. The findings during the model development suggested that it was necessary to develop the final model in 3D to enable the possibility of using the relative core permeability as the control parameter. The physical dimensions are in accordance with the sensor description, which improves the loss distribution and ensures a correct flux path in the model. This chapter presents a detailed description of the FEM model used in the simulations. The model is based on the findings in the 2D model and on recommendations in [1], [16] and [21].

5.3.1 Initial assumptions and definitions

A 3D model improves the simulation result but is more time consuming due to the increased number of nodes in the model. The 3D model enables the possibility of comparing the simulation results with the measurements. The comparison will be used to determine if the Jiles-Atherton method can be applied in Comsol with the help of JAMPS to simulate the power loss due to hysteresis and eddy current in ferromagnetic materials. The 3D model was developed based on the work and discoveries performed on the 2D axisymmetric model.

The measuring equipment scales the measured loss in the rod samples with the magnetic length provided by equipment calibrators[7]. The total weight needs to be scaled to get the weight of the rod volume in which the loss is calculated, as described in chapter 3.3.4.

In the Comsol model there are global definitions in terms of parameters. These parameters provide easy access to the values in the model. The easy access is beneficial since the simulation scenarios requires several changes in these values. The parameters with descriptions are displayed in Table 5.2. The usage will be described in the following chapters.

[7] The calibrated magnetic length of 85mm is the default value in the measuring equipment.

Table 5.2: Description of the parameter definitions utilized in the FEM model

Name	Description
f [Hz]	Coil current frequency
I_{max} [A]	Current amplitude in excitation coil from measurement file
numPeriod	The number of periods to be simulated
numStep	The number of timesteps per period
t_{step} [s]	Timestep in seconds: (1/f)/numStep
t_{stop} [s]	Total time to be simulated in seconds: (1/f)*numPeriod
Weight 1	Scaled weight for material sample 1 for calculation of specific loss
Weight 2	Scaled weight for material sample 2 for calculation of specific loss

5.3.2 Geometry

The 3D model geometry in Comsol is based on the geometry of the sensor description from chapter 3.3.1. To reduce the computation time, the geometry represents ¼ of the actual model. Figure 5.15 illustrates how the model is divided to end up with ¼ of the model. It is possible to perform this simplified calculation with the help of symmetry arguments presented in chapter 5.3.4. The symmetry arguments and model setup are adapted from [21].

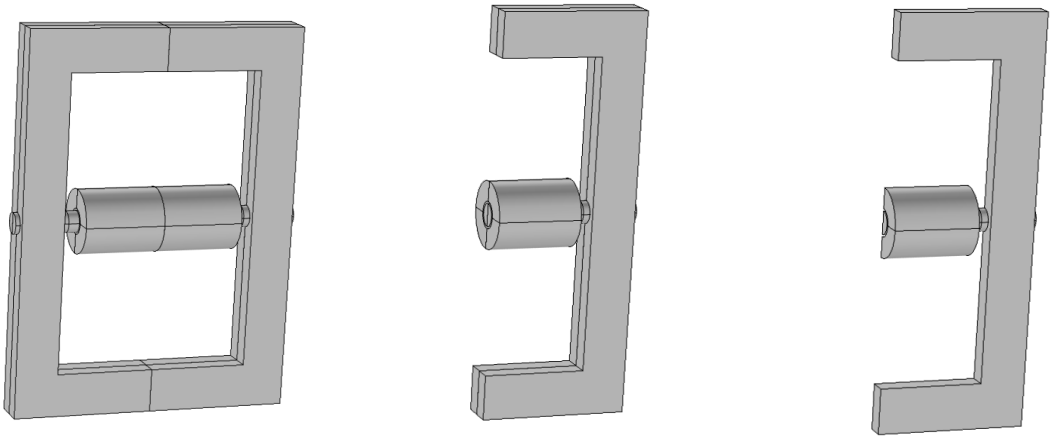

Figure 5.15: Reduction of 3D model to minimize simulation time

5.3.3 Materials

The materials are defined and assigned to the model geometry. There are five materials defined in the model:

- Air
- High permeability iron
- Cupper
- Material 1 (magnetic steel)
- Material 2 (magnetic steel)

The air is defined in the surrounding volume of the model, while the cupper is defined in the coil. The high permeability iron is defined in the core and has a very low conductivity ($\sigma = 1$ S/m) to prevent interference from the induced eddy currents. The laminations in the actual core ensures that the influence from the eddy currents are neglectable.

Material 1 and 2 represents two unknown compositions of magnetic steel. The material representation is the most important part of this study as this is the test object material. The magnetic steel rods in the model will be used to investigate if the Jiles-Atherton method can be utilized to calculate the specific power loss in the time domain. The process of obtaining the Jiles-Atherton parameter values was covered in detail in chapter 4.3. The materials get properties from the Jiles-Atherton property group which originates from the physics settings that will be described in the next section. The material definitions for the magnetic steel can be found in Table 5.3.

Table 5.3: Material definitions of the ferromagnetic materials used in the FEM model

Parameter		**Material 1 [S/m]**	**Material 2 [S/m]**
Conductivity		$4.5465 * 10^6$	$1.2784 * 10^6$
Jiles-Atherton parameters	**M_s**	1427100.592	974672.8
	a	533.7758585	1131.16
	k	456.34	2348.45
	c	0.402872374	0.2145793
	α	0.000782366	0.000836528973824

5.3.4 Physics

The study is defined in the magnetic field (mf) module in Comsol. The air is assigned the physics settings of Ampère's Law, shown in equation (5.10) to (5.13).

$$\nabla x \boldsymbol{H} = \boldsymbol{J} \tag{5.10}$$

$$\boldsymbol{B} = \nabla x \boldsymbol{A} \tag{5.11}$$

$$\boldsymbol{E} = -\frac{\partial \boldsymbol{A}}{\partial t} \tag{5.12}$$

$$\boldsymbol{J} = \sigma \boldsymbol{E} \tag{5.13}$$

In equation (5.10) H is the vector of the magnetic field strength and J is the current density, in equation (5.11) B is the vector describing the magnetic flux density and A is the magnetic vector potential. In equation (5.12) E is the electric field vector and A is the magnetic vector potential. In equation (5.13) J is the current density vector, σ is the conductivity and E is the electric field vector.

The material properties of the magnetic steel rods are implemented with the use of Ampère's Law in combination with the Jiles-Atherton method. The Jiles-Atherton method was covered in chapter 2.3 and requires five constant parameter values. The steel rods are assumed to be in an initial unmagnetized state. Thus, the initial magnetization M_0 is set to zero in the model definitions.

The symmetry arguments in this model are applied through the boundary conditions defined in the magnetic insulation and a perfect magnetic conductor. The magnetic insulation described in equation (5.14) is applied on the blue surfaces illustrated in Figure 5.16.

$$\boldsymbol{n}x\boldsymbol{A} = 0 \tag{5.14}$$

In equation (5.14) n is the normal vector and A is the magnetic vector potential. This ensures that the system remains closed and that the field is contained within the model.

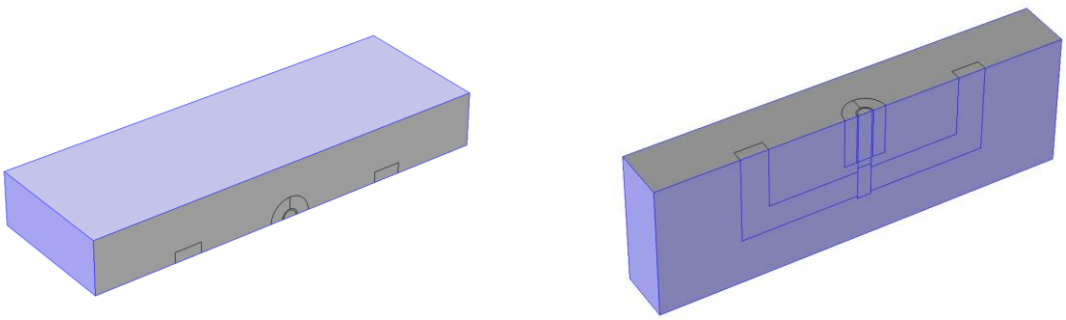

Figure 5.16: Selected surface for boundary condition 'Magnetic Insulation'.

The perfect magnetic conductor is explained with equation (5.15) and applied to the blue surface in the model geometry shown in Figure 5.17. H in equation (5.15) is the magnetic field

strength. This boundary condition makes the model behave as it continues in the length direction of the rod.

$$\boldsymbol{n}x\boldsymbol{H} = 0 \tag{5.15}$$

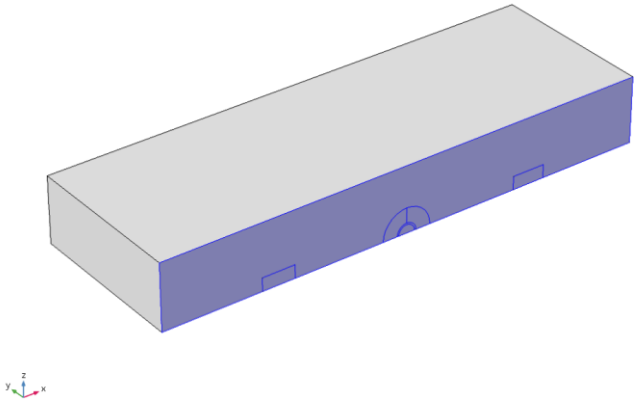

Figure 5.17: Selected surface for boundary condition 'Perfect Magnetic Conductor'.

The coil in the model geometry is defined with a physics setting named ‘Coil’. The coil is defined as a homogenized multi-turn coil with 900 turns. The argument for using 900 turns is that the coil in the measuring sensor has 900 turns. The coil conductivity is set to $6*10^6$ S/m and the wire cross-section area is set to the default setting based on the recommendation in [21].

The coil type is set to ‘numeric’ and the coil excitation is set to ‘current’. The coil excitation current is described in equation (5.16), where the I_{max} is the current amplitude and f is the frequency. The simulations will be based on a measured coil current amplitude and frequency and corresponding magnetic flux density.

$$I_{coil}(t) = I_{max}\sin(2\pi ft - \frac{151\pi}{288}) \tag{5.16}$$

The physics setting related to the coil is described in equation (5.17) and is based on the same theory as presented in chapter 2.1. $\mathbf{J}_e$ is the current density in the coil, I_{coil} is the current in the coil and N is the number of turns. A is the cross-section of the coil (blue area in Figure 5.18) and $\mathbf{e}_{coil}$ is a unit vector to describe the direction of the current.

$$\boldsymbol{J}_e = \frac{NI_{coil}}{A}\boldsymbol{e}_{coil} \tag{5.17}$$

In the coil geometry analysis, the multiplication factors of the coil length and area are set to two. These factors enable the possibility of simulating ¼ of the coil. The coil input and output are defined in the coil geometry analysis. Figure 5.18 illustrates the coil current input.

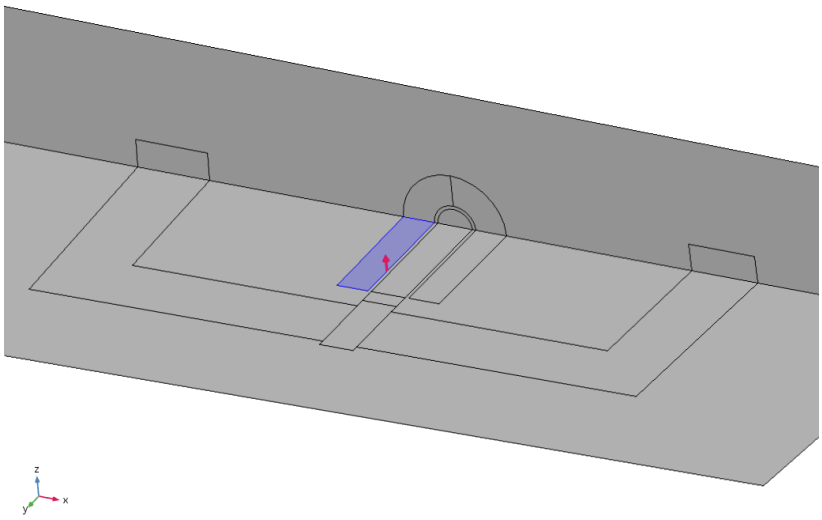

Figure 5.18: Definition of coil input in the 3D FEM model

The Gauge fixing technique in Comsol is used to determine a unique solution in the magnetic field study. Examples of the application of this technique can be found in [16] and [21].

5.3.5 Mesh

During the initial simulations, some tests were performed to ensure that the mesh size was sufficiently fine. Reducing the final mesh size had a limited effect on the simulation result. The mesh used in the simulations is divided in three tetrahedral meshes with different element sizes. The rod defined in the geometry has a custom maximum element size set to 0.1cm. The core and coil have a predefined mesh size set to 'extremely fine' where the maximum element size is 0.6cm. The surrounding air (remaining part of the model) has a predefined mesh set to 'finer' with a maximum element size of 1.65cm.

5.3.6 Study

The study consists of a coil geometry analysis and a time dependent analysis. The coil geometry analysis is a robust method used to supervise the coil in the model. The most important study is the time dependent study. All simulations are based on measurements performed on the test objects. Highlights from the measurement files are presented in chapter 6.1. The Comsol range function in (5.18) defines the time dependent study.

$$\text{Range}(0, \text{Step}, \text{Stop}) \tag{5.18}$$

'Step' is the timestep [s] in the simulation and 'Stop' is the duration [s] of the total simulation. The timestep per period is set to 50 steps and the number of periods per simulation is set to two. The simulation times in terms of steps and duration is calculated based on the frequency. The input values to the range function are displayed in Table 5.4.

Table 5.4: Time step and duration of two periods used in range function

f [Hz]	Length of time step [ms]	Duration of two periods [ms]
50	0.4	40
100	0.2	20
150	0.1333	13.3333
200	0.1	10

Two test simulations with 50Hz and 200Hz at 300mT target flux density were performed to determine which of the methods ‘MUMPS’ and ‘PARDISO’ that had the shortest computation time. In both test simulations ‘MUMPS’ finished more than 30 minutes faster than ‘PARDISO’. The solver configurations in the ‘Time-Dependent Solver’ is therefore set to the direct solver ‘MUMPS’.

5.3.7 Results and post-processing

The main objective with the simulations is to calculate the specific losses of the defined magnetic steel rod in the Comsol model. The magnetic flux density in the simulation is the most important indicator used to determine if the simulation has replicated the conditions in the measurements. Figure 5.19 shows the volume in which the average flux density is calculated for each time step in the simulation. This volume is equal to the part of the rod covered by the excitation coil. It is assumed that the secondary coil in the actual measurement sensor measures the voltage used to determine the measured loss (described in chapter 3.3.2). Thus, the flux densities are assumed to be comparable.

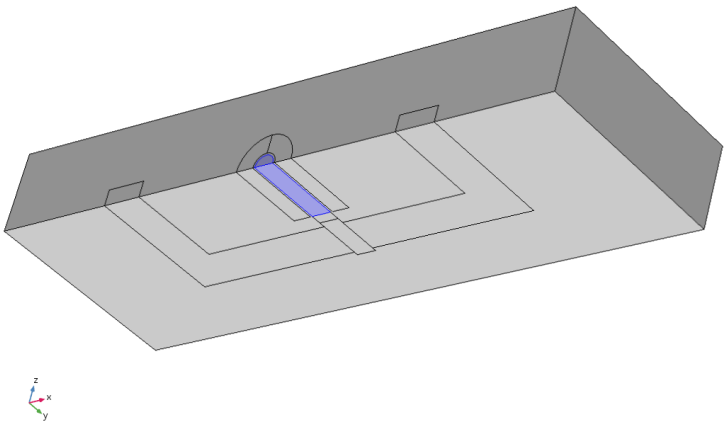

Figure 5.19: Volume selected for magnetic flux density calculation in 3D FEM model

The main contribution of the magnetic flux density is expected to be in the longitudinal direction of the rod. The second period is investigated because the flux density is assumed to

be in steady state after one period. The magnetic flux density is calculated in each relevant time step and the time variation is assumed to behave approximately sinusoidal. The volumetric average is calculated with the Comsol function ‘Volume Average’ with the expression ‘mf.By’, which is the magnetic flux density in the longitudinal direction of the rod.

The value of interest is the maximum flux density during steady state. The maximum value is determined with the function ‘Maximum’ found in the ‘Data Series Operation’ setting. The derived maximum flux density has to be manually compared with the measured value in every simulation to ensure that the target magnetic flux density is achieved in the simulation. A difference between the simulated and measured flux density has a direct influence on the validity of the comparison of the calculated losses.

The losses in the simulation is to be compared with the measured losses to determine if the losses can be simulated with the Jiles-Atherton method. The losses referred to as ‘the simulated losses’ are actually derived in the post-processing of the simulation. This implies that the simulated losses are calculated with user defined expressions. These calculations are derived in the next section. The loss measured with the instrument is the specific losses [W/kg] meaning that the weight of the rod must be included in the loss calculation of the simulated losses. The loss is calculated in ¼ of the rod as illustrated in Figure 5.20. Due to symmetry arguments the calculated losses are multiplied by four to get the total loss.

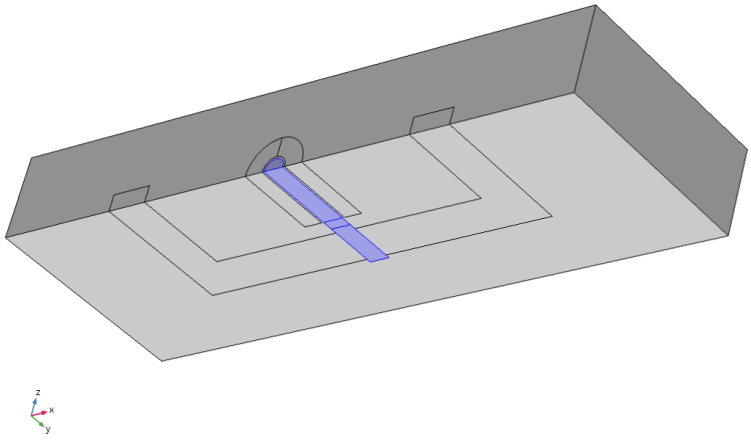

Figure 5.20: Volume selected for loss calculation in 3D FEM model

The losses are to be calculated in the volume of the rod. Thus, in the 'Derived Values' the option 'Volume Integration' is selected in the Comsol model. The domains selected for the volume integration are shown in Figure 5.20. The total losses are divided into eddy current and hysteresis losses in accordance with the assumptions in chapter 2.2. The first step in obtaining the losses is to define an expression that calculates the power loss in Watt for both eddy current and hysteresis loss.

Eddy current loss

The volumetric eddy current loss [W/m^3] is calculated at a given time step with a function in the magnetic fields physics known as mf.Qrh. The expression is found under "Magnetic Fields>Heating and losses>mf.Qrh - Volumetric loss density" [22]. The expression is included in the volume integral to obtain the eddy current loss in the FEM model. The eddy current loss changes for each time step, thus the time average is needed during one period during steady state of the magnetic flux density. The flux density is assumed to be in steady state after one period if the phase shift is successfully obtained. The 'timeavg' function in Comsol calculates the time average during a specified interval with a specified accuracy. Expression (5.19) is inserted into a volume integral to calculate the eddy current loss.

$$timeavg(start[ms], stop[ms], mf.Qrh, 10^{-6}) \tag{5.19}$$

The variables 'start[ms]' and 'stop[ms]' are the time in milliseconds that describes the start and stop of the second period in the simulation. The times are calculated for each frequency. The number 10^{-6} is a tolerance level selected based on recommendations in [16].

Hysteresis loss

The hysteresis loss in the rod geometry is calculated based on suggestions in [21]. The B-field and H-field in all directions are collected at each time step of the second period in the simulation as shown in equation (5.20).

$$timeavg(start[ms], stop[ms], \frac{dB_x}{dt} * H_x + \frac{dB_y}{dt} * H_y + \frac{dB_z}{dt} * H_z, 10^{-6}) \tag{5.20}$$

The volume integral of the term $\frac{dB}{dt} * H$ describes the dissipated loss in a specified time step. Figure 5.21 illustrates that the power can be negative in a time instance because both $\frac{dB}{dt}$ and H have negative values during the period. When one of the values is negative it can be interpreted that the material is feeding power back to the source. The green area illustrates the positive power values and the pink areas represent two values; one positive and one negative. This depends on whether the material is magnetizing or demagnetizing. The pink areas are effectively not contributing to the loss.

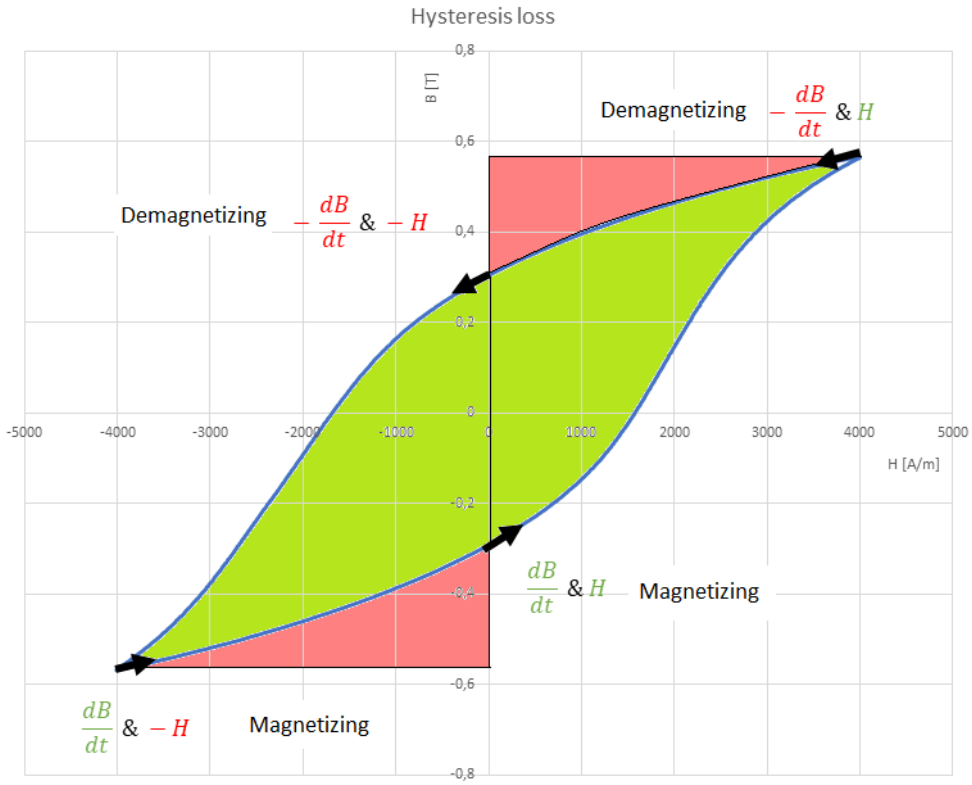

Figure 5.21: Explanation of 'negative energy dissipation' in a ferromagnetic material

The time average of the power in one period results in the hysteresis power dissipated in material per period. Thus, equation (5.20) is added in the volume integral and provides the hysteresis loss in Watt, during the second period of the simulation. The time average function was carefully described in the section that covers the calculation of simulated eddy current loss.

The total loss

The total simulated loss which is to be compared with the total loss in the measurement result is a combination of the hysteresis loss and the eddy current loss during the second cycle. The loss is multiplied by four because the FEM model represents ¼ of the actual rod. The total loss is divided by the scaled weight, described in chapter 3.3.4, to get a comparable total simulated specific loss. Expression (5.21) is added in a volume integral to get the total specific loss.

$$[timeavg(eddy) + timeavg(hysteresis)] * \frac{4}{weight_{scaled}} \tag{5.21}$$

The timeavg(eddy) and timeavg(hysteresis) refers to the expressions in (5.19) and (5.20) respectively.

6 AC measurements and simulation results

The highlights from the AC measurements performed with the measuring equipment is presented in this chapter. The AC measurements are used as reference values during comparisons and analytical calculations. The simulation results are presented in terms of a comparison of the total measured and simulates losses in the two materials. The measures and simulated eddy current and hysteresis losses will be investigated and presented in terms of a comparison.

6.1 AC measurement results

The AC measurements performed on the two materials are presented in the following chapters. A brief analysis of the frequency dependency is presented in the respective chapters.

6.1.1 AC measurement results in material 1

The measurements were performed at four different magnetic flux densities at four different frequencies. The total specific power losses measured on material 1 are displayed in Table 6.1 arranged according to the frequency and flux density.

Table 6.1: Measured total specific loss in material 1

		Magnetic flux density target value			
		100mT	**200mT**	**300mT**	**400mT**
Frequency	**50Hz**	0.66 W/kg	2.31 W/kg	5.03 W/kg	9.09 W/kg
	100Hz	1.76 W/kg	6.33 W/kg	14.42 W/kg	27.27 W/kg
	150Hz	3.12 W/kg	11.60 W/kg	27.30 W/kg	53.40 W/kg
	200Hz	4.72 W/kg	17.99 W/kg	43.54 W/kg	87.27 W/kg

Figure 6.1 shows the losses in Table 6.1 as a plot where each line represents a flux density. P is the power and f is the frequency. From the figure it can be seen that the losses increase exponentially with an increase in frequency. The measurement series ‘100mT’ appear to be approximately linear in the plot, but this is only due to the scaling of the y-axis in the plot. Table 6.1 confirms that the specific loss increases exponentially. The increase is investigated in

chapter 6.2 where the eddy current and hysteresis are examined further. From the total losses it is difficult to find the specific relationship between eddy current and hysteresis loss.

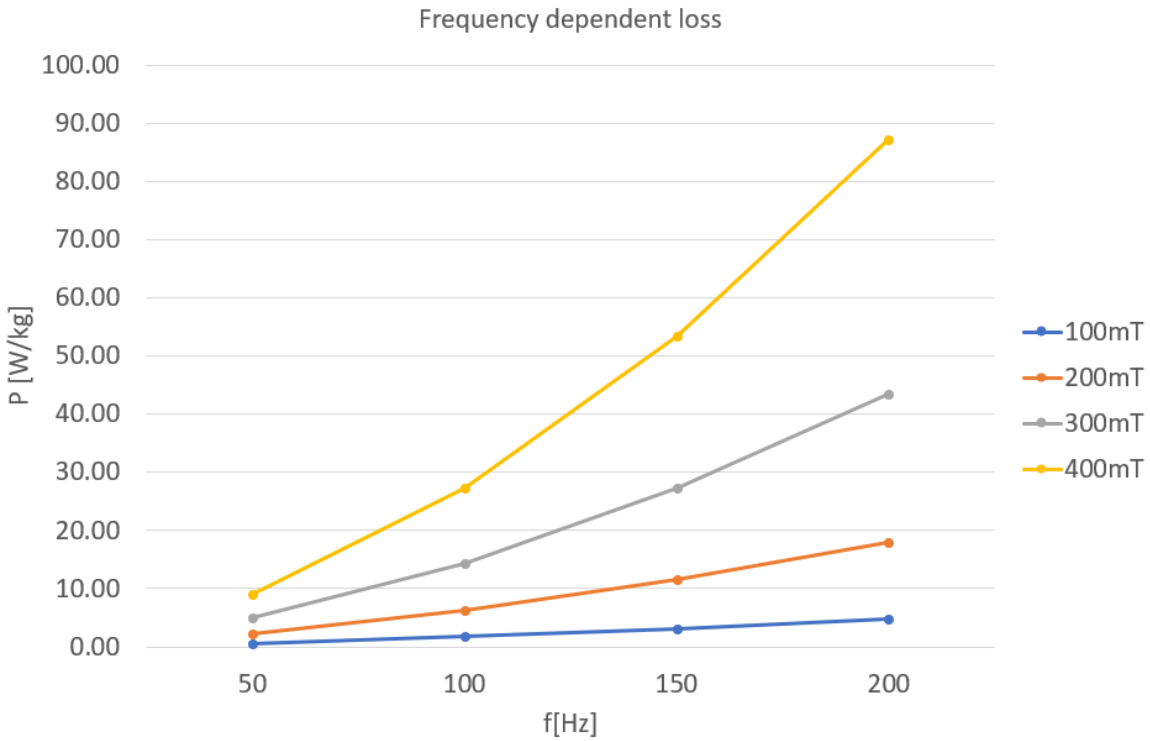

Figure 6.1: Measured frequency dependent total loss in material 1

6.1.2 AC measurement results in material 2

Chapter 4.2 show that a higher H-field is required to obtain the same flux density in material 2 compared with material sample 1. This implies a higher current needed to obtain the same magnetic flux density in the material. The measured specific total AC losses are displayed in Table 6.2. The specific losses are slightly higher in material sample 2 than in material sample 1. On average the specific losses for material sample 2 are approximately 20% higher than the specific losses in material sample 1. The current needed to generate the target flux density is on average approximately 92% higher in material 2 compared with material 1. This is not investigated further in this thesis but it is clear that the two materials are of a different composition. Material 2 has a much lower conductivity compared with material 1 and thus the eddy current losses will be lower in material 2 with the same coil excitation current as in

material 1. The materials behave differently and thus there is not a clear connection between the measured losses in the different materials.

Table 6.2: Measured total specific loss in material 2

		Magnetic flux density target value			
		100mT	**200mT**	**300mT**	**400mT**
Frequency	**50Hz**	0.59 W/kg	2.92 W/kg	7.03 W/kg	12.80 W/kg
	100Hz	1.76 W/kg	7.98 W/kg	18.77 W/kg	33.93 W/kg
	150Hz	3.45 W/kg	14.83 W/kg	34.30 W/kg	62.02 W/kg
	200Hz	5.60 W/kg	23.23 W/kg	53.06 W/kg	95.71 W/kg

Figure 6.2 is a plot of the specific losses displayed in Table 6.2. The data is grouped into series based on the magnetic flux density. It is clear that the losses are frequency dependent in such a way that the specific losses increase exponentially with an increase in the frequency. The separated losses are examined further in chapter 6.3 where the eddy current loss and hysteresis loss are treated separately.

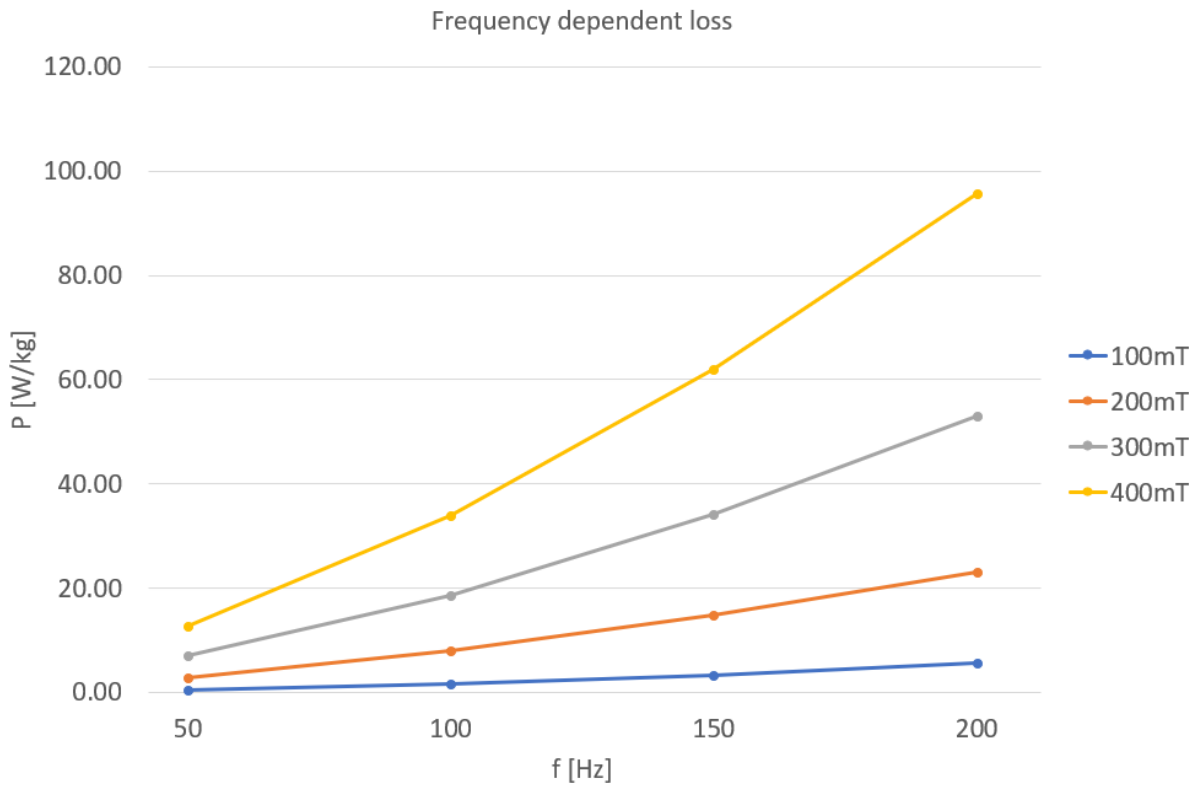

Figure 6.2: Measured frequency dependent loss in material 2

6.2 Comparison of measured and simulated losses

The measured total AC losses presented in the previous chapter are compared with the simulated results obtained with the FEM model described in chapter 5.3. The simulation target value is the maximum B-field obtained in the AC measurement. The relative permeability in the core of the model was changed until the simulated maximum flux density was approximately equal to the measured maximum flux density. When the target maximum flux density was reached in the simulation the losses in the model were calculated.

6.2.1 Total losses in material 1

Table 6.3 shows an example of the result tables found in Appendix D.1. The simulated total losses are compared with the corresponding measured losses.

Table 6.3: Comparison of measured and simulated total losses at 300mT in material 1

Simulation result at 300mT average flux density				
f [Hz]	**$P_{tot\text{-}measured}$ [W/kg]**	**$P_{tot\text{-}simulated}$ [W/kg]**	**Difference [W/kg]**	**Difference [%]**
50	5.03	4.62	0.41	-8.28
100	14.42	13.58	0.84	-5.85
150	27.30	26.59	0.71	-2.57
200	43.54	42.90	0.64	-1.47

The simulations are performed with target flux densities at 100, 200, 300 and 400mT. The target flux densities were simulated at the frequencies 50, 100, 150 and 200Hz respectively.

Table 6.3 shows that at 300mT the Jiles-Atherton parameters yielded a difference in the loss simulation between -8.28% and -1.47% compared to the measured total loss. The difference with respect to the measured total loss increments as the frequency increases.

Figure 6.3 provides an overview of the difference between the simulated and measured total losses for material sample 1.

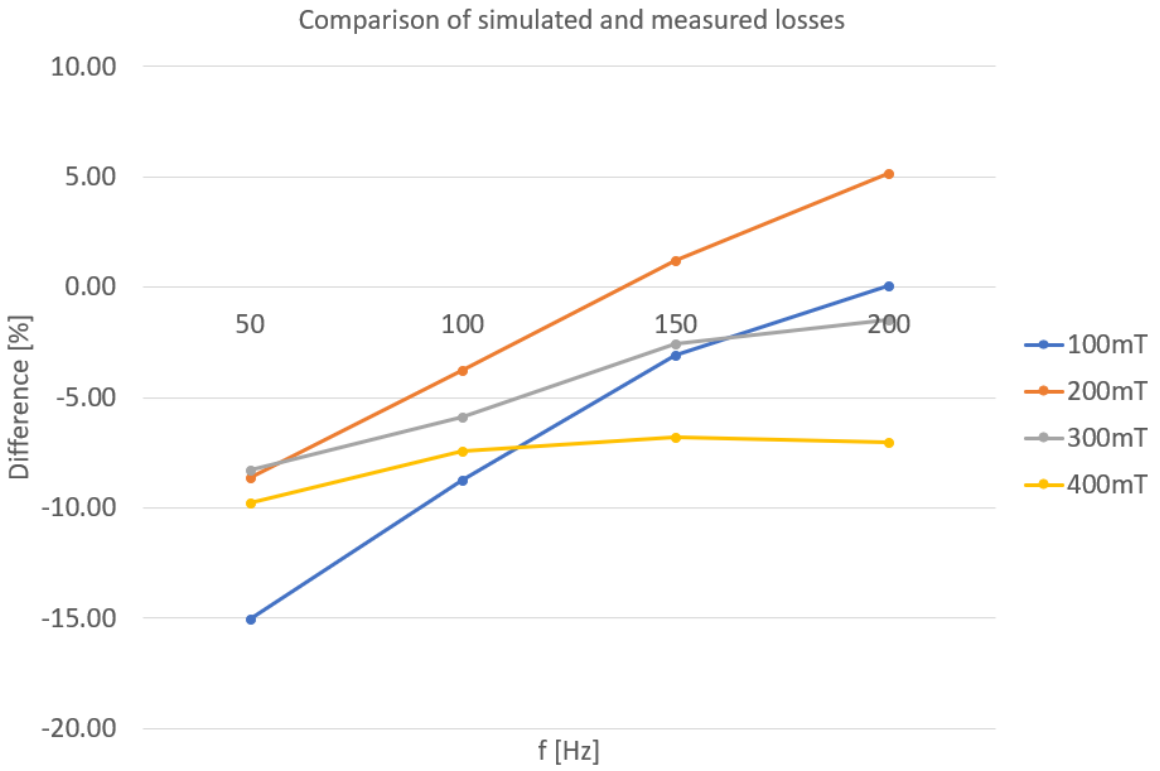

Figure 6.3: Difference between the simulated and measured frequency dependent total loss in material 1

The highest difference between the measured and simulated total loss is -15.04% with a target magnetic flux density of 100mT with a coil current frequency of 50Hz. 15 of the 16 simulated losses have a difference in the range of -9.74% to 5.14% compared with the measured losses. The detailed simulation results of material sample 1 with comparisons of the total losses can be found in Appendix D.1.

6.2.2 Total losses in material 2

The Jiles-Atherton parameters used in the simulations yielded an overestimation of the total losses in material 2. Table 6.4 shows the simulation result at 400mT target flux density with a comparison of the simulated and measured total losses in material sample 2. The results in Table 6.4 are the set of simulated values in material sample 2 which were closest to the measured total losses.

Table 6.4: Comparison of measured and simulated total losses at 400mT in material 2

Simulation result at 400mT average flux density				
f [Hz]	$P_{tot\text{-}measured}$ [W/kg]	$P_{tot\text{-}simulated}$ [W/kg]	Difference [W/kg]	Difference [%]
50	12.80	14.21	-1.41	10.98
100	33.93	36.91	-2.98	8.79
150	62.02	65.44	-3.41	5.50
200	95.71	99.31	-3.60	3.76

The simulation results of material sample 2 are presented in Figure 6.4 in terms of a comparison of the measured and simulated total losses.

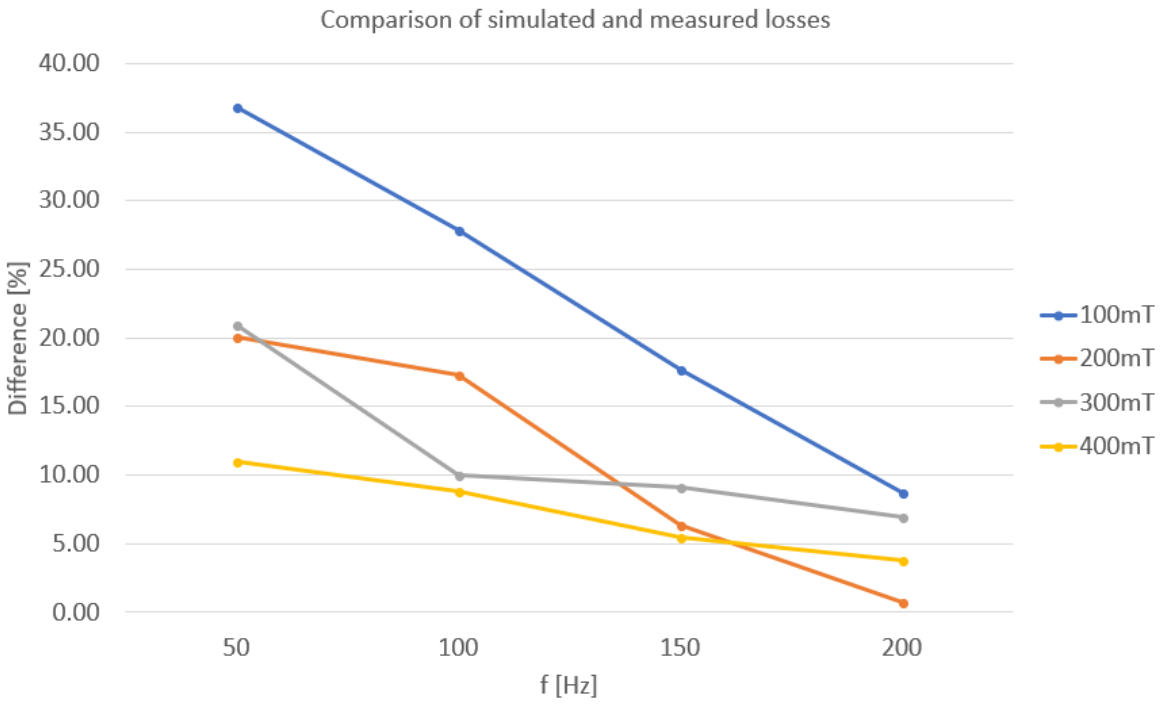

Figure 6.4: Difference between the simulated and measured frequency dependent total loss in material 2

Figure 6.4 shows that the simulated losses for material sample 2 has a larger difference between the simulated and measured total loss compared with material sample 1. The largest difference between the simulated and measured total loss is found in the measurement series of 100mT at 50Hz with a difference of 36.79%. The difference appears to be connected to the frequency of the simulation. An increase in the frequency corresponds to a reduction in the difference, meaning that the simulations of material sample 2 with the lowest difference are performed at 200Hz. The difference in the total losses are lower when the magnetic flux density increase. The reduction in the difference varies in each measurement series, but on average the 400mT series are closest to the measured series. The most accurate simulation in material sample 2 is with a target magnetic flux density of 200mT at 200Hz where the difference is 0.7%. The complete simulation results with comparisons are found in Appendix D.2.

6.3 Comparison of hysteresis and eddy current loss

The total loss in the material samples were assumed to consist of two parts; hysteresis loss and eddy current loss. The results from the comparisons are found in Appendix E for both materials. The simulated losses are compared with the corresponding measured losses. The comparisons of the losses are presented for each material sample. The simulated eddy current and hysteresis losses are calculated according to the description in chapter 5.3.7.

6.3.1 Measured and simulated hysteresis and eddy current losses for material 1

The total losses previously presented shows that the difference between the measured and calculated loss has a difference of approximately ±10% for material sample 1. Figure 6.5 displays the comparison of the simulated and measured eddy current losses for material sample 1. The measurements are divided into groups based on the magnetic flux density target value. It can be seen from Figure 6.5 that the eddy current losses have a lower difference between measured and simulated loss as the target flux density increases. The difference seems to be reduced as the frequency increases. The difference ranges from 3.06% at 400mT 200Hz to 151.55% at 100mT 50Hz.

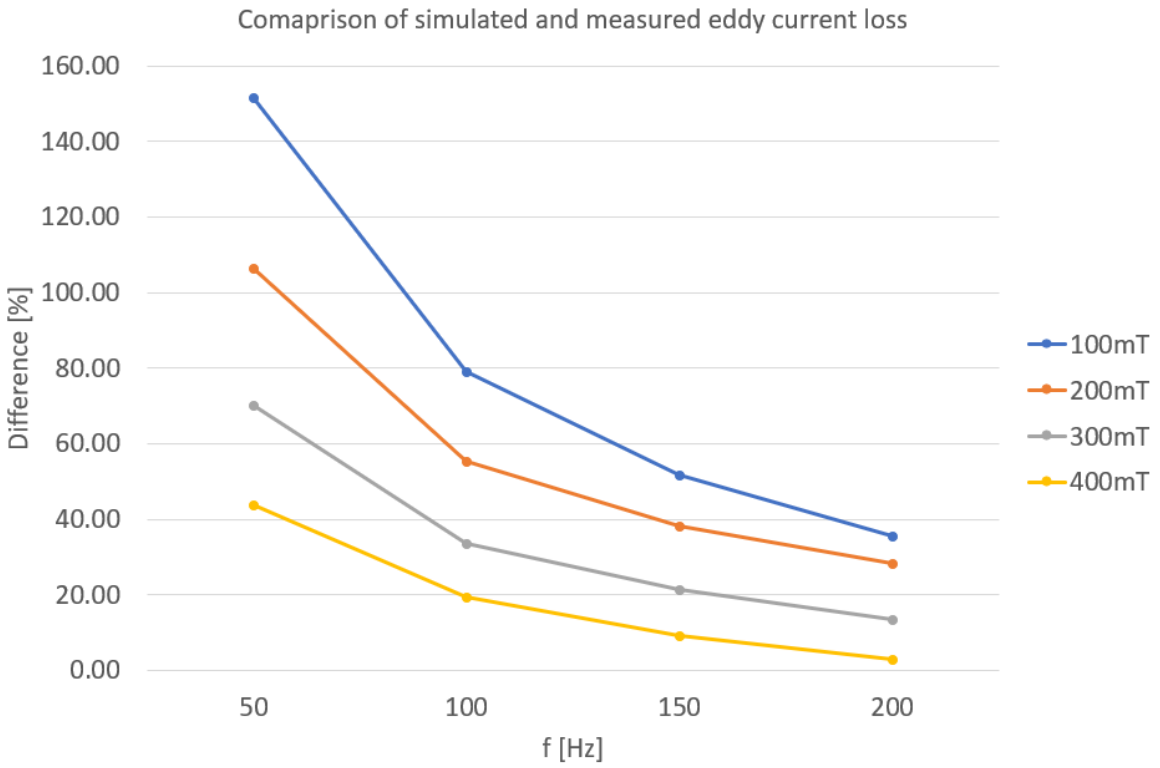

Figure 6.5: Difference between the simulated and measured eddy current loss in material 1

Figure 6.6 shows the comparison of the simulated and measured hysteresis losses. The difference between the total losses is relatively low and the difference between the eddy current losses is relatively high. Thus, the difference between the measured and simulated hysteresis losses in material sample 1 has a high difference in the opposite direction. Compared to the measured losses, the simulated eddy current losses are overestimated and the simulated hysteresis losses are underestimated.

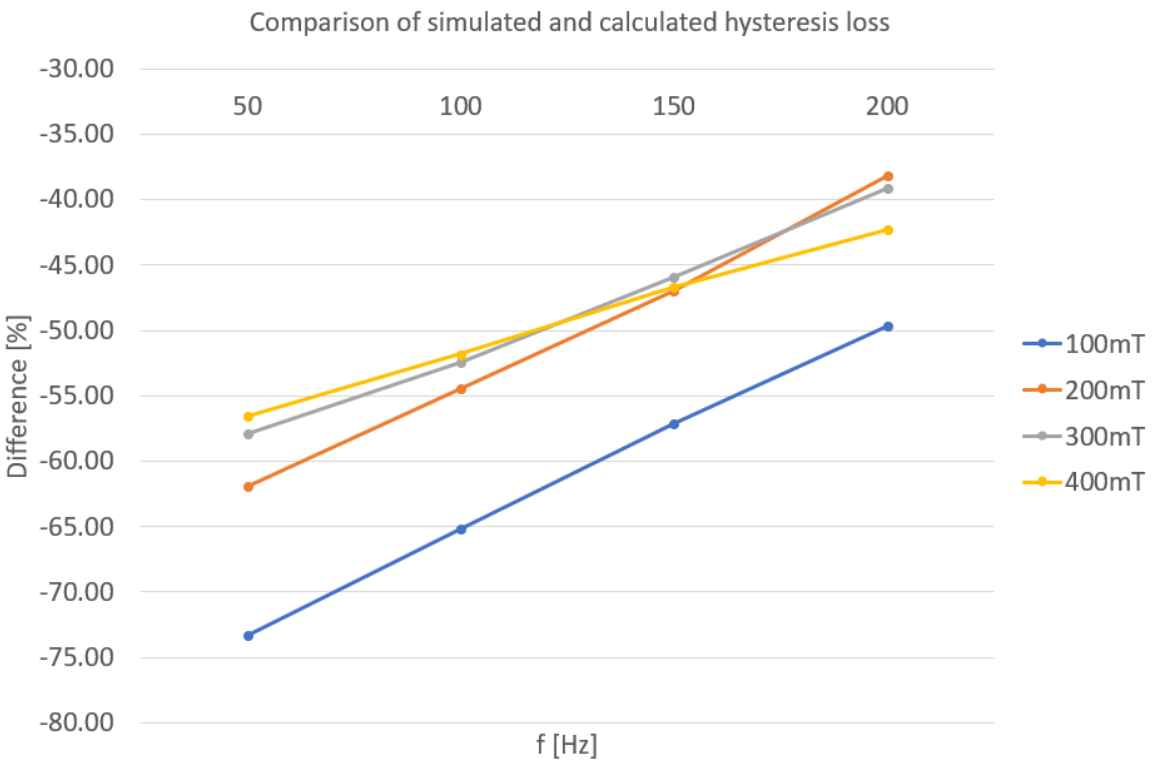

Figure 6.6: Difference between the simulated and measured hysteresis loss in material 1

The hysteresis losses in Figure 6.6 shows that the simulation series of 100mT stands out and has the highest difference of -73.28% at 50Hz. The simulation series of 200, 300 and 400mT have a relatively equal behavior in terms of change in magnetic flux density and coil current frequency all in the range of -61.90% at 50Hz to -38.12% at 200Hz.

6.3.2 Measured and simulated hysteresis and eddy current losses for material 2

The total simulated losses in material sample 2 are overestimated compared with the measured losses. Figure 6.7 shows the comparison of the simulated and measured eddy current losses in material sample 2.

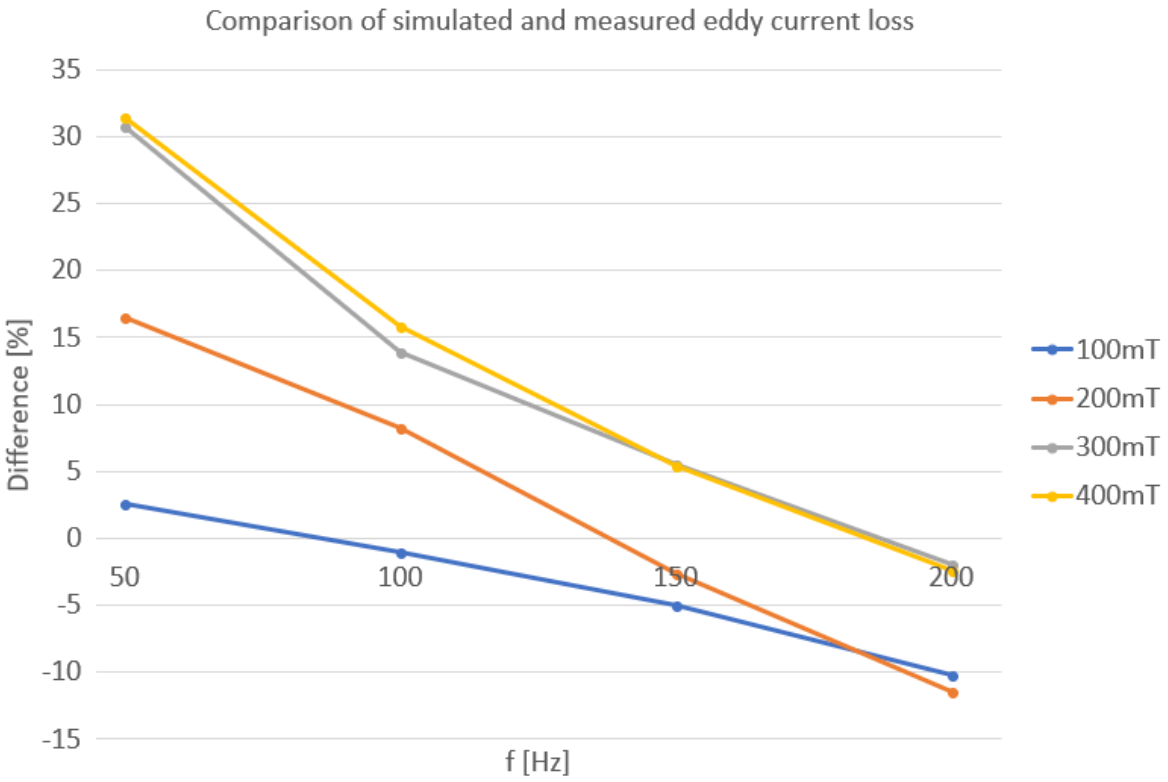

Figure 6.7: Difference between the simulated and measured eddy current loss in material 2

The differences between the measured and simulated losses are in the range of 31.48% to -11.44% and decreases as the frequency increase. Compared with the difference between measured and simulated eddy current losses form material sample 1 (3.06% to 151.55%), the range is concentrated in material sample 2.

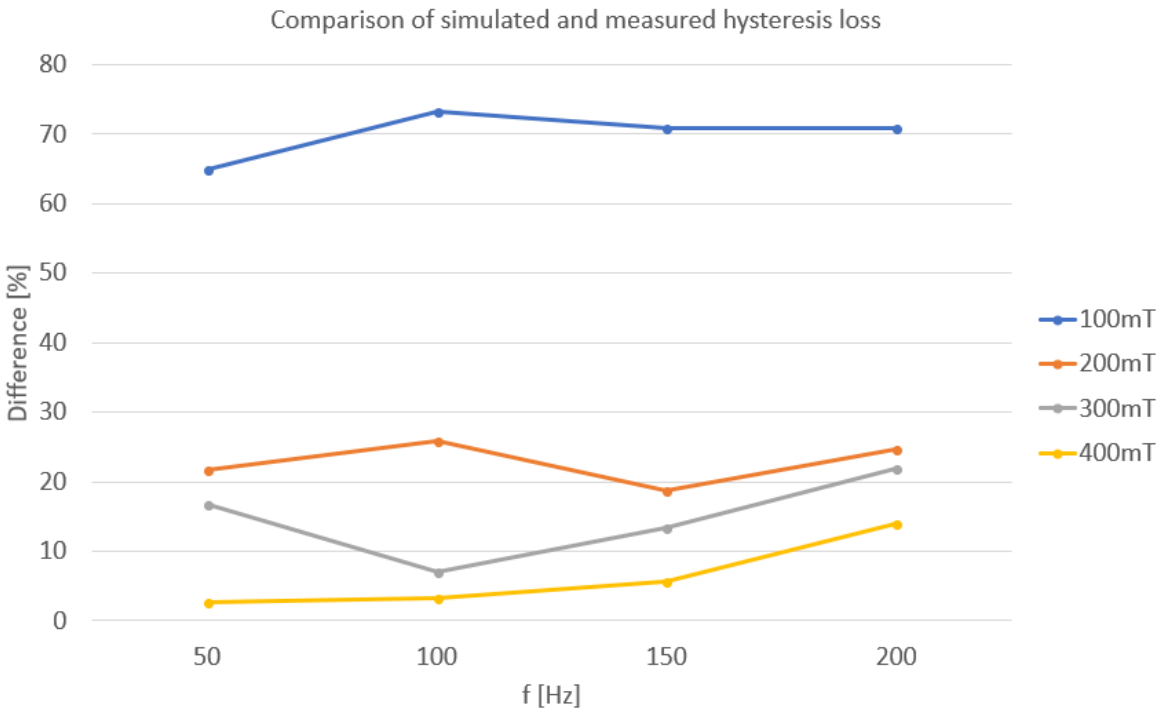

Figure 6.8: Difference between the simulated and measured hysteresis loss in material 2

Figure 6.8 displays the comparison of the measured and simulated hysteresis loss in material 2. The difference in all other measurement series seems to be influenced by the frequency, but not these losses. The difference between the measured and simulated hysteresis losses are approximately constant for the different frequencies, but at different levels depending on the magnetic flux density. Increased magnetic flux density decreases the difference between the measured and simulated loss. The simulated hysteresis losses have a range from the highest difference of 73.26% at 100mT and 100Hz to the lowest difference of 2.6% at 400mT and 50Hz.

7 Discussion

This chapter discusses different aspects of the work performed in the thesis, with emphasis on encountered challenges and factors that have undesired impacts on the results derived in the thesis. Uncertainties are addressed in combination with suggested improvements suited for future work.

7.1 Introduction and theory

The scope of the thesis is broad and indicates an experimental approach. It was not clear regarding how to solve the main challenges in the problem description. The potential challenges were not sufficiently mapped out and the thesis quickly became extensive and covered a lot of different topics. The topics covered by the thesis varies from developing a software, developing a FEM model and performing measurements with advanced measuring equipment. The invested time in the thesis exceeded the scope of expected work hours at the level in which the thesis is written. The quality of each topic could have been improved by limiting the topics.

The main goal with the thesis was to develop a FEM model and compare simulated losses with actual measured losses in material samples. The initial idea was that the work, including the development of the verification model, could be performed with a relative high degree of ease. This turned out to be the main challenge in the thesis work.

The application areas of the work performed in the thesis are larger than the initial motivation for the thesis, which was direct electrical heating of oil pipes on the seabed. Many of the topics investigated in this thesis are generally valid in several applications. Either in terms of power dissipation in heating applications or in loss efficiency calculations regarding electrical machines.

7.2 The development of JAMPS

The initial script demanded extensive knowledge in Matlab programming and yielded a limited result. This was improved dramatically in the Jiles-Atherton method parameter search (JAMPS) software when the graphical user interface was implemented. The software can be distributed as a Windows application with a setup file. Handling input files directly in the software eliminated all requirements of programming skills.

Due to the time constraint of the project and the large variety of topics that needed to be covered, the software development was finished when the functionality was deemed satisfactory for this application. During the characterization of the materials a few errors (known as bugs) were

encountered. The origin of the bugs was not examined thoroughly as they were inconsistently appearing with relatively long time intervals. The interruption was not regarded as critical because of the few attempts needed to perform the calculations. The bug seemed to be related to the number of measurements as the error occurred with a high number of measurements in loops without a reduction in JAMPS. The error was not consistently caused by the high number of measurements in the loops. For some loops with a high number of measurements, the calculations were performed with ease.

The initial parameters, used as the first guess in the optimization code, have a large influence on the values under investigation. The algorithm tries to check several variations, but the initial values determines the computation time and iterations needed in JAMPS to determine a set of parameters. Any set of initial values will provide a set of parameter values, but a method for determining initial parameters that are closer to the solution would be beneficial.

The simulations were frequently interrupted due to a run-time error. This caused a significant delay in the thesis work because there was no indication of what caused the run-time error. After a lot of trouble-shooting, it was discovered that there are parameter values generated in JAMPS which theoretically is a valid solution but causes a 'zero matrix' problem in Comsol. This problem occurred if the parameter c in the Jiles-Atherton method became less than 0.05. The recommended range for the c parameter is 0 to 1 and this presented some challenges when selecting the initial condition. From experience, the computation time per iteration increased exponentially with an increase in the initial parameter value of c.

The improvement method embedded in the software is a practical and close to necessary function to obtain usable parameter values. There are many local solutions that are found in the software as the parameter values get tuned in with several decimal points. The solution is not able to improve the parameter values by increasing the number of iterations if the local minima is encountered. The improve function not only uses the previous solution as initial values for the next optimization round, but it has to change the values slightly by rounding the numbers. The optimizing algorithm embedded in Matlab makes extreme parameter value guesses during the first iterations and with fewer decimal places it reduces the chances of obtaining the same local minima.

The critical part of the objective function is the term where the difference between the measured and simulated B-field value is of great importance. The expression is inspired by the well-known least square method, but it is modified to drastically change the objective function value if the difference increase. This is especially useful during the first iterations in the optimizing

process because this is when the difference between the measured and simulated loop is largest. The expression is not mathematically proven to give a faster or more accurate solution than other methods. Thus, it could be useful to investigate if other expressions or methods can improve both computation time and quality of the Jiles-Atherton parameter values.

There is a strong correlation between the selected curves, in the JAMPS software, and the error in the simulation result. It is clear that curves within a certain flux density span are desirable and corelated with the desired flux density in the simulation. The Jiles-Atherton modelling must be done with care and knowledge about the flux density to be simulated.

7.3 Measurement performed on the magnetic steel rod

There are several factors that can be the source of errors and offsets in the work performed in this thesis. There will always be uncertainties and inaccuracies related to measurements where a high level of precision is needed. The conductivity of the rod was to be calculated based on measurement of the resistance in the magnetic steel rods. The resistance is low in the rod materials and a potential error in the measurements would influence the validity of the simulated losses. The first calculated conductivities were wrong by a factor of 10 due to a flaw in the calculations. This caused a lot of problems and was discovered first after several simulations. The model development based on these values was disregarded.

The uneven contact surface between the rod and core in the measuring sensor influences the validity of the measurements due to the introduction of airgaps. These airgaps change the reluctance of the magnetic circuit significantly and is difficult to model. It is assumed that this is the main reason for the high degree of difficulty to obtain a relative flux density in the core that yields the target magnetic flux density at a given coil current in the simulation.

The measured weight of the rod samples is significant in the calculation of the specific losses. The sensitivity of the scale can potentially introduce errors in the simulated losses, but it does not compromise the validity of the loss comparisons. The calculation of the specific losses is based on the measured weight in both the simulation and in the measurement. This can possibly introduce inaccuracies compared with the actual loss, but the error would be equal in both the simulated and measured loss. Thus, the values are still valid for comparisons used to determine the level of loss replication.

The rods did not have a constant thickness, which influence the rod volume used in the FEM model. The effect of a varying thickness was neglected in the FEM model due to the assumable low impact on the results. This is however something that can introduce small inaccuracies in

the simulation. Ideally the rods should be perfect cylinders, but it cannot be guaranteed that the rods are perfectly straight due to the lack of appropriate measuring equipment.

The investigated materials are of an unknown type and this caused some challenges. The materials are assumed to be isotropic and non-oriented in this thesis. This is to simplify the simulation by having the same material description in all spatial directions. It reduces the number of measurements and increase the accuracy of the measurements on the cylinders because the rod orientation is not important during the measurements. Several of the provided rods yielded distorted 'DC-loops' in the measurement results. The reason was not investigated due to the time constraint of the thesis and availability of other rod samples with correct material properties. The distorted loops were used initially but discarded as the JAMPS software did not manage to find satisfying Jiles-Atherton parameters to describe the material. This resulted in the need for several time-consuming DC-measurements of other rod samples.

Temperature dependencies in the material was not considered due to the limited time scope. The rod measurements are influenced by the temperature, but it is assumed that the temperature in the rod was constant during the measurements of the AC losses. The impact of temperature variations should be considered in future work.

7.4 Development of the FEM model

If there are deviations in the final loss comparisons, despite of a satisfying FEM model, it is difficult to decide if the error is due to the Jiles-Atherton method or if it is the obtained method parameters.

The relative permeability in the core is the parameter to be adjusted in the FEM model to achieve the target flux density in each simulation. This is done because the relative permeability of the core is one of the unknown parameters. The relative permeability combines the airgaps between the core and rod in the actual sensor. This indicates that even if the relative permeability of the core was known, there would be uncertainties regarding the simulated magnetic circuit because of the irregularities in the contact surface (small airgaps). The validity of the FEM simulation could be improved by using a sensor of higher quality, because it is difficult to model the small airgaps due to the poor contact surface in the core.

There is no available documentation of the core in the sensor, but it resembles a sheet core and thus it is assumed to have low eddy current losses. The model of the core is simplified and modelled as a solid material. The conductivity in the core material is set to 1 S/m to prevent the eddy currents in the core from distorting the flux or eddy current in the rod. It is assumed that

this measure will have the same effect as the sheet core. In a more realistic FEM model, the conductivity of the core should be measured and the sheets in the core would be included.

The exact physical size of the core is not possible to measure accurately since the core is incapsulated. The measurements are assumed to be sufficiently accurate, but it will likely introduce a small error in the loss calculations.

The excitation coil in the model is defined as a current source, because it is difficult to obtain a solution with the coil defined as a voltage source. This is a simplification which introduces inaccuracies in the simulation. The source in the measuring sensor is a voltage source which ensured that the flux in the sensor was sinusoidal. When the coil is defined as a current source, the current becomes sinusoidal and the time variation in the magnetic flux is not purely sinusoidal. The distorted flux can be observed in the flux density plot in Figure 5.2 from chapter 5.2.2. This is a numerical issue and can be solved by adding a circuit in Comsol. The development of this circuit was too time consuming and not prioritized as long as the current source showed promising results.

The decaying DC term in the time varying flux density is assumed to be neglectable after the first period due to the phase shift introduced in the coil current expression. The magnetic flux density is not in a perfect steady state due to small variations between the simulated frequencies and flux densities. This small offset will influence the loss calculation and can be improved to a limited extent.

The simulated magnetic flux density is determined by the relative permeability of the core in the model. The time needed per simulation is approximately three hours. The number of required simulations to obtain an acceptable magnetic flux density (±1mT) is considerably reduced if the phase shift is implemented in the coil current. Thus, the time to obtain an acceptable simulated magnetic flux density is significantly reduced.

It was necessary to develop the model in 2D due to the limited computer resources and the total computation time. All FEM models were adapted to Comsol 5.2a and 3 because the simulations were performed on three independent computers simultaneously. One calculation that needed 2 hours was not problematic to overcome. The challenge was the number of simulations needed to develop a trustworthy model and obtaining the relative permeability of the core. This challenge demanded over 1000 simulations with different computation time. If the simulations were to be performed on one computer there would not have been enough time to perform the simulations. The need for manual parameter adjustments after each calculation made it

necessary to monitor the simulations to start new simulations as fast as possible. Thus, the simulations became vary time consuming. This could have been avoided by simulating in batches using a ‘super computer’.

The simulation results can be improved by increasing the number of time steps per period and creating a finer mesh in the model. These measures would improve the simulation results. Measures were made to develop a mesh and time step that gave acceptable computing time and a trustworthy simulation result.

7.5 Simulation result and comparisons

In general, the total losses are simulated with a satisfactory low error in the different scenarios. As mentioned, the B-H loop selection in the JAMPS software is crucial to obtain a satisfactory loss simulation. The B-H loops should be selected based on the desired flux density in the simulation.

There is a significant difference between the measured and simulated eddy current and hysteresis losses. It is an interesting observation that the separated losses have a significant difference, while the difference between the total losses are within an acceptable level.

The total loss is assumed to be without anomalous loss in the simulations because the measuring instrument describes the separated losses without anomalous loss. The size of the anomalous loss is not known and can potentially introduce an error in the simulated total loss.

The total loss is measured and the separated losses are calculated in the instrument software based on the measured total loss. If there is anomalous loss in the measured total loss, the contribution from the anomalous loss would be included in the measured eddy current and hysteresis loss. The anomalous loss in the FEM model is not included in the total loss. This introduces an uncertainty in the results, but it is very difficult to identify this factor. If the simulated total losses are close to the measured total loss, this suggests that the contribution from the anomalous loss is small. The effect of the anomalous losses cannot be discarded while there is a difference between the measured and simulated loss, as described in chapter 6.2.

To investigate the validity of the measured eddy current and hysteresis loss provided by the measuring equipment it was decided to make an attempt to describe the measured losses analytically. The analytical description of the losses is based on the theory presented in chapter 2.2. If the analytical expressions describe the measured losses with a satisfactory low error, the loss separation performed in the equipment software is in accordance with commonly accepted theory. This is the main argument for the work presented in chapter 7.6.

7.6 Comparison of measured and analytically calculated losses

The comparisons between the measured and simulated eddy current and hysteresis losses rely on the validity of measured losses. The arguments and calculations carried out by the measuring equipment software are not provided in the instrument documentation. Thus, the main argument for calculating the analytical losses is to investigate the behavior of the measured eddy current and hysteresis losses. This investigation will give an indication of the validity of the assumption that the anomalous losses in the material are negligible.

The analytical hysteresis losses are calculated based on equation (2.7) presented in chapter 2.2.1 and the analytical eddy current losses are based on equation (2.9) presented in chapter 2.2.2. The analytically calculated hysteresis and eddy current losses are compared with the corresponding measured loss. Thus, the units of the losses have to be equal to perform the comparison. The selected unit is Watt because it simplifies the calculations. The difference [%] between the measured and analytically calculated loss is presented in the following chapters.

7.6.1 Analytical eddy current loss

The analytical eddy current losses are calculated with equation (7.1) for material sample 1 and equation (7.2) for material sample 2.

$$P_{Eddy-Material\,1} = 0.00055791 * f^2 * B^2_{Max-target} \quad (7.1)$$

$$P_{Eddy-Material\,2} = 0.00046328 * f^2 * B^2_{Max-target} \quad (7.2)$$

P is the power, f the frequency and $B_{Max\text{-}target}$ the maximum flux density. The constant, K_e, used in equation (7.1) and (7.2) are displayed in Table 7.1 and includes the volumes of the steel rods. Figures illustrating the comparison between the simulated, calculated and measured losses are shown in Appendix F.

Table 7.1: Parameters for analytical calculation of eddy current loss

$K_{e\text{-material 1}}$	$K_{e\text{-material 2}}$
0.00055791	0.00046328

The constants are determined based on the measured eddy current losses with the Matlab script in Appendix G. The script searches for the optimal parameter value until a convergence criterion or the maximum number of iterations is met (1000). The optimizing script uses the measured eddy current loss to calculate the parameters that express all of the losses with the lowest absolute power difference compared to the measured losses.

The parameter is found based on the measured eddy current losses, thus it is expected that at least one of the analytically calculated loss series should be described with a low error. The parameters should describe all the measured losses to confirm that the behavior of the measured eddy current losses is in accordance with the commonly accepted theory.

The comparison of the analytically calculated and the measured eddy current losses can be found in Appendix E. The overview of the comparison of the analytically calculated and measured eddy current losses in material 1 and 2 will be presented in the following sections.

Material 1

The overview from the comparison of the analytically calculated and measured eddy current losses in material 1 is shown in Figure 7.1.

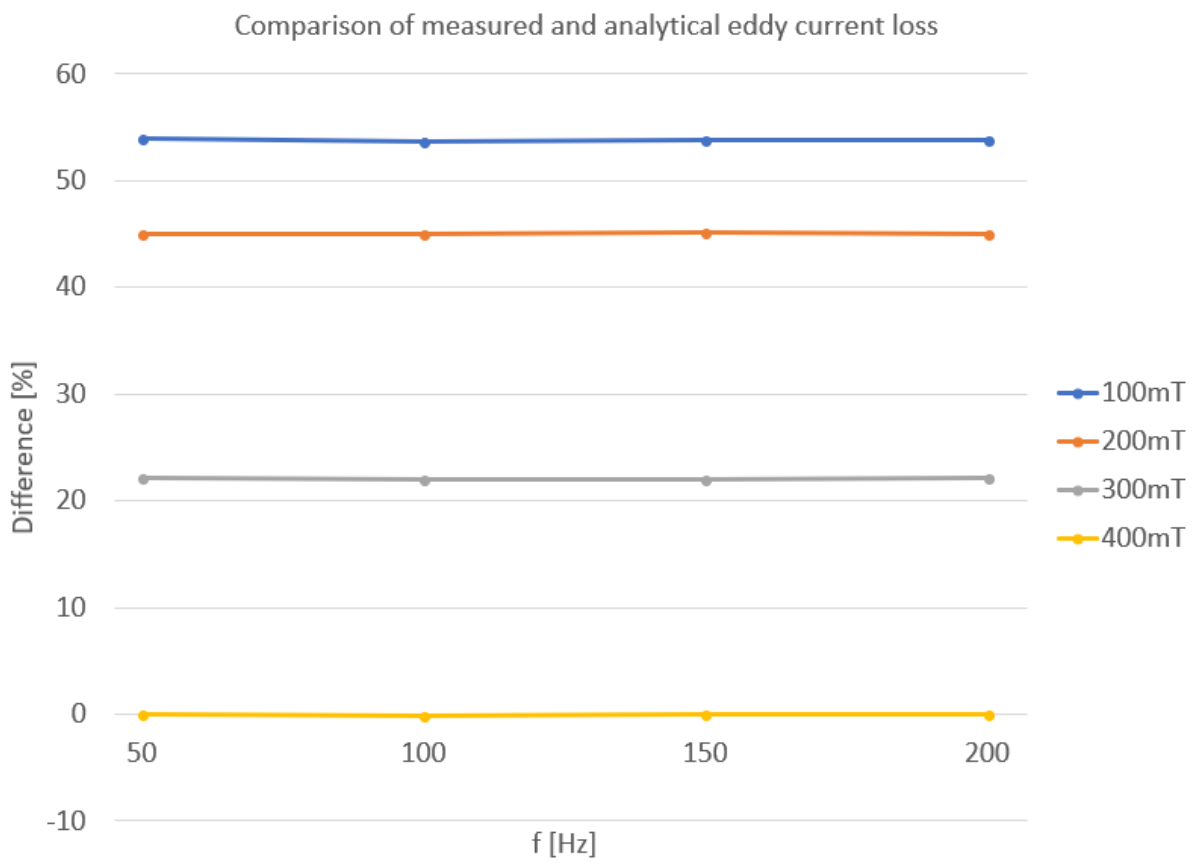

Figure 7.1: Difference between the measured and analytical eddy current loss in material 1

The plot in Figure 7.1 show that at 400mT the analytically expressed loss has a low difference. The parameter in the analytical expression is optimized in Appendix G based on the absolute difference. This indicates that an increase in the difference results in a high absolute difference between the measured and analytically calculated eddy current loss at 400mT.

For the lower magnetic flux densities, the difference is relatively high. The analytical expression of the series at 100mT the difference is approximately 55%. This indicates that the measuring instrument use another method to calculate the eddy current loss.

Based on this comparison, it cannot be concluded that the difference between the measured and simulated eddy current loss described in chapter 6.3.1 is caused by an error in the simulation. There is uncertainty connected to how the instrument calculates the eddy current loss. The difference between the measured and analytically calculated loss is significant. Thus, the behavior of the measured eddy current loss is not in accordance with the commonly accepted theory.

Material 2

The overview from the comparison of the analytically calculated and measured eddy current losses in material 2 is shown in Figure 7.2.

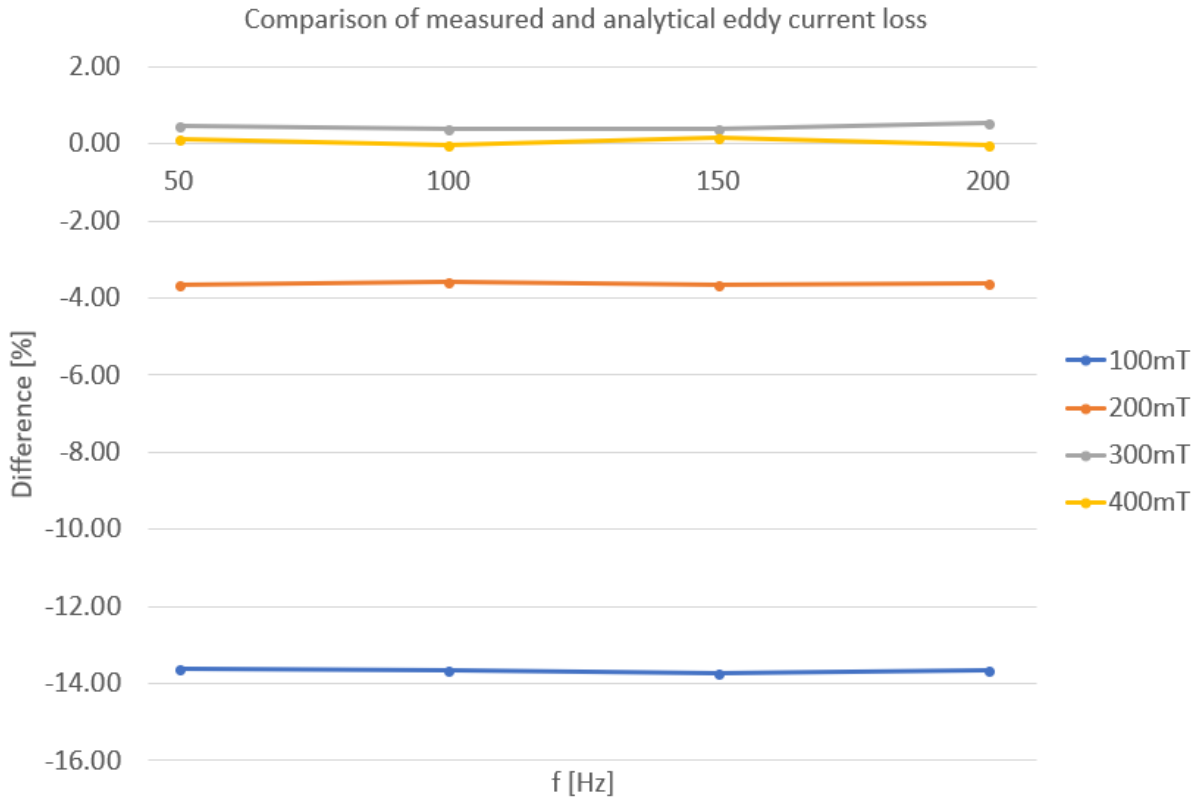

Figure 7.2: Difference between the measured and analytical eddy current loss in material 2

The plot in Figure 7.2 shows that at 400mT the measured loss is expressed analytically with a very low error. The difference is largest in the series at 100mT, with a difference of approximately -14%. In general, the measured eddy current loss is described analytically with a relatively low difference and behaves approximately in accordance with the commonly accepted theory. There is still uncertainty connected to how the instrument calculates the eddy current loss because the method is not provided in the manual describing the measuring equipment.

The low difference between the simulated and measured eddy current loss in material 2, described in chapter 6.3.2, can be explained by a successful loop selection in JAMPS. It can also indicate that there is less contribution of the anomalous loss in material 2, due to the low conductivity compared with material 1, see chapter 3.2.1.

7.6.2 Analytical hysteresis loss

The analytically calculated hysteresis losses are based on the measured hysteresis losses of material sample 1 and 2. Equation (7.3) and (7.4) are used to calculate the hysteresis losses for material sample 1 and 2 respectively.

$$P_{Hysteresis-Material\,1} = 0.022023 * \mathrm{f} * B_{Max-target}^{1.5926} \quad (7.3)$$

$$P_{Hysteresis-Material\,2} = 0.077141 * \mathrm{f} * B_{Max-target}^{2.2839} \quad (7.4)$$

P is the power, f the frequency and $B_{Max\text{-}target}$ the maximum flux density. Table 7.2 shows the constants used to calculate the analytically calculated hysteresis losses based on the measured hysteresis loss.

Table 7.2: Parameters for analytical calculation of hysteresis loss

	K_h	**n**
Material sample 1	0.022023	1.5926
Material sample 2	0.077141	2.2839

The volume of the rod samples is included in the constant K_h. The Matlab script utilized to calculate the parameter values K_h and n in Table 7.2 can be found in Appendix H. The script searches for the optimal parameter values until a convergence criterion or the maximum number of iterations is met (1000). The measured hysteresis losses are used in combination with the corresponding measured magnetic flux density in the Matlab script where the n parameter is in the range of 1.5 to 2.5 [2].

The parameters are based on the measured hysteresis losses. Thus, it is expected that at least one of the analytically calculated loss series is described with a low error. This is however not an indication of the behavior of the measured losses because the parameters should describe all the measured hysteresis losses with the same parameters.

The comparison of the analytically calculated and the measured hysteresis losses can be found in Appendix E. The analytical expression used to calculate the hysteresis losses, found in equation (7.3) and (7.4), is expected to be linear with respect to the frequency. Figures illustrating the comparison between the simulated, calculated and measured losses are shown in Appendix F. The overview of the comparison of the analytically calculated and measured hysteresis losses in material 1 and 2 will be presented in the following sections.

Material 1

The overview from the comparison of the analytically calculated and measured hysteresis losses in material 1 is shown in Figure 7.3.

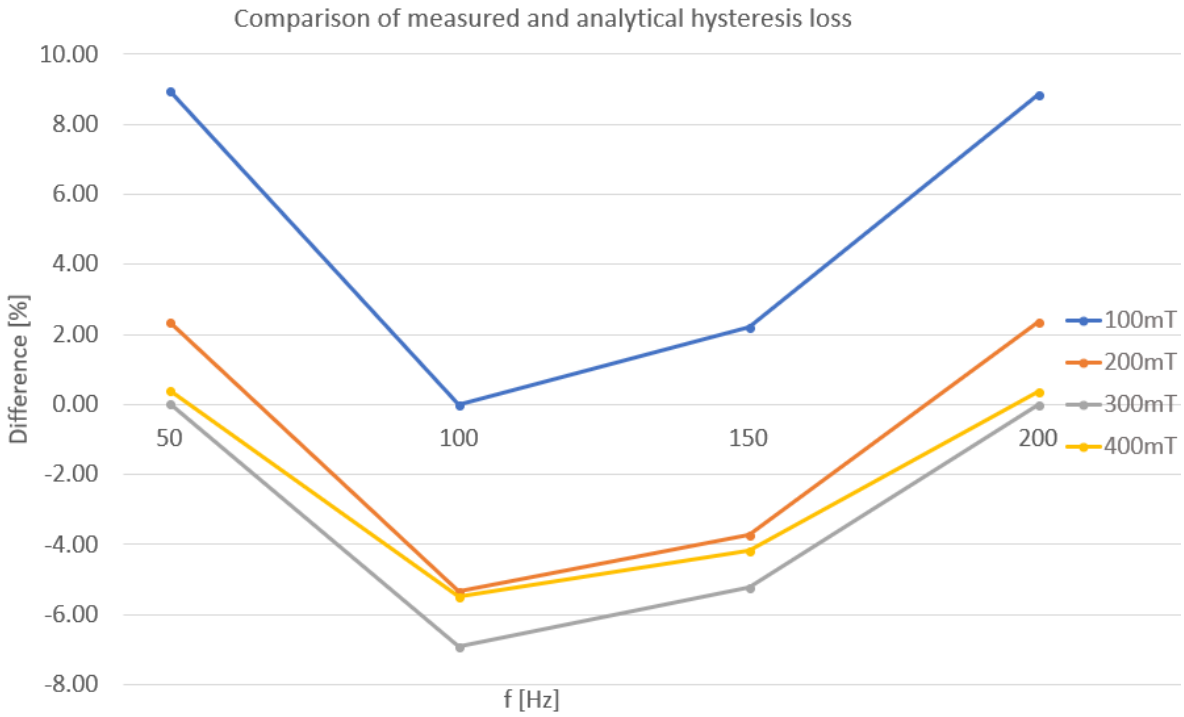

Figure 7.3: Difference between the measured and analytical hysteresis loss in material 1

The analytical expression of the hysteresis losses in material 1 is linear with respect to the frequency. The measured hysteresis losses in material 1 are not strictly linear with respect to the frequency, as shown in Appendix F. This introduce a frequency dependent difference in each measurement series. This can be observed in Figure 7.3 as a U-shape in the plotted difference.

The variation of all series is within ±10%. This result is assumed to be acceptable and the difference between the magnetic flux density series is investigated further. The series of 200, 300 and 400mT have a small difference and behave similar to each other. The 100mT series stands out and has an approximate difference in the range of 5 to 9% compared to the other magnetic flux density series.

The behavior of the measured hysteresis losses in material 1 approximately according to the commonly accepted theory.

Material 2

The overview from the comparison of the analytically calculated and measured hysteresis losses in material 2 is shown in Figure 7.4.

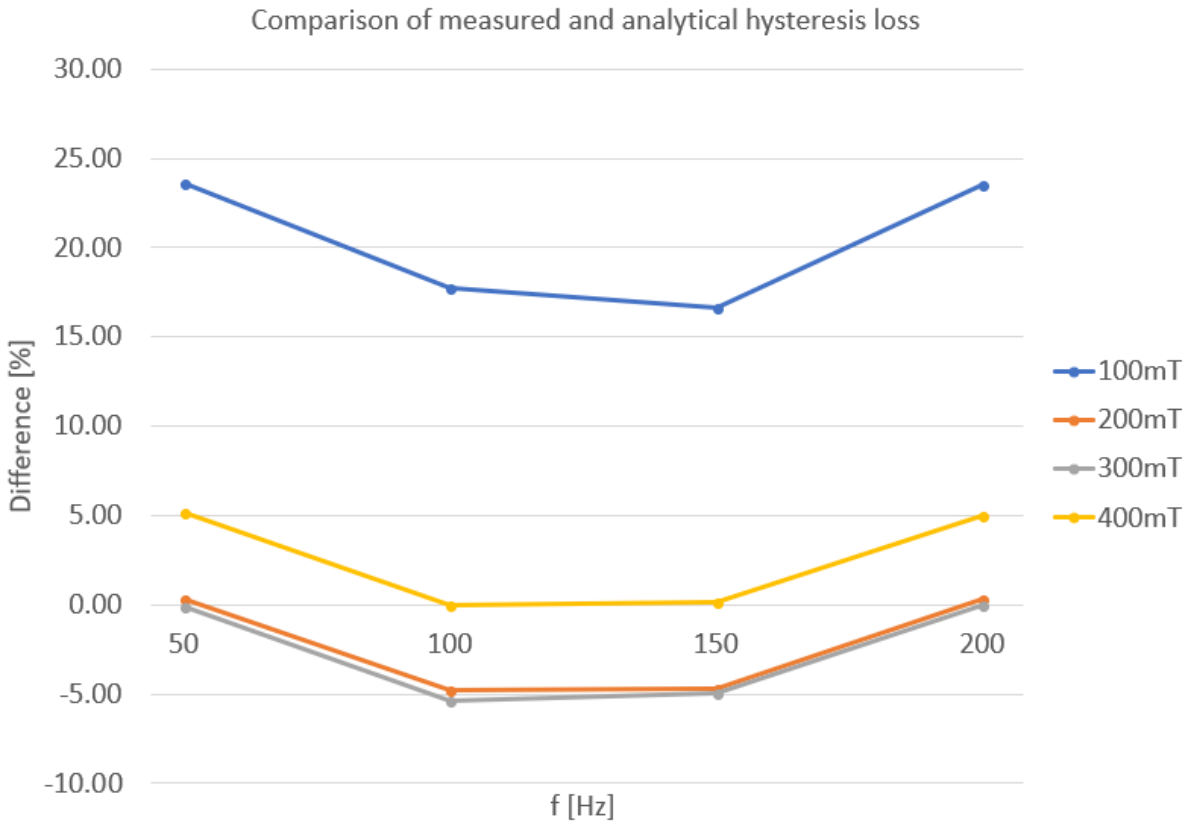

Figure 7.4: Difference between the measured and analytical hysteresis loss in material 2

As described in material 1, the analytical expression of the hysteresis loss in material 2 is also linear with respect to the frequency. The measured hysteresis losses in material 2 is not strictly linear, as seen in Appendix F. This introduce a frequency dependency in the plotted difference,

as shown in Figure 7.4. At 100mT the difference increases with approximately 8% when the frequency increase from 150 to 200Hz. This representation is assumed to be acceptable and the difference between the magnetic flux density series is investigated further.

The series of 200 and 300mT have a small difference and behave similar to each other. The 100 and 400mT series stand out and have an approximate difference relative to the 200 and 300mT series of 5% and 28% respectively.

The measured hysteresis losses in material 2 is not successfully described analytically according to the commonly accepted theory. The difference in the comparison can originate from the FEM model, but it can also be due to the presence of anomalous losses.

7.7 Further work

The recommendations for further work depends on the desired application in which this method is to be utilized.

The 'improvement method' in the software is practical but mainly based on trial and error rather than theory. The objective function can be developed further in terms of developing an improved algorithm that governs the optimizing process. The 'error calculation' in JAMPS should be changed to focus on the individual loops rather than the total error. The optimizing process is uninterruptable in the current version of JAMPS. This is a practical feature that should be added in newer versions.

JAMPS calculates the Jiles-Atherton parameter values based on the DC loops provided as input from the measuring equipment. The software tries to calculate the B-field with the Jiles-Atherton method based on the measured H-field in the DC loops. An 'error' is calculated to indicate the difference between the measured and simulated AC losses. JAMPS can be improved by investigating the correlation between the error and the DC loops. A technique should be developed to decide which DC loops to select as input in JAMPS.

A function for selecting the initial Jiles-Atherton parameter values in the optimizing process in JAMPS should be developed. This could be done with by creating a categorized database with Jiles-Atherton parameter values, DC loop(s) and magnetic flux density range. By using the database, one could also get suggestions about which DC loops to select as input in JAMPS.

There are areas that can be improved in the FEM model. A 'super computer' should be used to reduce the simulation time. This makes it possible to increase the number of time steps and create a finer mesh. An improved description of the core would increase the accuracy, but it

would require a better description of the sensor used in the measurements. An improved comparison of the measured and simulated losses can be done if the physical sensor data and calculations in the MPG-Expert software is known. This could be done by proposing a collaboration with Brockhaus. The JAMPS software is used in combination with DC loops measured with a Brockhaus instrument, implying that both parties would benefit from the hypothetical collaboration.

The method developed in this thesis can be applied to other geometries and materials. The main challenge with choosing other ferromagnetic materials is to account for potential anomalous losses in the FEM model. Simulating different geometries in a FEM model is not necessarily difficult, but the verification of the new geometries need a setup where the losses can be measured and verified.

In theory, it is possible to expand the method to be applied in the description of anisotropic materials (eg. orientated steel). The Jiles-Atherton is applied in Comsol by the superposition principle. Each spatial direction in the material can be defined with a unique set of Jiles-Atherton parameter values. The challenge with this implementation is how the initial DC measurements should be performed to obtain the directional responses. The procedure of obtaining the parameter values can be done as described in this thesis. The amount of work to characterize anisotropic materials would be three times the amount of work required for characterization of an isotropic material (non-oriented steel).

Based on the comparison in chapter 7.6 it is recommended to investigate the anomalous contribution in the total measured loss. If the anomalous loss is a significant part of the total loss, methods for including the anomalous loss in FEM simulations should be investigated.

8 Conclusion

The work of this thesis comprises the development of a software that obtain Jiles-Atherton parameter values for new materials based on measured hysteresis loops. The Jiles-Atherton method should be implemented in a FEM model and verified in terms of comparison of simulated and measured AC losses.

The software 'JAMPS' (Jiles-Atherton Parameter Search) was developed and used as the tool for obtaining the Jiles-Atherton parameters of two different ferromagnetic materials. The verification of the Jiles-Atherton FEM implementation was performed in a Comsol model developed to simulate the measurement equipment used to measure the induced loss in the cylindric material samples.

The measured AC losses in material 1 and 2 were frequency dependent and exponentially increasing with an increase in the frequency. The simulations and measurements were performed with the target flux densities 100, 200, 300 and 400mT at the frequencies 50, 100, 150 and 200Hz. The measured AC losses were used as a reference and compared with the simulated material losses from the FEM model and yielded the following results:

- The difference between the simulated and measured total losses in material 1 is in the range -15% to 5%
- The difference between the simulated and measured total losses in material 2 is in the range 0% to 37%

16 simulations were performed per material, which constitutes 32 different simulations in total. 25 of these loss simulations are within a difference of ±10% compared to the corresponding measured loss. In general, the simulation of the total losses was performed with a satisfactory low error and the implementation of the Jiles-Atherton method is regarded as a success. During the verification process it was discovered that the initial selection of B-H loops in JAMPS is corelated to the accuracy of the simulation of the total loss. There is a potential of improving the accuracy of the simulated total loss if a method is developed to determine which B-H loops that should be used in JAMPS.

A Brockhaus measuring instrument was used to measure the losses. The software in the measuring instrument separates the hysteresis and eddy current losses. These losses were compared with the corresponding simulated losses.

The comparison of the measured and simulated eddy current and hysteresis losses in material 1 showed a significant difference between the measured and simulated losses:

- The difference between the measured and simulated eddy current losses is in the range 3% to 152%
- The difference between the measured and simulated hysteresis losses is in the range -73.28% to -38.12%

The comparison of the measured and simulated eddy current and hysteresis losses in material 2 showed a significant difference between the measured and simulated losses:

- The difference between the measured and simulated eddy current losses is in the range -12% to 32%
- The difference between the measured and simulated hysteresis losses is in the range 3% to 73%

The method used by the measuring equipment software to separate the losses is not provided in the equipment documentation. Thus, an investigation of the separated losses was performed in terms of an attempt of expressing the measured eddy current and hysteresis losses analytically with commonly accepted theory. The separated losses were not satisfactory expressed analytically. This indicates that the difference between the measured and simulated eddy current and hysteresis losses may be due to the presence of anomalous loss. In further work it is recommended to investigate the relevance and possibility of including the anomalous loss in a FEM model.

9 Bibliography

[1] M. E. Tangen, "*Study of frequency dependent loss in carbon steel by the Jiles-Atherton method*", NTNU IME, Specialization project in TET5500. December 2017.

[2] D. C. Hanselman, "*Brushless Permanent Magnet Motor Design*", Second Edition, pp. 19-34. Publisher: The Writer's Collective, 2003.

[3] E. Westgaard, O. W. Andersen and B. Taraldsen, "*Elektriske maskiner*", Chap. 1.9 – "*Jernets magnetiske egenskaper*". Publisher: Norges Tekniske Høgskole, 1982.

[4] C. G. Stefanita, "*Traditional Magnetism*", Chap.: "*Magnetism*", Publisher: Springer Berlin, 2012. DOI: https://doi.org/10.1007/978-3-642-22977-0_1

[5] M. Najgebauer, "*Models for Prediction of Energy Loss in Soft Magnetic Materials*", XXI International PhD Workshop OWD 2010, pp. 477-482. October 2010.

[6] G. Bertotti, "*Physical interpretation of eddy current losses in ferromagnetic materials. I. Thoretical considerations*", Journal of Applied Physics, Vol.57(6), pp. 2110-2117. March 1985.

[7] C. P. Steinmetz, "*On the law of hysteresis*", Proc. IEEE, vol. 72, pp. 196–221, Feb. 1984.

[8] S. J. Chapman, *"Electric Machinery Fundamentals"*, Fifth Edition, p. 29. Publisher: McGraw-Hill Education, 2012.

[9] G. H. Shirkoohi and A. J. Moses, "*Anisotropic dependence of hysteresis and eddy current components of iron loss in non-oriented steels*", Journal of Magnetism and Magnetic Materials, 1994, pp. 440-442.

[10] R. H. Pry and C. P. Bean, "*Calculation of the Energy Loss in Magnetic Sheet Materials Using a Domain Model*", Journal of Applied Physics, March 1958, Vol.29(3), pp.532-533.

[11] K. M Lee, S. Y. Park, M. Y. Huh, J. S. Kim and O. Engler, "*Effect of texture and grain size on magnetic flux density and core loss in non-oriented electrical steel containing 3.15% Si*", Journal of Magnetism and Magnetic Materials, 2014, pp. 324-332.

[12] Y. Gao, Y. Matsuo and K. Muramatsu, "*Investigation on Simple Numeric Modeling of Anomalous Eddy Current Loss in Steel Plate Using Modified Conductivity*", IEEE Transactions on Magnetics, Vol. 48. No. 2, pp. 635-638. February 2012.

[13] F. Liorzou, B. Phelps, and D. L. Atherton, "*Macroscopic Models of Magnetization*", IEEE Transactions on Magnetics, VOL. 36, NO. 2, March 2000.

[14] A. Ladjimi and A. Babouri, "*Modelling of Frequency Effects in a Jiles-Atherton Magnetic Hysteresis model*", Revue Roumaine Des Sciences Techniques-Serie Electrotechnique Et Energetiqu, 2016 Jul-Sep, Vol.61(3), pp. 217-220.

[15] A. J. Bergqvist, "*A Simple Vector Generalization of the Jiles-Atherton Model of Hysteresis*", IEEE Transactions on Magnetics, Vol. 32. No. 5, pp. 4213-4215.

[16] P. Grahn, "*Simulating Ferromagnetic Materials in COMSOL MULTIPHYSICS®*", archived webinar, 2017. URL: https://www.comsol.com/video/simulating-ferromagnetic-materials-in-comsol-multiphysics?wvideo=0w6gpmbyxi. Access date: 02.06.2018.

[17] A. Chen, A. Nysveen and M. Høyer-Hansen, "*Analytical Calculation and FEM Simulation of Electric Parameters of Steel Pipe for DEH systems*", Proceedings of Intermag, 2018.

[18] R. Szewczyk, "*Jiles-Atherton model library fork OCTAVE/MATLAB*", Git repository, 2016. URL: https://github.com/romanszewczyk/JAmodel. Access date: 02.06.2018.

[19] M. E. Tangen, "*JAMPS – Software for determining the Jiles-Atherton parameters based on measured B-H loops*", Git repository, 2018. URL: https://github.com/magtan/JAMPS. Access date: 02.06.2018.

[20] MathWorks, "*Documentation*", The MathWorks, Inc., 2018. URL: https://se.mathworks.com/help/. Access date: 27.05.2018.
[21] Comsol Multiphysics, "*Vector Hysteresis Modeling*", Application ID: 20671, 2017. URL: https://www.comsol.com/model/vector-hysteresis-modeling-20671. Access date: 27.05.2018.
[22] Comsol Multiphysics, "*Eddy Currents in a Cylinder*", Application ID: 128, 2017. URL: https://www.comsol.com/model/eddy-currents-in-a-cylinder-128. Access date: 07.06.2018.

Appendix A: Simplified user manual for JAMPS

Follow the instructions in the installer, shown in Figure 9.1. If the installation is successful, the message in Figure 9.2 will appear. The simplified manual is available as a separate pdf file in [19].

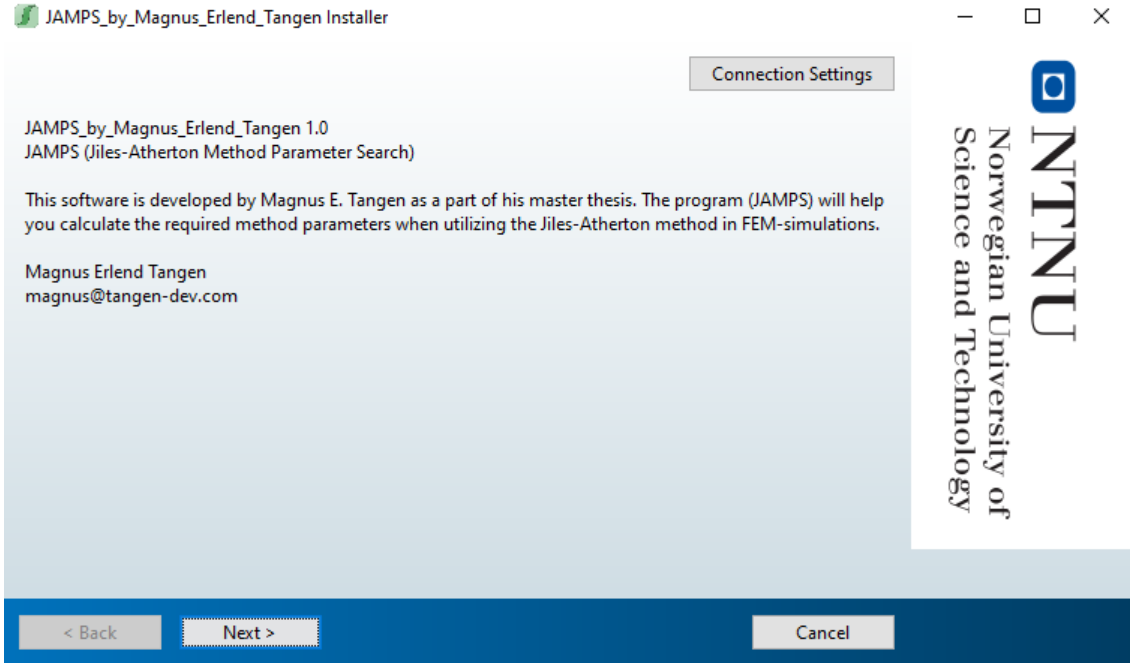

Figure 9.1: JAMPS manual - Installer

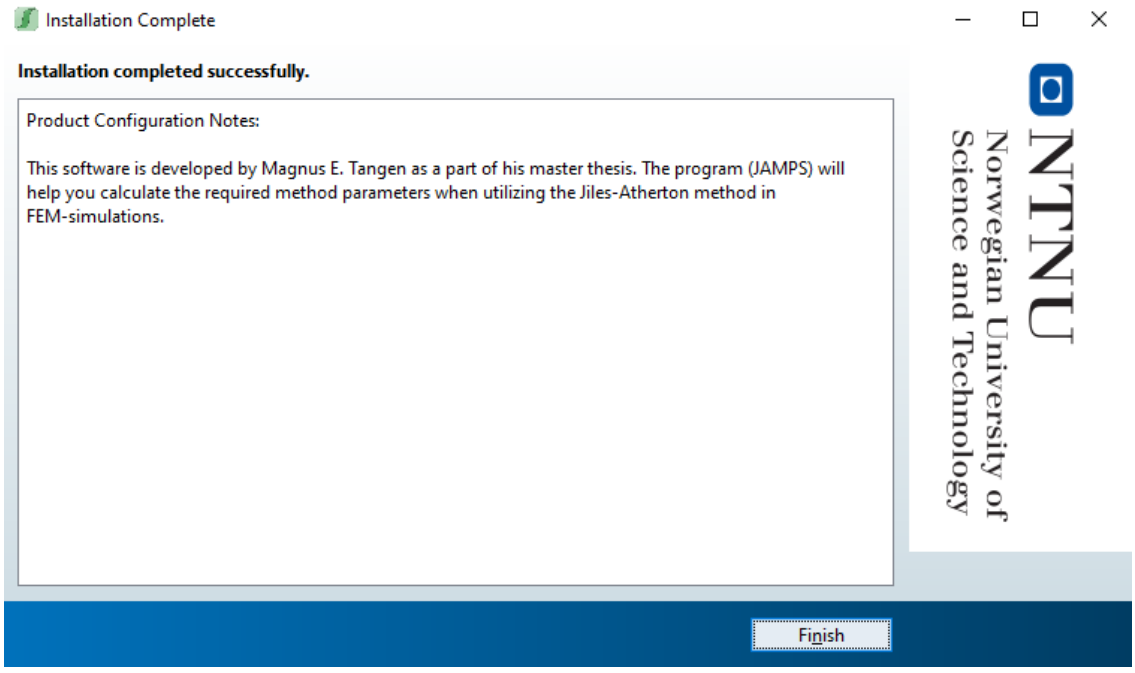

Figure 9.2: JAMPS manual - Installation complete message

Launch the JAMPS software. The guide is always displayed in the upper right corner. The guide describes the visible elements and choices available in the software window, as shown in Figure 9.3.

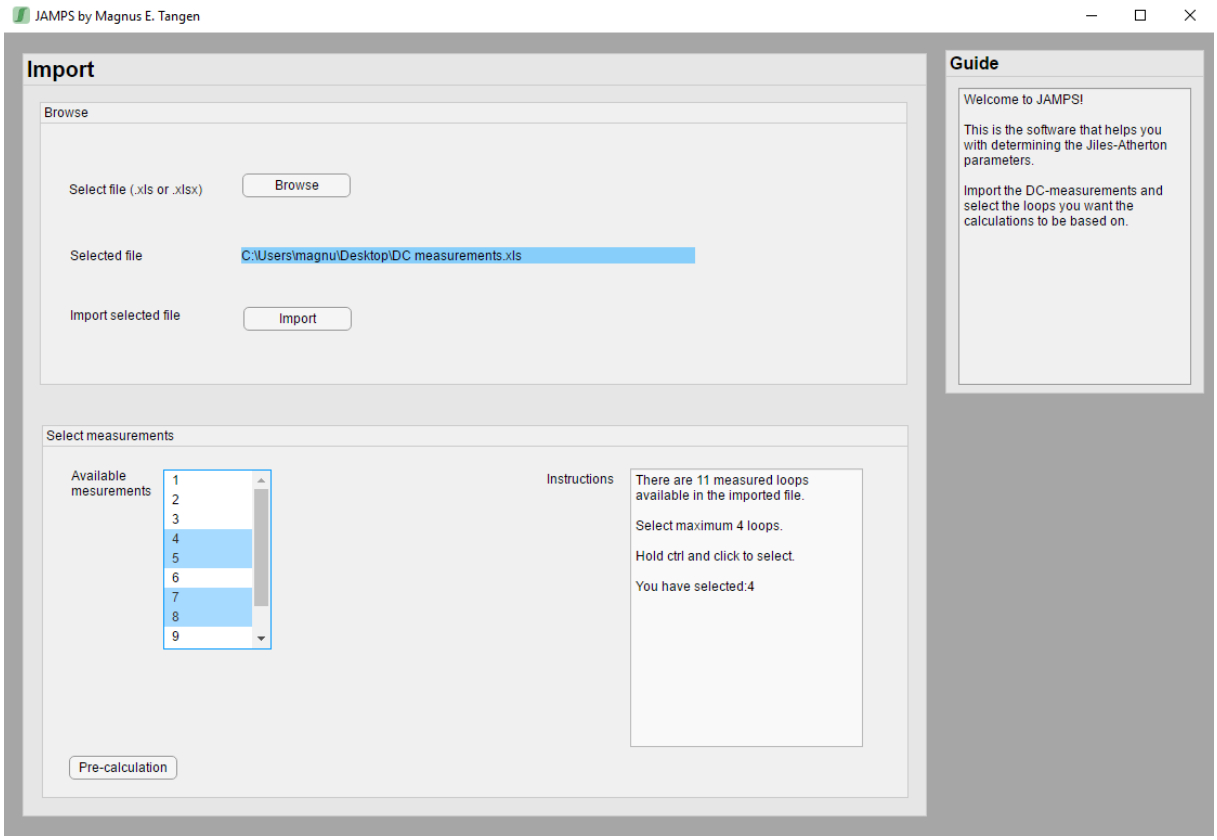

Figure 9.3: JAMPS manual - Import and select hysteresis loops from measurement file

1 Browse -> select a DC measurement file (.exe) -> import.

2 The measurement file often consists of several DC hysteresis loops. The program detects and numbers the available DC hysteresis loops. The numbering is based on when the loops appear in the measurement file. Select the measurements from ‘Available measurements’ by clicking on the number while pressing the ‘ctrl’ button. The program let the user select maximum four measurement sets (loops).

3 Click ‘Pre-calculation’ to proceed to the Pre-calculation, as seen in Figure 9.4.

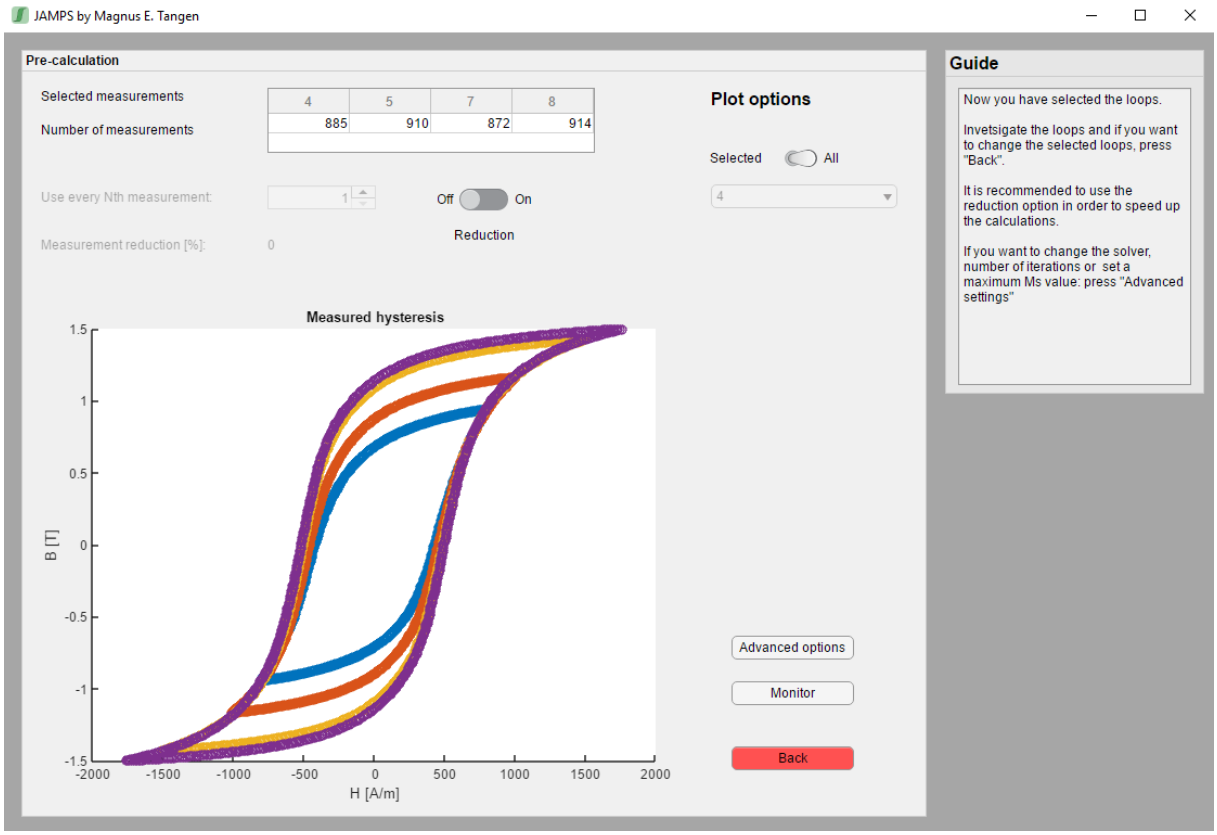

Figure 9.4: JAMPS manual - Pre-calculation page with plotted loops for inspection

Pre-calculation lets the user inspect all selected curves.

1 By flicking the Reduction switch to ‘On’ the number of measurements used in the parameter search can be reduced, as seen in Figure 9.5.

2 By flicking the Plot options switch to ‘Selected’ the selected curves can be investigated separately, as seen in Figure 9.6.

3 ‘Advanced options’ takes you to the advanced options menu, as seen in Figure 9.7.

4 ‘Monitor’ takes you to the optimizing panel where the parameter search can be initiated, as seen in Figure 9.8.

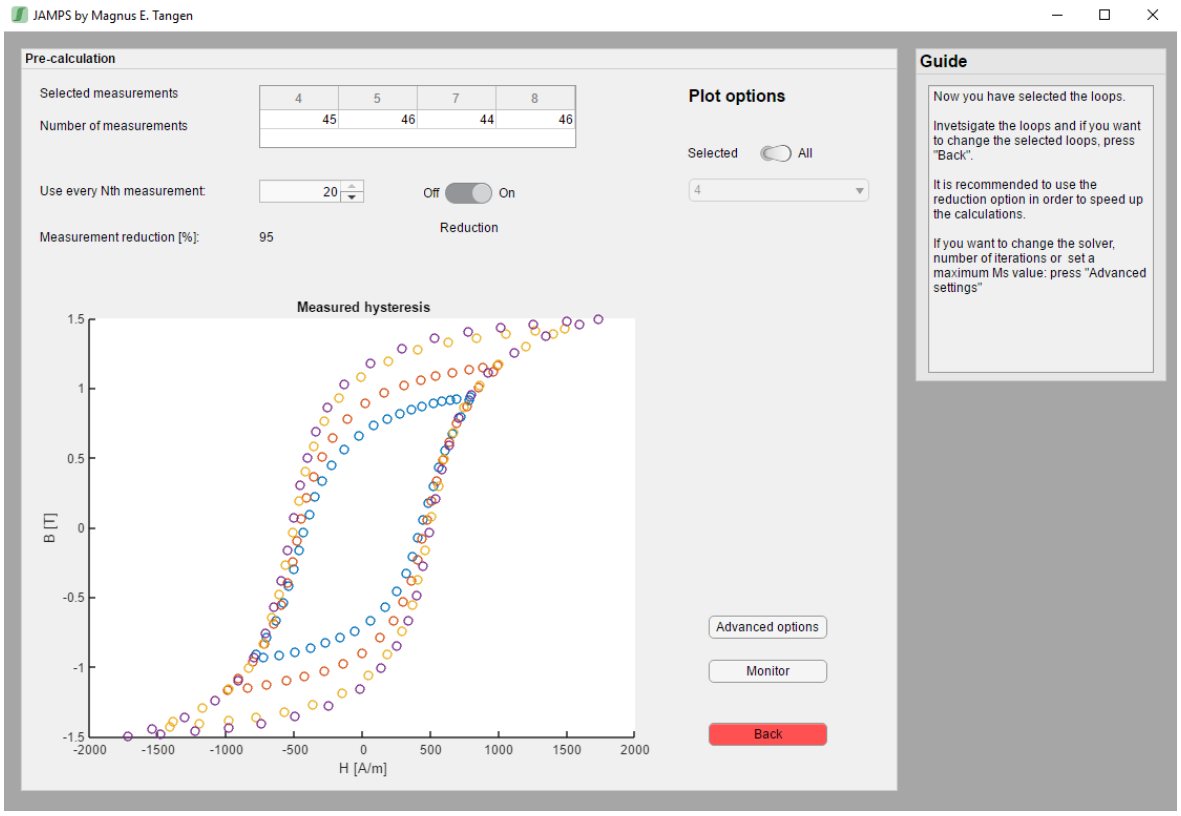

Figure 9.5: JAMPS manual - Reduction of measurements in selected DC hysteresis loops

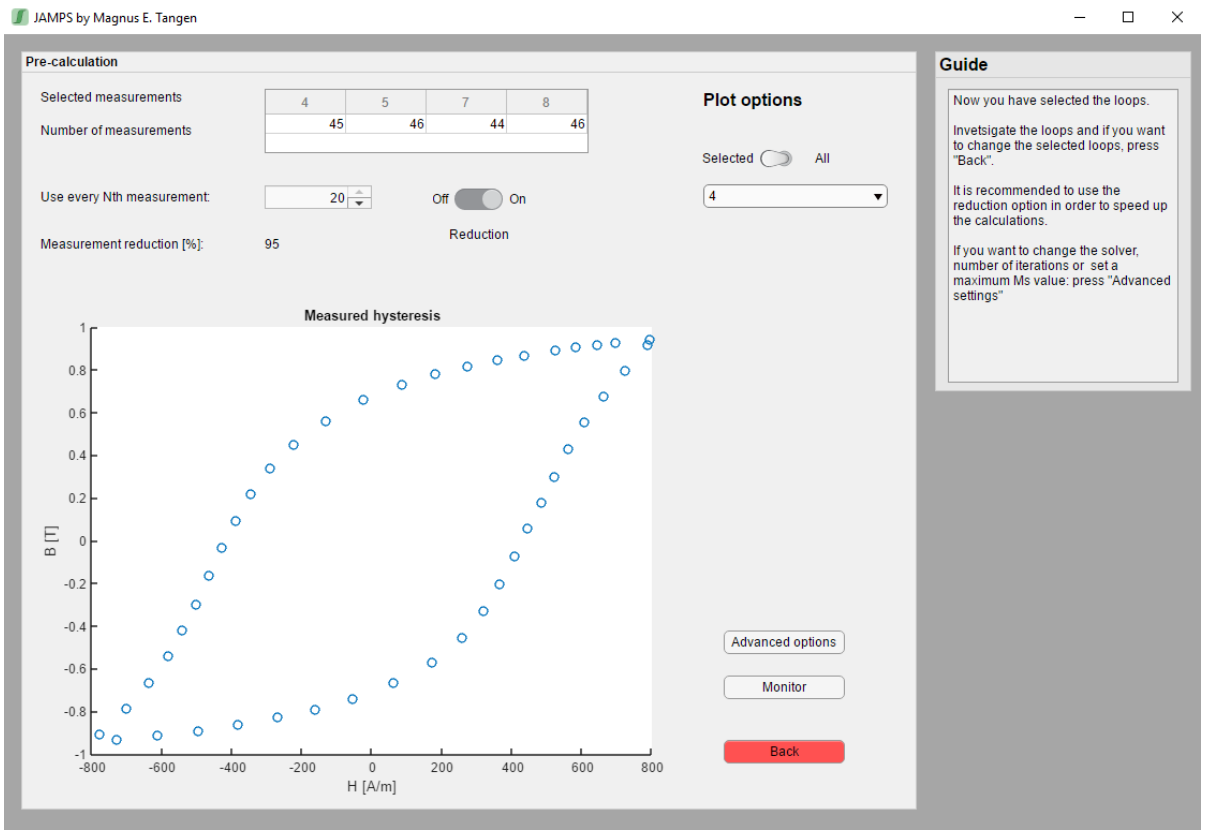

Figure 9.6: JAMPS manual - Individual investigation of selected DC hysteresis loops

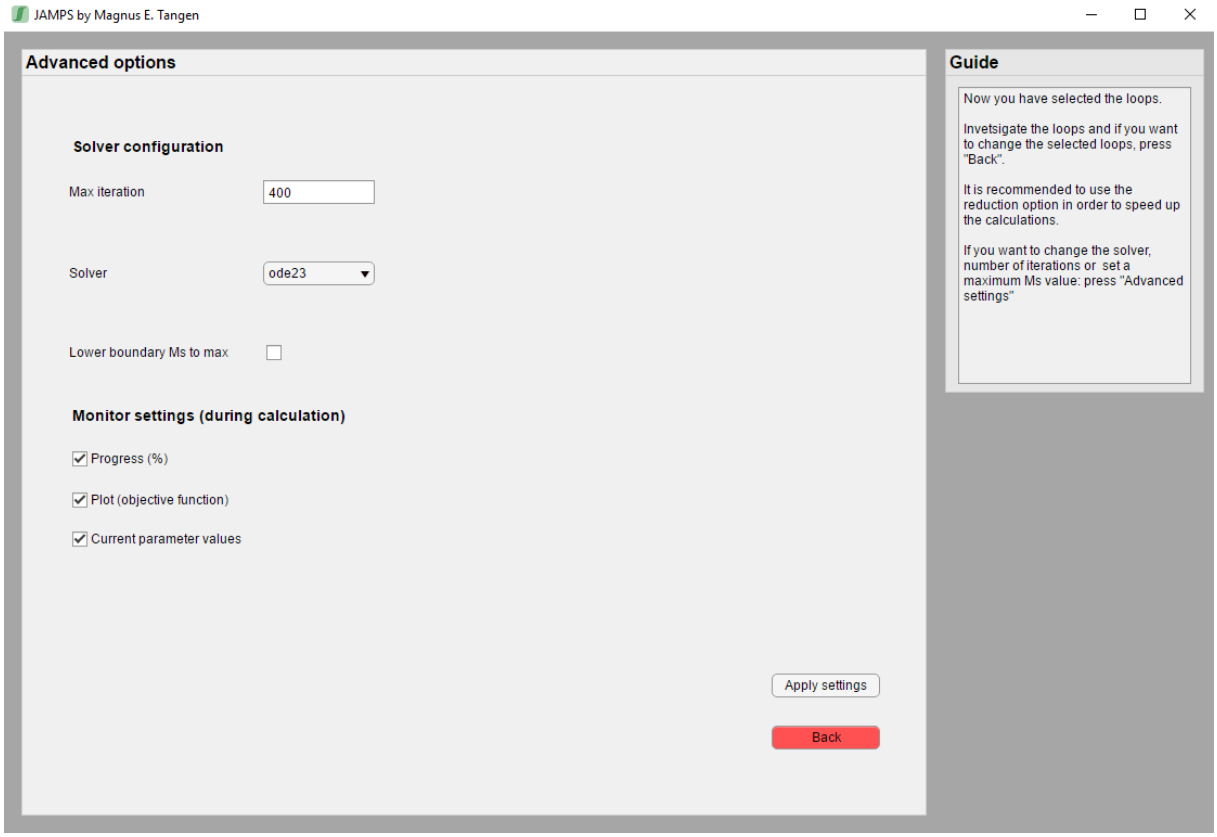

Figure 9.7: JAMPS manual - Advanced settings menu

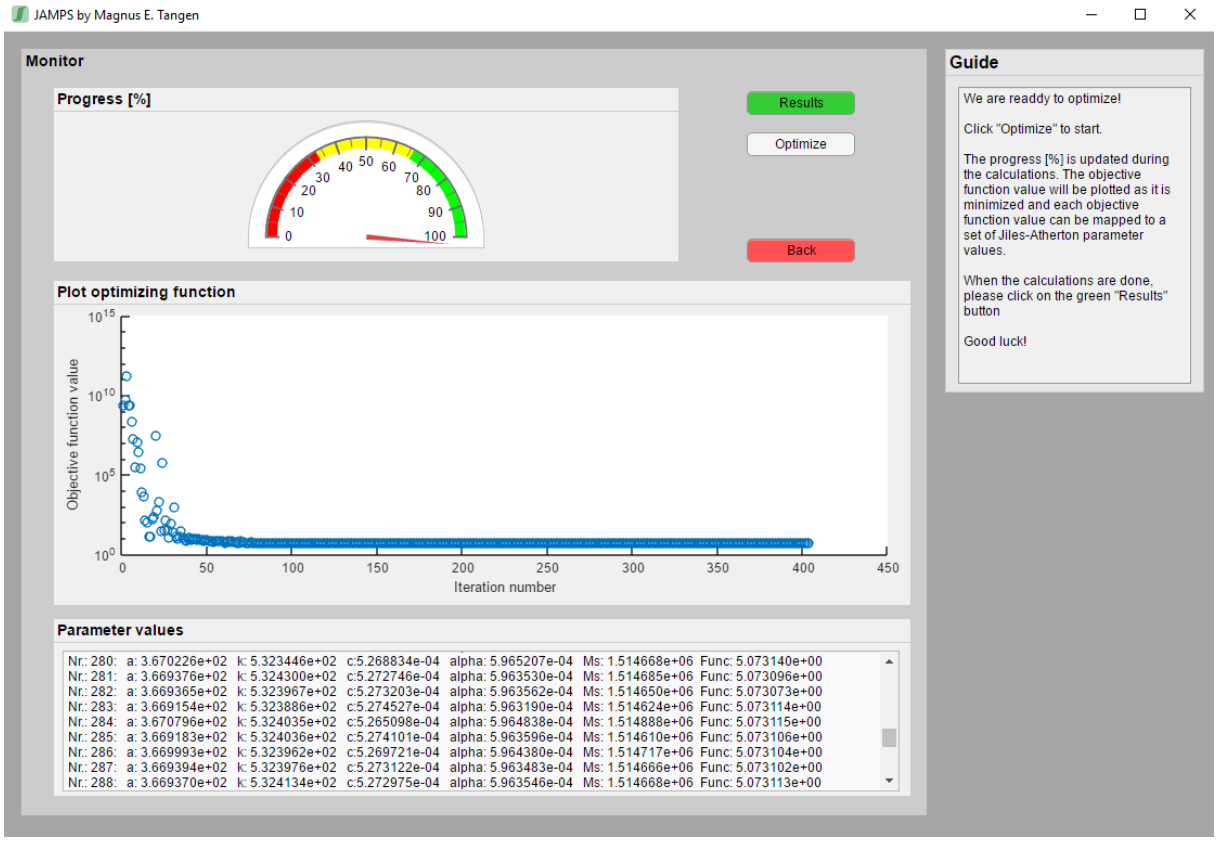

Figure 9.8: JAMPS manual - Monitoring the parameter search

1 The parameter search is initiated by clicking the ‘Optimize’ button.

2 When the simulation is finished the green ‘Result’ button appears. Investigate the results by pressing the ‘Result’ button, see Figure 9.9.

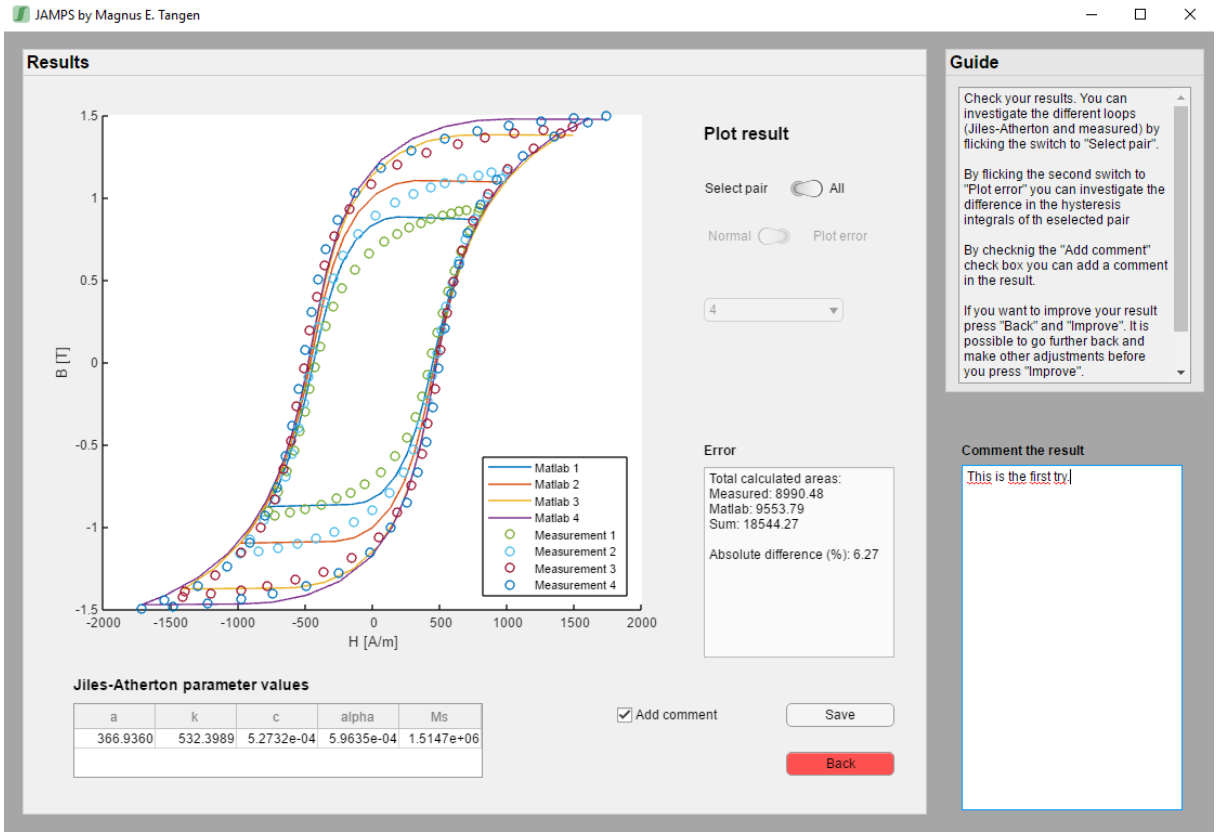

Figure 9.9: JAMPS manual - Parameters and plotted result

1 Investigate the separate loops by flicking the plot result switch to ‘Select pair’.

2 Add a comment by checking the checkbox ‘Add comment’.

3 Save the result by clicking the ‘Save’ button.

Appendix B: Obtaining the phase shift with parametric sweep

Example:

$i(t) = I_{max} \sin(2\pi ft - \varphi)$

Lets say that parametric sweep 1 showed that the phase shift which gave the lowest $B_{max} - B_{min}$ was $\varphi = \frac{25\pi}{48}$

The new range was calculated as follows:

Range max = $\frac{24\pi*3}{48*3} = \frac{72\pi}{144}$ Step = $\frac{\pi}{144}$

Range min = $\frac{26\pi*3}{48*3} = \frac{78\pi}{144}$

Parametric sweep 2 showed that $\varphi = \frac{75\pi}{144}$ gave a better solution.

The final parametric sweep shows that the steady state solution in the flux density is obtained with $\varphi = \frac{151\pi}{288}$

Appendix C: Power loss and H_{max} as a function of rod distortion in the sensor

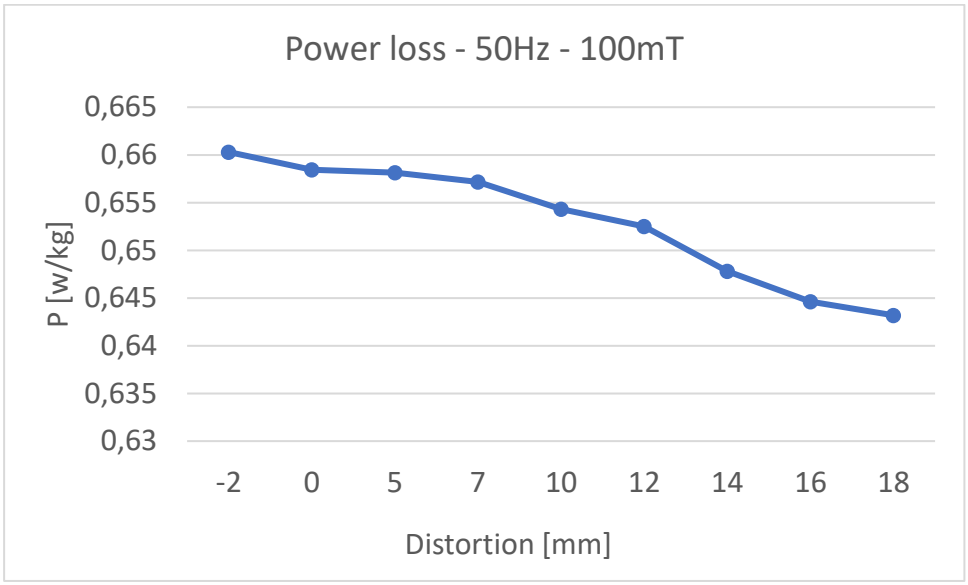

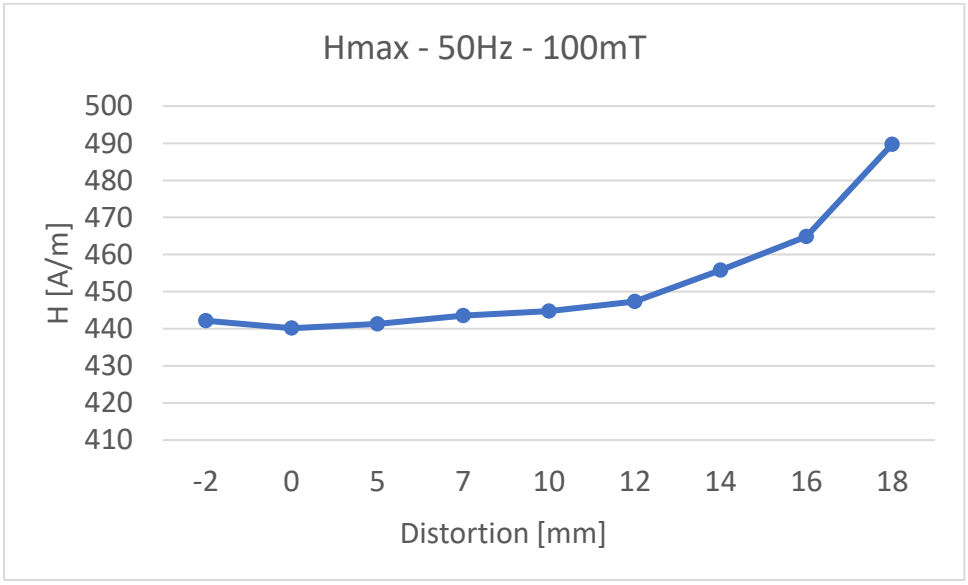

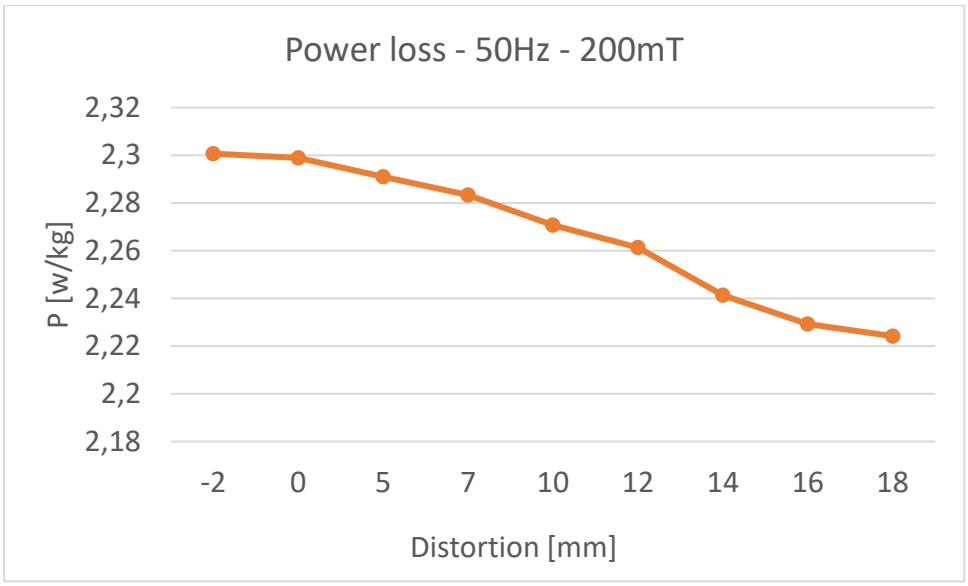
Power loss - 50Hz - 200mT
2,32
2,3
2,28
2,26
2,24
2,22
2,2
2,18
P [w/kg]
-2
0
5
7
10
12
14
16
18
Distortion [mm]

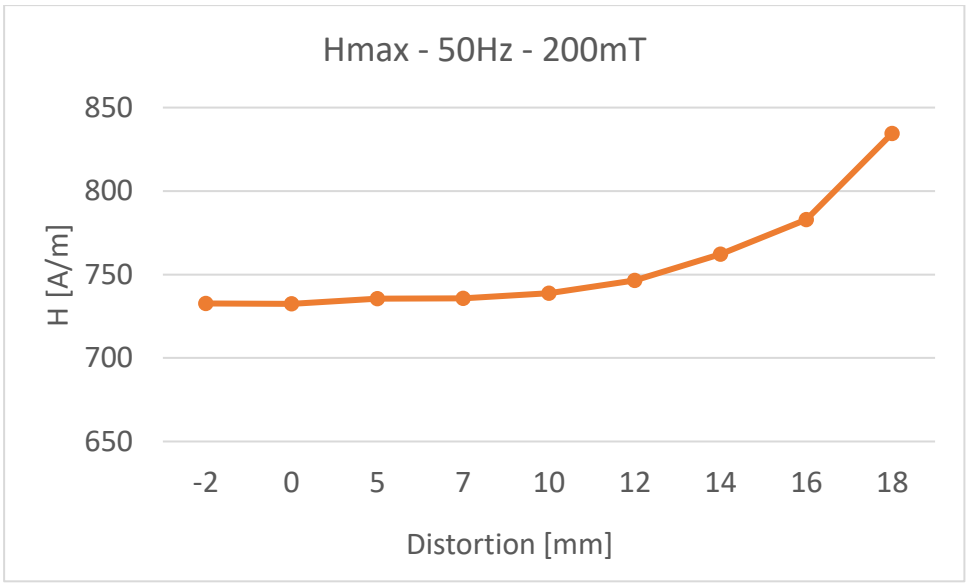
Hmax - 50Hz - 200mT
850
800
750
700
650
H [A/m]
-2
0
5
7
10
12
14
16
18
Distortion [mm]

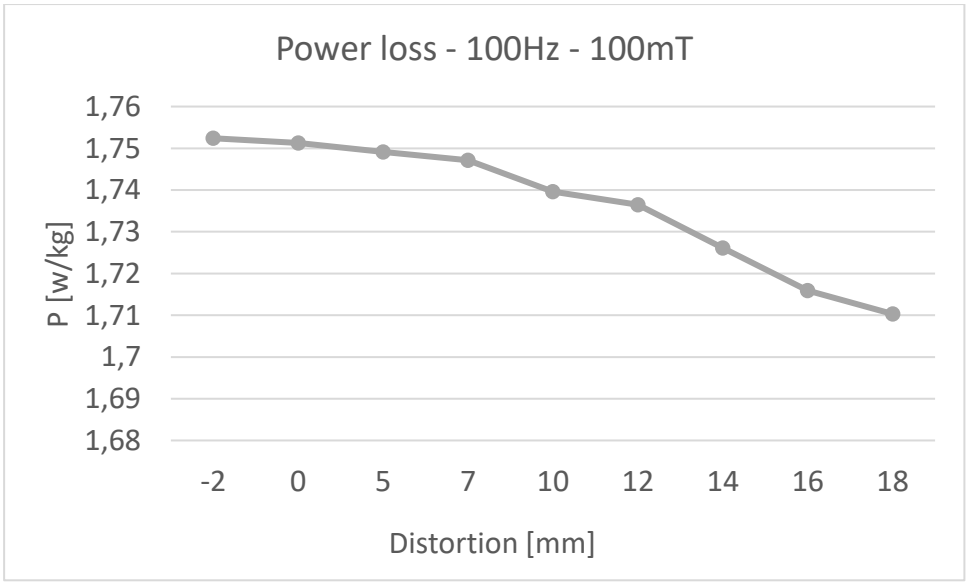
Power loss - 100Hz - 100mT
1,76
1,75
1,74
1,73
1,72
1,71
1,7
1,69
1,68
P [w/kg]
-2
0
5
7
10
12
14
16
18
Distortion [mm]

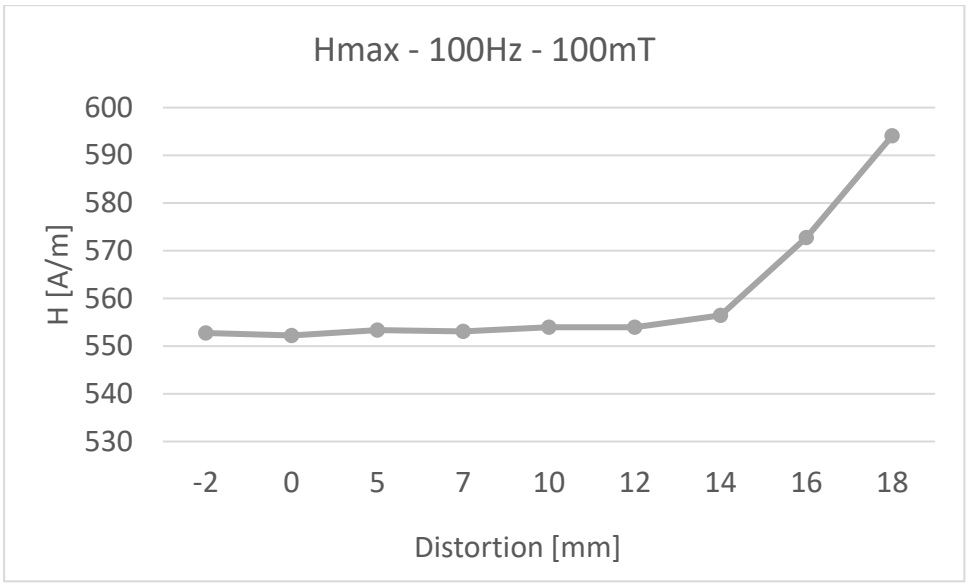
Hmax - 100Hz - 100mT
600
590
580
570
560
550
540
530
H [A/m]
-2
0
5
7
10
12
14
16
18
Distortion [mm]

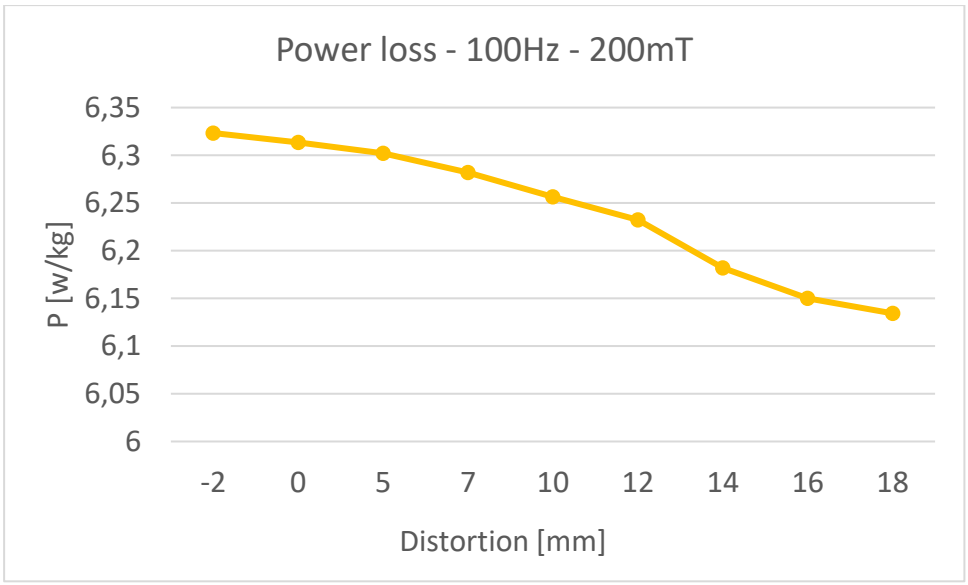
Power loss - 100Hz - 200mT
6,35
6,3
6,25
6,2
6,15
6,1
6,05
6
P [w/kg]
-2
0
5
7
10
12
14
16
18
Distortion [mm]

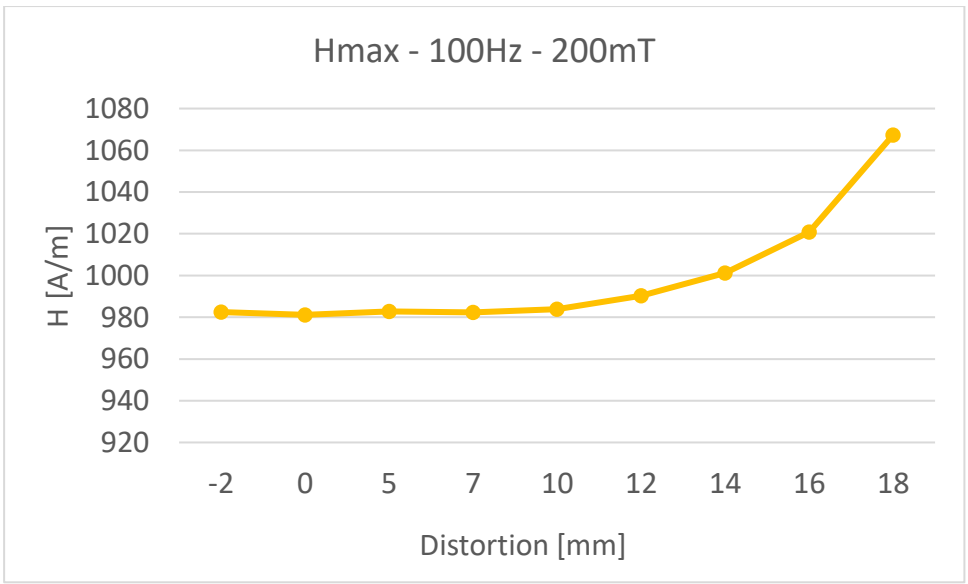
Hmax - 100Hz - 200mT
1080
1060
1040
1020
1000
980
960
940
920
H [A/m]
-2
0
5
7
10
12
14
16
18
Distortion [mm]

Appendix D.1: Simulation results for material sample 1

Simulation result at 100mT average flux density				
f [Hz]	**$P_{tot\text{-}measured}$ [W/kg]**	**$P_{tot\text{-}simulated}$ [W/kg]**	**Difference [W/kg]**	**Difference [%]**
50	0.66	0.56	0.10	-15.04
100	1.76	1.60	0.15	-8.73
150	3.12	3.02	0.10	-3.05
200	4.72	4.72	0.00	0.05

Simulation result at 200mT average flux density				
f [Hz]	**$P_{tot\text{-}measured}$ [W/kg]**	**$P_{tot\text{-}simulated}$ [W/kg]**	**Difference [W/kg]**	**Difference [%]**
50	2.31	2.11	0.20	-8.62
100	6.33	6.09	0.24	-3.77
150	11.60	11.75	-0.14	1.23
200	17.99	18.92	-0.93	5.14

Simulation result at 300mT average flux density				
f [Hz]	**$P_{tot\text{-}measured}$ [W/kg]**	**$P_{tot\text{-}simulated}$ [W/kg]**	**Difference [W/kg]**	**Difference [%]**
50	5.03	4.62	0.42	-8.28
100	14.42	13.58	0.84	-5.85
150	27.30	26.59	0.70	-2.57
200	43.54	42.90	0.64	-1.47

Simulation result at 400mT average flux density				
f [Hz]	**$P_{tot\text{-}measured}$ [W/kg]**	**$P_{tot\text{-}simulated}$ [W/kg]**	**Difference [W/kg]**	**Difference [%]**
50	9.09	8.21	0.89	-9.74
100	27.27	25.25	2.02	-7.42
150	53.40	49.77	3.63	-6.79
200	87.27	81.12	6.14	-7.04

Appendix D.2: Simulation results for material sample 2

Simulation result at 100mT average flux density				
f [Hz]	**$P_{tot\text{-}measured}$ [W/kg]**	**$P_{tot\text{-}simulated}$ [W/kg]**	**Difference [W/kg]**	**Difference [%]**
50	0.59	0.81	-0.22	36.79
100	1.76	2.25	-0.49	27.88
150	3.45	4.06	-0.61	17.70
200	5.60	6.09	-0.49	8.69

Simulation result at 200mT average flux density				
f [Hz]	**$P_{tot\text{-}measured}$ [W/kg]**	**$P_{tot\text{-}simulated}$ [W/kg]**	**Difference [W/kg]**	**Difference [%]**
50	2.92	3.50	-0.58	20.02
100	7.98	9.36	-1.38	17.31
150	14.83	15.77	-0.93	6.30
200	23.23	23.39	-0.16	0.70

Simulation result at 300mT average flux density				
f [Hz]	**$P_{tot\text{-}measured}$ [W/kg]**	**$P_{tot\text{-}simulated}$ [W/kg]**	**Difference [W/kg]**	**Difference [%]**
50	7.03	8.51	-1.47	20.94
100	18.77	20.65	-1.88	10.04
150	34.30	37.42	-3.11	9.07
200	53.06	56.73	-3.67	6.91

Simulation result at 400mT average flux density				
f [Hz]	**$P_{tot\text{-}measured}$ [W/kg]**	**$P_{tot\text{-}simulated}$ [W/kg]**	**Difference [W/kg]**	**Difference [%]**
50	12.80	14.21	-1.41	10.98
100	33.93	36.91	-2.98	8.79
150	62.02	65.44	-3.41	5.50
200	95.71	99.31	-3.60	3.76

Appendix E: Comparison of eddy current and hysteresis losses

Comparison of analytically calculated and measured eddy current losses and measured and simulated eddy current loss. The values in Table 9.1 are the loss difference in percentage of the measured loss.

Table 9.1: Comparison of analytically calculated and measured eddy current loss and measured and simulated eddy current loss

		Material 1		**Material 2**	
f [Hz]	**$B_{max\text{-}target}$ [mT]**	**Analytical [%]**	**Simulated [%]**	**Analytical [%]**	**Simulated [%]**
50	100	54.01	151.55	-13.62	2.62
	200	44.98	106.52	-3.64	16.52
	300	22.15	70.14	0.45	30.81
	400	-0.01	43.88	0.10	31.48
100	100	53.63	79.05	-13.64	-1.02
	200	44.96	55.40	-3.56	8.26
	300	21.99	33.63	0.41	13.97
	400	-0.09	19.57	-0.02	15.83
150	100	53.81	51.85	-13.72	-5.04
	200	45.18	38.21	-3.67	-2.56
	300	22.07	21.49	0.41	5.55
	400	-0.01	9.15	0.16	5.44
200	100	53.87	35.62	-13.67	-10.16
	200	44.98	28.51	-3.61	-11.44
	300	22.13	13.39	0.54	-1.98
	400	-0.06	3.06	-0.03	-2.43

Comparison of analytically calculated and measured hysteresis losses and simulated and measured hysteresis loss. The values in Table 9.2 are the loss difference in percentage of the measured loss.

Table 9.2: Comparison of analytically calculated and measured hysteresis loss and measured and simulated eddy current loss

		Material 1		**Material 2**	
f [Hz]	**$B_{max\text{-}target}$ [mT]**	**Theoretical [%]**	**Simulated [%]**	**Theoretical [%]**	**Simulated [%]**
50	100	8.96	-73.28	23.58	64.94
	200	2.37	-61.90	0.33	21.74
	300	0.02	-57.92	-0.11	16.80
	400	0.41	-56.54	5.15	2.60
100	100	0.01	-65.17	17.76	73.26
	200	-5.33	-54.42	-4.81	25.76
	300	-6.91	-52.42	-5.38	6.93
	400	-5.48	-51.80	0.00	3.32
150	100	2.23	-57.12	16.62	70.81
	200	-3.71	-46.98	-4.68	18.73
	300	-5.22	-45.88	-4.94	13.28
	400	-4.16	-46.64	0.19	5.58
200	100	8.87	-49.70	23.49	70.82
	200	2.37	-38.12	0.36	24.59
	300	0.01	-39.10	-0.01	21.81
	400	0.39	-42.31	4.99	13.86

Appendix F: Plotted comparison of eddy current and hysteresis losses

Material 1 – Comparison of eddy current loss

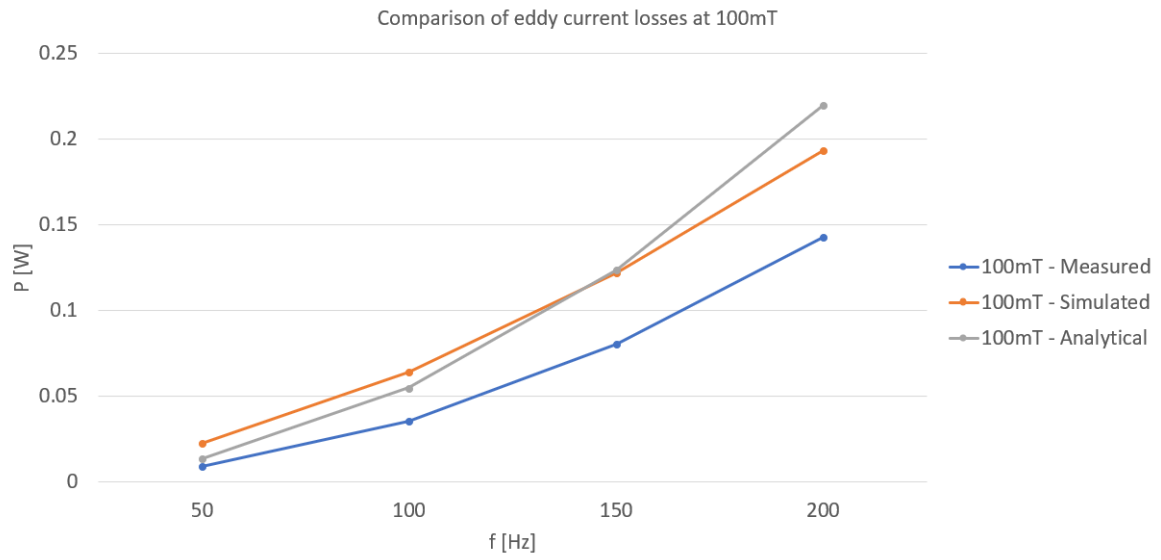

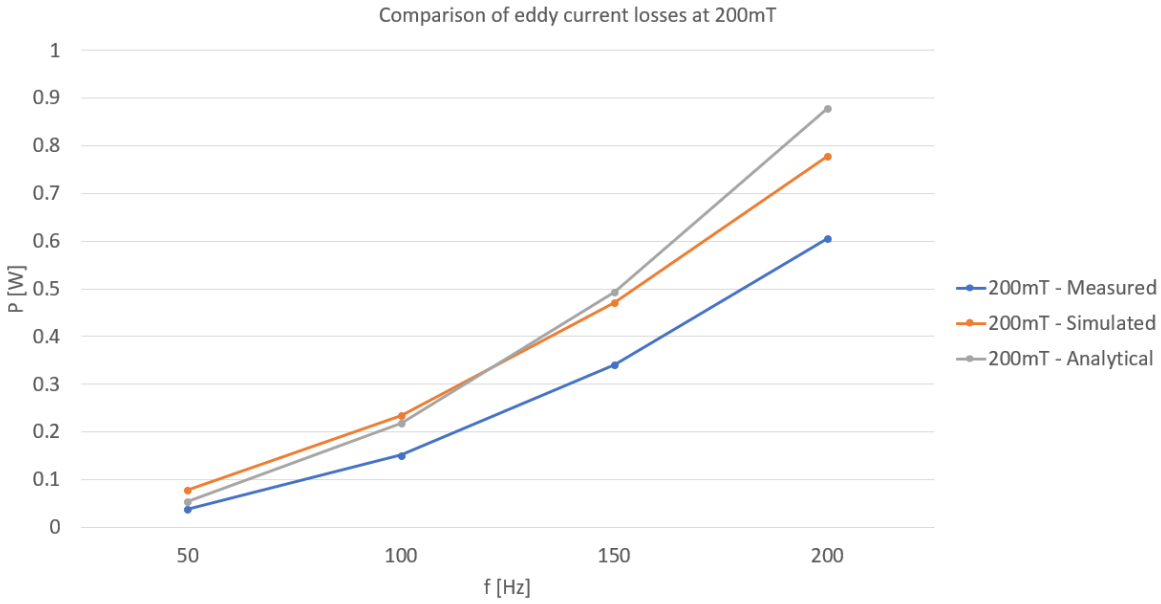

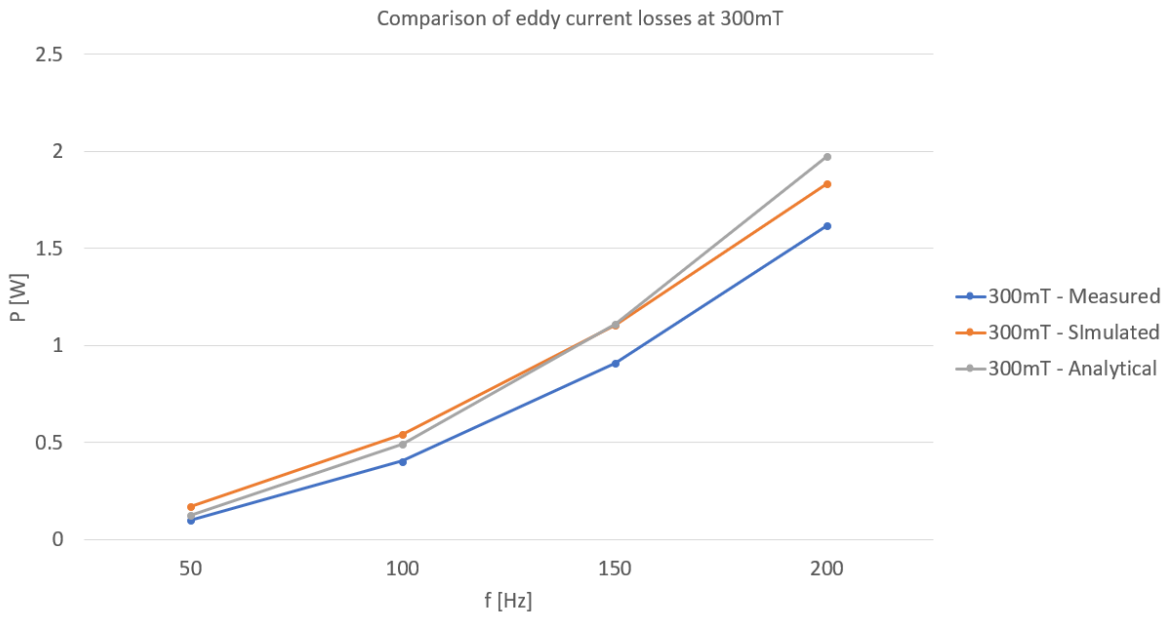
Comparison of eddy current losses at 300mT
2.5
2
1.5
1
0.5
0
P [W]
50
100
150
200
f [Hz]
300mT - Measured
300mT - SImulated
300mT - Analytical

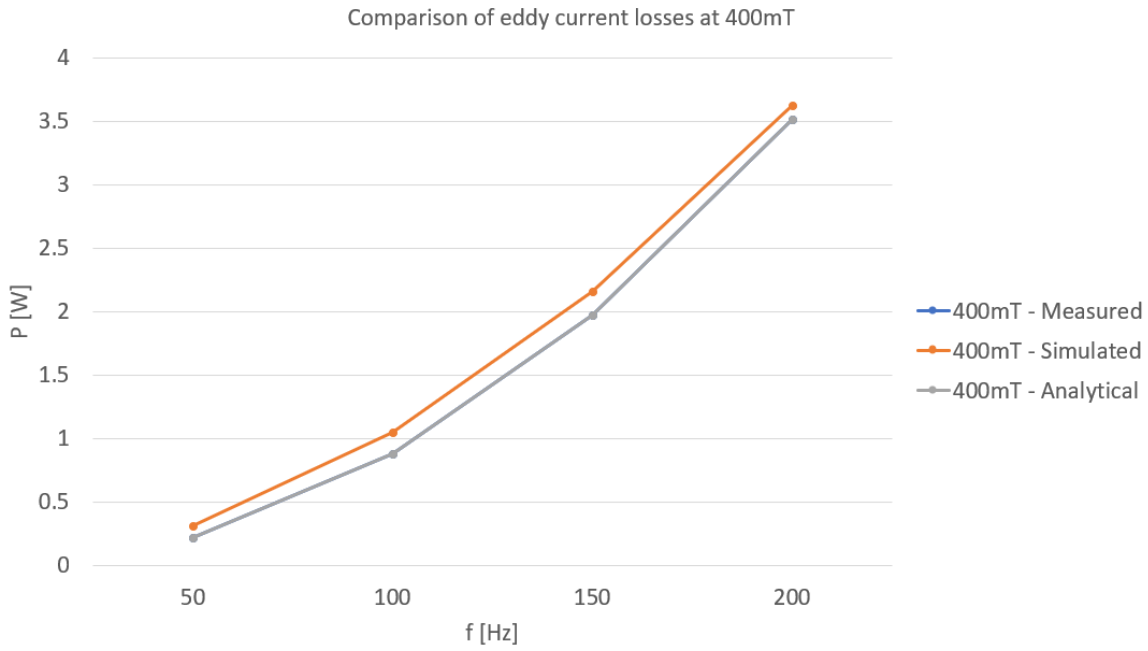
Comparison of eddy current losses at 400mT
4
3.5
3
2.5
2
1.5
1
0.5
0
P [W]
50
100
150
200
f [Hz]
400mT - Measured
400mT - Simulated
400mT - Analytical

Material 1 – Comparison of hysteresis loss

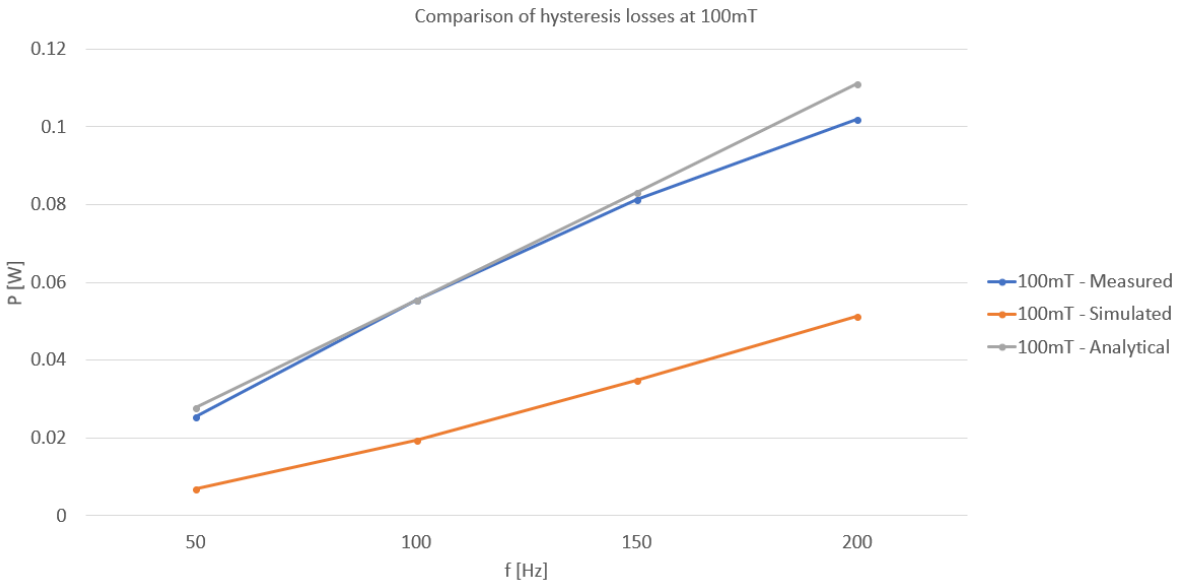

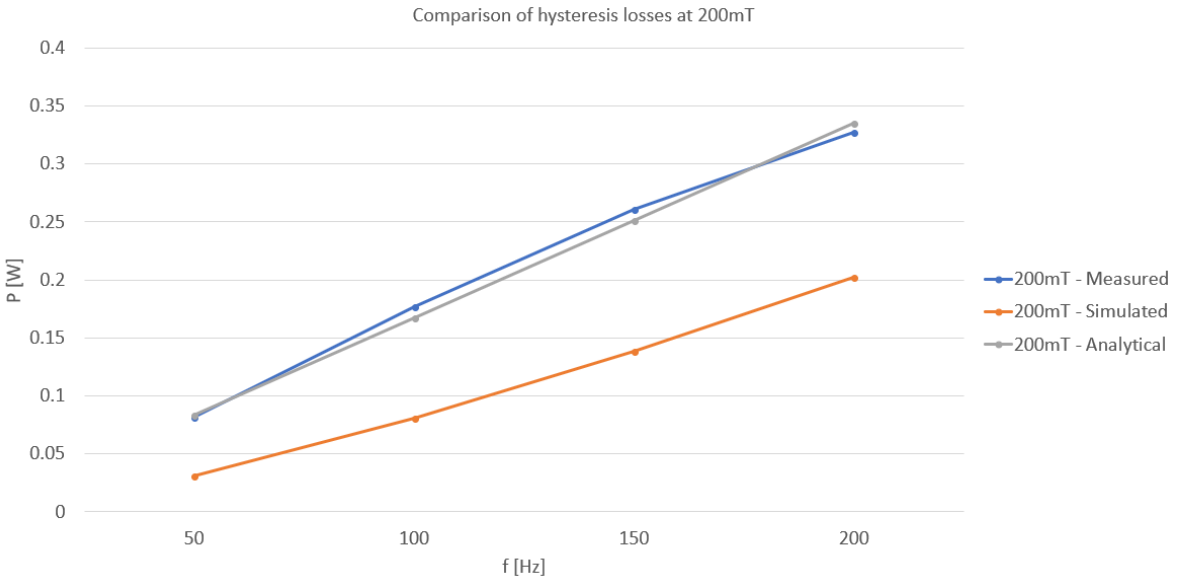

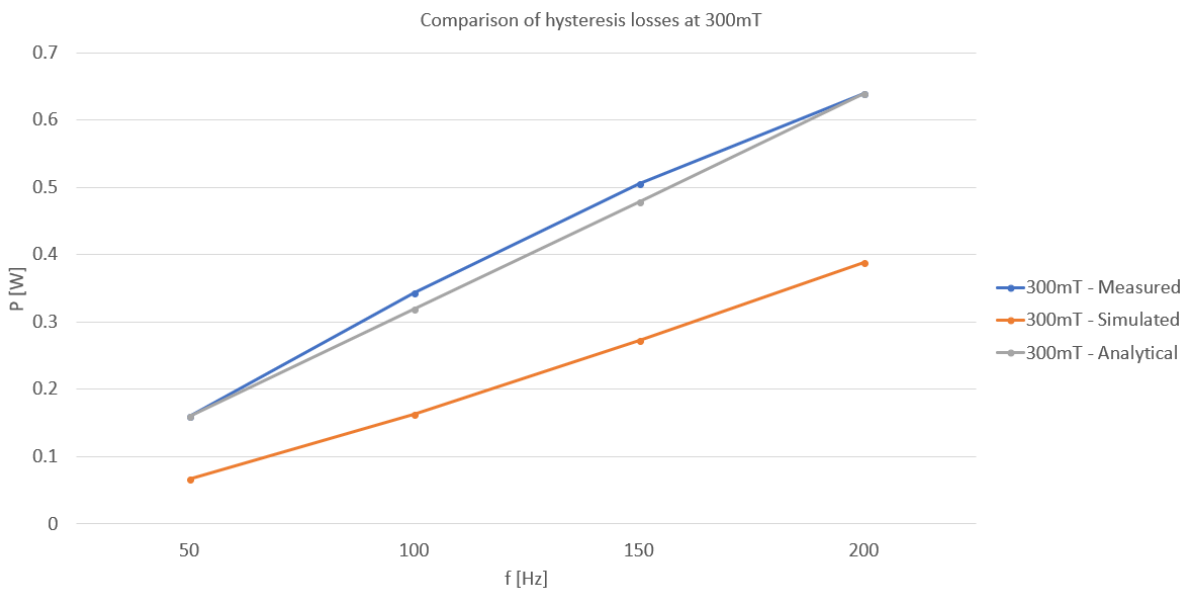
Comparison of hysteresis losses at 300mT
0.7
0.6
0.5
0.4
0.3
0.2
0.1
0
P [W]
50
100
150
200
f [Hz]
300mT - Measured
300mT - Simulated
300mT - Analytical

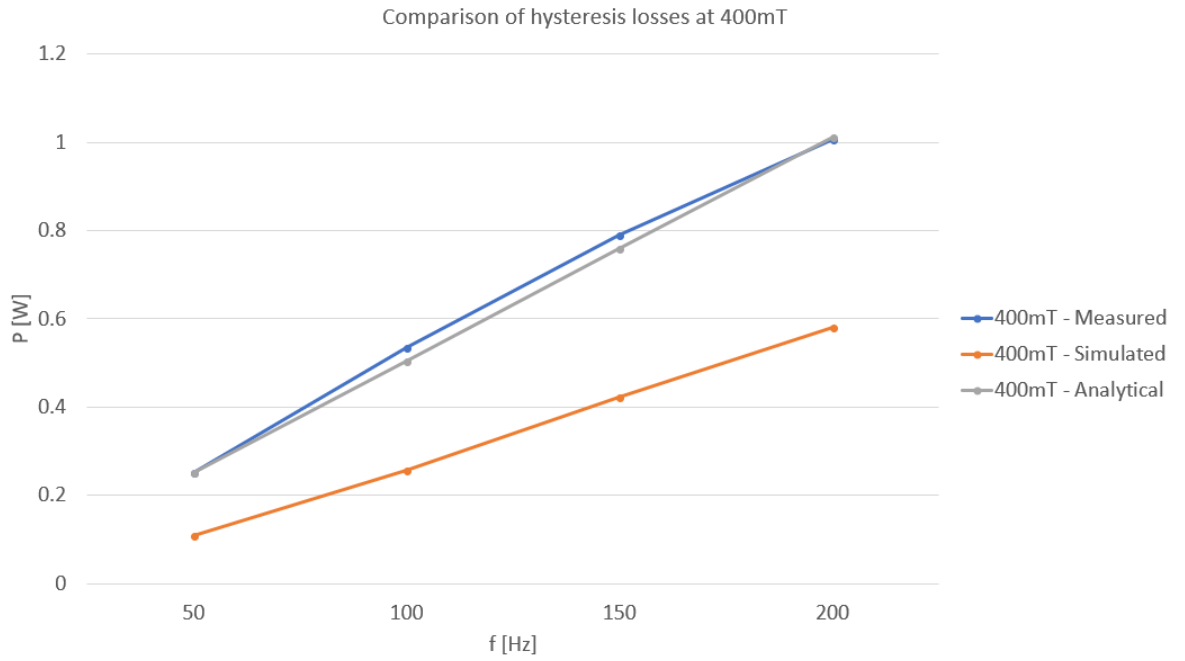
Comparison of hysteresis losses at 400mT
1.2
1
0.8
0.6
0.4
0.2
0
P [W]
50
100
150
200
f [Hz]
400mT - Measured
400mT - Simulated
400mT - Analytical

Material 2 – Comparison of eddy current loss

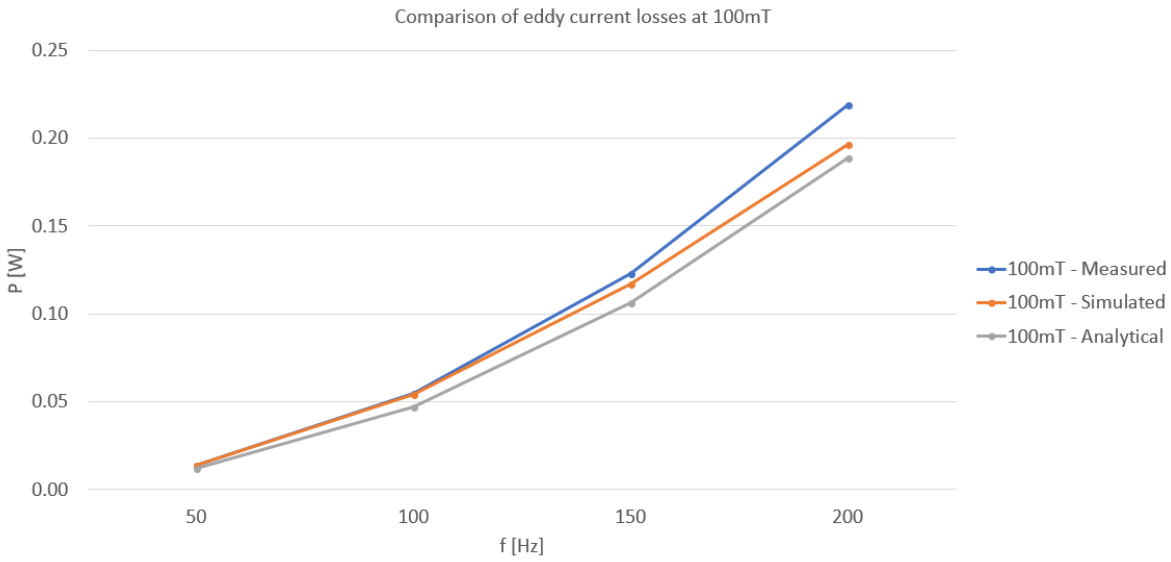

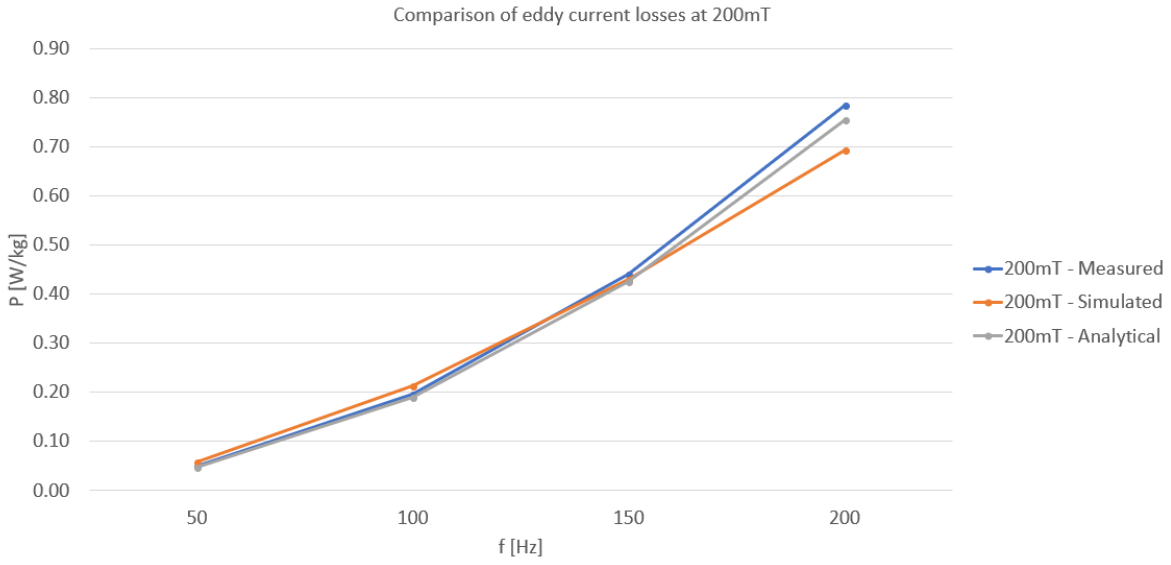

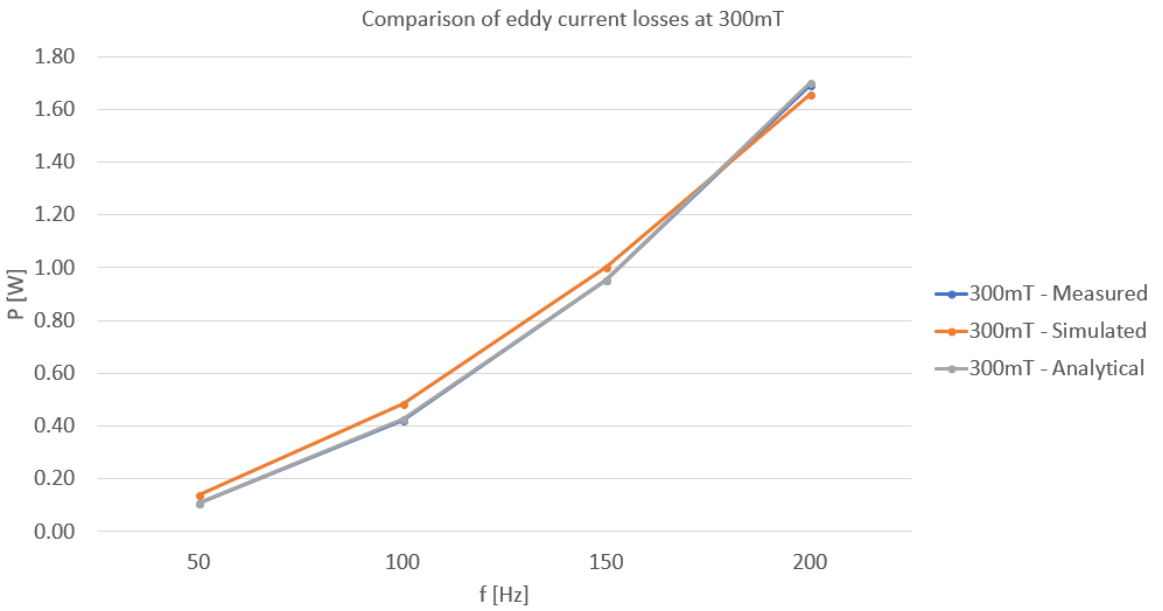
Comparison of eddy current losses at 300mT
1.80
1.60
1.40
1.20
1.00
0.80
0.60
0.40
0.20
0.00
P [W]
50
100
150
200
f [Hz]
300mT - Measured
300mT - Simulated
300mT - Analytical

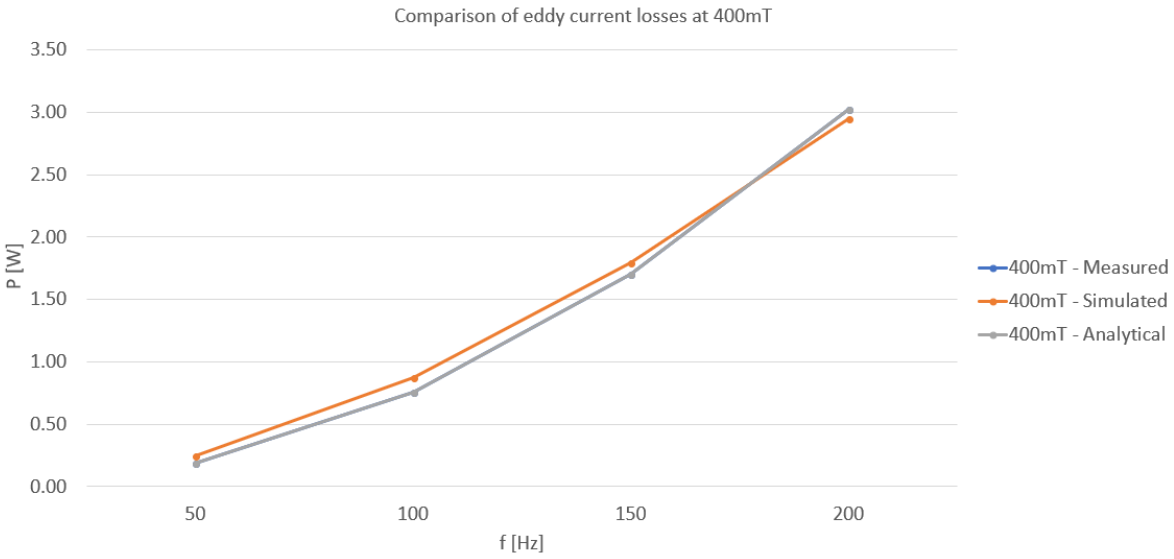
Comparison of eddy current losses at 400mT
3.50
3.00
2.50
2.00
1.50
1.00
0.50
0.00
P [W]
50
100
150
200
f [Hz]
400mT - Measured
400mT - Simulated
400mT - Analytical

Material 2 – Comparison of hysteresis loss

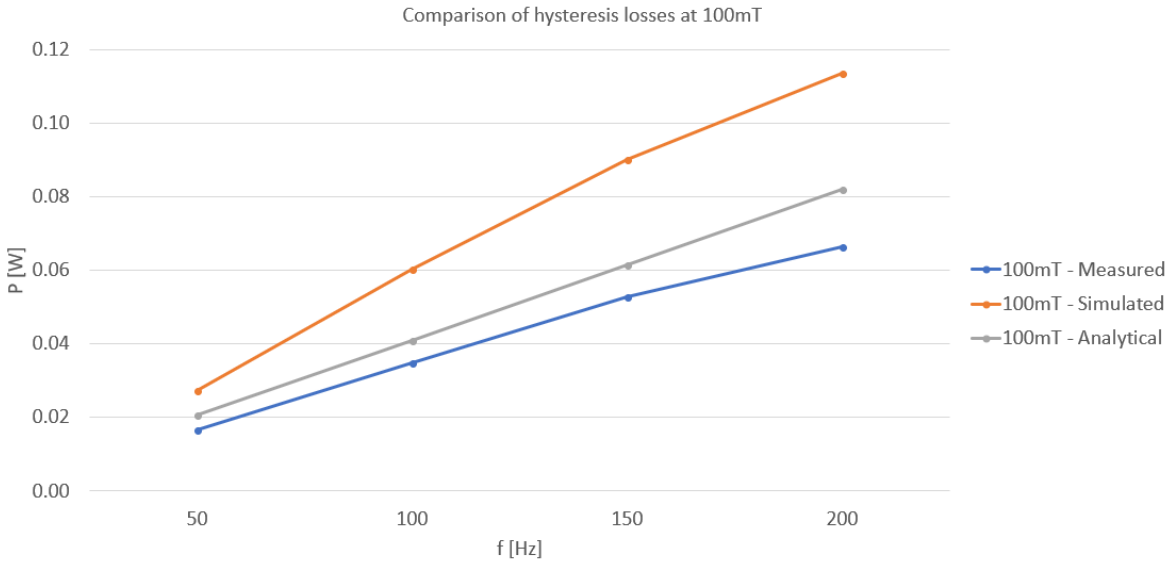

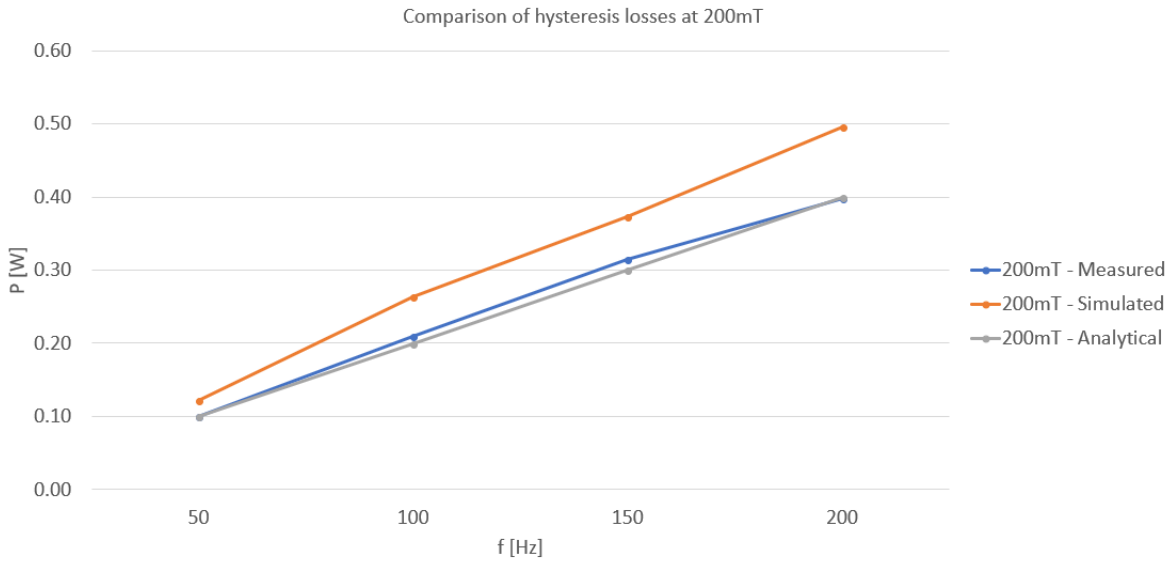

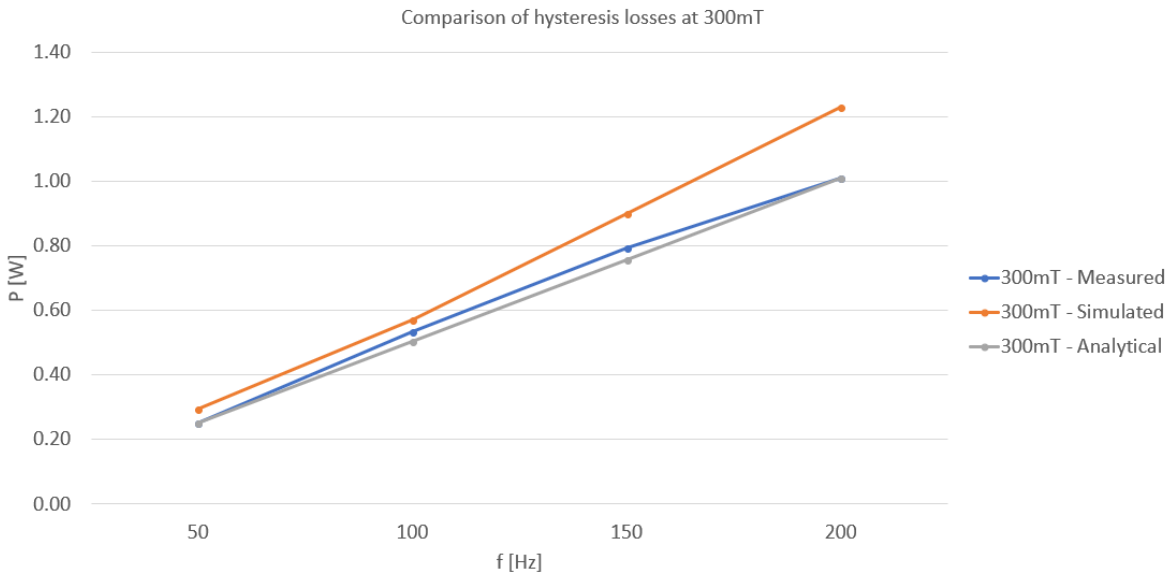
Comparison of hysteresis losses at 300mT
1.40
1.20
1.00
0.80
0.60
0.40
0.20
0.00
P [W]
50
100
150
200
f [Hz]
300mT - Measured
300mT - Simulated
300mT - Analytical

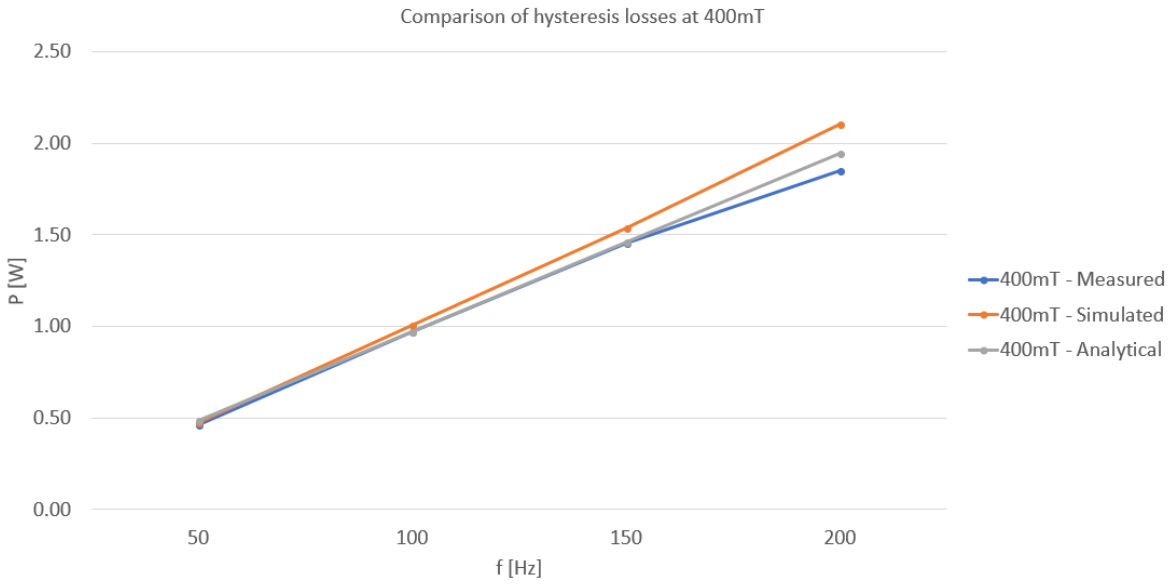
Comparison of hysteresis losses at 400mT
2.50
2.00
1.50
1.00
0.50
0.00
P [W]
50
100
150
200
f [Hz]
400mT - Measured
400mT - Simulated
400mT - Analytical

Appendix G: Matlab script - Determination of analytical eddy current loss parameters

```
options=optimset('Display','iter','MaxFunEvals',1000000);

optiFun1 = @(b) optimizeEddyCurrent(b(1));
b_init = [0.000576778];
b_min = fminsearch(optiFun1, b_init, options);

function func = optimizeEddyCurrent(k)
% Rod 6
%     bmax50 = [0.099212997 0.198320007 0.297549988 0.396790009];
%     bmax100 = [0.099078003 0.198300003 0.297350006 0.396720001];
%     bmax150 = [0.099126999 0.198399994 0.297359985 0.39676001];
%     bmax200 = [0.099165001 0.198309998 0.29751001 0.396769989];
%
%
%     p50 = [0.00891434 0.037836847 0.101092746 0.219622419];
%     p100 = [0.035649069 0.151346351 0.404360629 0.878842027];
%     p150 = [0.080194341 0.34034921 0.90931138 1.976358265];
%     p200 = [0.142625286 0.605343942 1.617307804 3.515368107];


%Rod 25175
    bmax50 = [0.100989998 0.201919998 0.302839996 0.403959991];
    bmax100 = [0.100980003 0.202 0.302769989 0.403709991];
    bmax150 = [0.10093 0.201889999 0.302769989 0.404049988];
    bmax200 = [0.100959999 0.201949997 0.302970001 0.403690002];

    p50 = [0.013675 0.049005 0.105741 0.188802];
    p100 = [0.054690 0.196019 0.422878 0.755177];
    p150 = [0.123057 0.440809 0.951287 1.698982];
    p200 = [0.218801 0.784087 1.691704 3.020503];

    tot = 0;

    for i=1:4
        fifty = (k*(50.^2)*(bmax50(i).^2));
        hundred = (k*(100.^2)*(bmax100(i).^2));
        hundredandfifty = (k*(150.^2)*(bmax150(i).^2));
        twohundred = (k*(200.^2)*(bmax200(i).^2));

        fprintf("50Hz losses: " + num2str(fifty)+"\n");
        fprintf("100Hz losses: " + num2str(hundred)+"\n");
        fprintf("150Hz losses: " + num2str(hundredandfifty)+"\n");
        fprintf("200Hz losses: " + num2str(twohundred)+"\n");
        fprintf("k: " + num2str(k)+"\n");
        fprintf("i: " + num2str(i)+"\n");

%         dev1 = abs(((fifty*100)/p50(i))-100);
%         dev2 = abs(((hundred*100)/p100(i))-100);
%         dev3 = abs(((hundredandfifty*100)/p150(i))-100);
%         dev4 = abs(((twohundred*100)/p200(i))-100);
```

```
        dev1 = abs(fifty-p50(i));
        dev2 = abs(hundred - p100(i));
        dev3 = abs(hundredandfifty - p150(i));
        dev4 = abs(twohundred - p200(i));
        %The relative deviation in percentage is added together and minimized
        tot = tot+dev1+dev2+dev3+dev4;
    end

    func = tot;
end
```

Appendix H: Matlab script - Determination of analytical hysteresis loss parameters

```
options=optimset('Display','iter','MaxFunEvals',1000);
optiFun1 = @(b) optimizeHysteresis(b(1), b(2));
b_init = [0.1, 2];
b_min = fminsearch(optiFun1, b_init, options);

function func = optimizeHysteresis(k, n)
    %Rod 6
%     bmax50 = [0.099212997 0.198320007 0.297549988 0.396790009];
%     bmax100 = [0.099078003 0.198300003 0.297350006 0.396720001];
%     bmax150 = [0.099126999 0.198399994 0.297359985 0.39676001];
%     bmax200 = [0.099165001 0.198309998 0.29751001 0.396769989];
%
%     p50 = [0.025499374 0.081785168 0.15971504 0.251609992];
%     p100 = [0.055440635 0.176835878 0.342857223 0.534456207];
%     p150 = [0.08142244 0.261015051 0.505101031 0.790750604];
%     p200 = [0.101999572 0.327114751 0.6388187 1.006626572];

%     %Rod 25175
    bmax50 = [0.100989998 0.201919998 0.302839996 0.403959991];
    bmax100 = [0.100980003 0.202 0.302769989 0.403709991];
    bmax150 = [0.10093 0.201889999 0.302769989 0.404049988];
    bmax200 = [0.100959999 0.201949997 0.302970001 0.403690002];

    p50 = [0.016602994 0.099526347 0.252266755 0.462771564];
    p100 = [0.034835748 0.209975452 0.532293422 0.971850292];
    p150 = [0.052705092 0.314072452 0.794673648 1.457775487];
    p200 = [0.066411978 0.398105387 1.009005958 1.851015];

    tot = 0;

    for i=1:4
        fifty = (k*50*(bmax50(i).^n));
        hundred = (k*100*(bmax100(i).^n));
        hundredandfifty = (k*100*(bmax150(i).^n));
        twohundred = (k*200*(bmax200(i).^n));

        fprintf("50Hz losses: " + num2str(fifty)+"\n");
        fprintf("100Hz losses: " + num2str(hundred)+"\n");
        fprintf("150Hz losses: " + num2str(hundredandfifty)+"\n");
        fprintf("200Hz losses: " + num2str(twohundred)+"\n");
        fprintf("k: " + num2str(k)+"\n");
        fprintf("n: " + num2str(n)+"\n");
        fprintf("i: " + num2str(i)+"\n");

%         dev1 = abs(((fifty*100)/p50(i))-100);
%         dev2 = abs(((hundred*100)/p100(i))-100);
%         dev3 = abs(((hundredandfifty*100)/p150(i))-100);
%         dev4 = abs(((twohundred*100)/p200(i))-100);
        dev1 = abs(fifty - p50(i));
        dev2 = abs(hundred - p100(i));
```

```
        dev3 = abs(hundredandfifty - p150(i));
        dev4 = abs(twohundred - p200(i));
        %The relative deviation in percentage is added together and minimized
        tot = tot+dev1+dev2+dev3+dev4;
        %Recommendation in theory
        if(1.5 > n) || (n > 2.5)
        tot = tot+10000;
        end
    end
 func = tot;
end
```